The University of Alberta

Stratigraphy and Palaeoclimatology of Loess of the Loess Plateau, China during the last interglacial-glacial cycle.

By

Charles Dean Rokosh ©

A Thesis

Submitted to the Faculty of Graduate Studies and Research

in Partial Fulfillment of the Requirements for the Degree of

Doctor of Philosophy

Department of Earth and Atmospheric Sciences

Edmonton, Alberta, Canada

Spring 2001

National Library of Canada
Acquisitions and Bibliographic Services
395 Wellington Street
Ottawa ON K1A 0N4
Canada

Bibliothèque nationale du Canada
Acquisitions et services bibliographiques
395, rue Wellington
Ottawa ON K1A 0N4
Canada

Your file Votre référence

Our file Notre référence

The author has granted a non-exclusive licence allowing the National Library of Canada to reproduce, loan, distribute or sell copies of this thesis in microform, paper or electronic formats.

L'auteur a accordé une licence non exclusive permettant à la Bibliothèque nationale du Canada de reproduire, prêter, distribuer ou vendre des copies de cette thèse sous la forme de microfiche/film, de reproduction sur papier ou sur format électronique.

The author retains ownership of the copyright in this thesis. Neither the thesis nor substantial extracts from it may be printed or otherwise reproduced without the author's permission.

L'auteur conserve la propriété du droit d'auteur qui protège cette thèse. Ni la thèse ni des extraits substantiels de celle-ci ne doivent être imprimés ou autrement reproduits sans son autorisation.

0-612-60340-7

Canada

University of Alberta

Library Release Form

Name of Author: Charles Dean Rokosh

Title of Thesis: Stratigraphy and Palaeoclimatology of Loess of the Loess Plateau, China during the last Interglacial-Glacial cycle.

Degree: Doctor of Philosophy

Year this degree granted: 2001

Permission is hereby granted to the University of Alberta Library to reproduce single copies of this thesis or sell such copies for private, scholarly or scientific research purposes only.

The author reserves all other publication and other rights in association with the copyright in this thesis, and except as herein provided, neither the thesis nor any substantial portion thereof may be printed or otherwise reproduced in any material form whatever without the author's prior written permission.

C. Dean Rokosh

Charles Dean Rokosh
#75, 3115 - 119 St.
Edmonton, Alberta
T6G 5N5

December 8, 2001

University of Alberta

Faculty of Graduate Studies and Research

The undersigned certify that they have read , and recommend to the Faculty of Graduate Studies and Research for acceptance, a thesis titled 'Stratigraphy and Palaeoclimatology of loess of the Loess Plateau, China during the last interglacial-glacial cycle' submitted by Charles Dean Rokosh in Partial Fulfillment of the Requirements for the Degree of Doctor of Philosophy.

Dr. N.W. Rutter (supervisor)

Dr. A.B.G. Bush

Dr. O. Catuneanu

Dr. M. Hickman

Dr. J.T. Teller (external)

Approved by the committee on October 9, 2000.

Abstract

A regional study of loess-palaeosol stratigraphy and sedimentology, during the last interglacial-glacial cycle, has used three different scales of observation to develop a new, conceptual model of loess deposition in the Chinese Loess Plateau. The model is based on spatial and temporal variations in loess grain size, accumulation rates and thickness, and indicates that variations in loess characteristics are part of an evolving desert-loess depositional system. In this system, the desert is the main source of loess and influences loess distribution via desert expansion and contraction during glacial and interglacial periods, respectively. Desert expansion and contraction was forced, in part, by changes in soil moisture that is influenced by extent of the Fennoscandian ice-sheet and the atmospheric circulation pattern that it induces downstream.

Within the last glacial unit (~12-74 ky), lateral changes in stratigraphy from desert sand to loess (proximal to the source), or loess to soil (distal from the source) are driven by variations in the balance between loess accumulation rates and pedogenesis. In addition, vertical alternations of loess and palaeosols are driven by changes in accumulation rates along a shifting climatic gradient. At a higher resolution, correlations suggest that millenial-scale variations in grain size propagate through the central Loess Plateau. The geometry of the high resolution correlations is similar to the geometry of the Malan formation and its' members, suggesting that the Malan loess is stratified, and that there was a relatively consistent wind direction during deposition of the Malan..

These results suggests that there are global effects (changes in ice volume), regional effects (i.e. changes in Eurasian ice sheets), and local effects (i.e. changes in the position of the desert margin) that have an influence on loess-palaeosol stratigraphy and

loess deposition in China. However, not all variations in loess-palaeosol stratigraphy or sedimentology are related to climate change. Some high frequency variations may result from non-climatic effects, rather than global or hemispherical climatic change.

Acknowledgments

My endeavor to get a Ph.D. in Quaternary Geology has been the most exciting and arduous journey that I have ever undertaken. The journey has also taken its toll on my family, though we have endured through love and support for each other. My feelings of guilt for not spending more time with my children are finally rested. I pledge to each of you that I will be available to guide you through your own journeys.

I must first thank my friend and mentor Nat Rutter. This journey could absolutely not have completed without your continued intellectual, financial and emotional support. You are truly a gentleman and a scholar. My discussions with Charlie Schweger and Ted Evans, academic or otherwise, have always been fruitful and fun. You helped me construct a strong and well-balanced intellectual foundation, from which I shall surely build a productive career. I look forward to many more encounters. To the gentlemen of my examination committee: Marvin Dudas, Carl Mendoza and Karlos Meuhlenbachs: I have never been shy to ask a question and you have never failed to take the time to answer. Many thanks.

One of the most enjoyable experiences of graduate school is building new friendships. Although there are more people to name than space to say thanks, I must mention the great group of the old 1-16: Solweig Balzer, Jeff Bond, Arlene Collins, Loren Davis, Julie Esdale, Ted Little, Louise Leslie and Paul Wilson. Great discussions and thirst quenching beer are an unbeatable combination. Beer and pool with Robin Wylie and Ian Campbell always 'hit the spot'. I want to single out Solly for putting my graduate writing ability on the right track, and especially Ted for our discussions on every aspect of life and science. Ted is the best office mate that a student could have, a real

gentleman and a scholar. This thesis was greatly improved due to editing by Celina, Ian, Loren, Robin, Solly and (notably) Ted.

To my father (especially), brother, sister and in-laws your support restored my spirit when I needed it the most. I cannot tell you how much I appreciated getting unwavering support even after a decade of undergraduate and graduate school. Lastly and certainly not the least (in fact the most!!), my dearest Karen, we have done this together. Thanks for your love, patience and support. Your turn!!

Shortly after writing this acknowledgement my dear wife Karen passed away (01/98). I dedicate this thesis to my beloved Karen. Without her unwavering support and encouragement this work could not have been done. I miss you so much

Table of Contents

List of Tables

List of Figures

Chapter 1 Introduction

1.1 Introduction 1
1.2 Geographical setting 4
1.3 Objective and Rationale 5
1.4 Contributions to Quaternary Geology 6
1.5 Format 6
1.6 References 8

Chapter 2 Prior Research

2.1 Introduction 13
2.2 Early Loess research in China 14
2.2.1 Introduction: Pre 1949 14
2.2.2 Loess History 14
2.2.3 Introduction: Post 1949 22
2.2.4 Trends in Research After 1949 23
2.3 References 25

Chapter 3 Comparison of loess grain size and accumulation rates during the last interglacial and glacial periods in the central Loess Plateau, China: links to climatic forcing. (Paper #1)

3.1 Introduction 30
3.2 Geography 34
3.3 Methods 37
3.4 Stratigraphy along the transect 38
3.4.1 Methodology 38
3.4.2 Temporal and spatial observations of grain size variations along transect 41
3.4.2.1 Interpretation 43
3.4.3 Observations of trends in thickness 46
3.4.3.1 Interpretation of trends in thickness 49
3.4.3.2 Interpretation of variations in accumulation rates 51
3.5 Discussion of results and relationship to global ice volume variations 56
3.6 Conclusion 57
3.7 References 59

Chapter 4 Regional lithofacies and pedofacies variations along a north to south climatic gradient during the last glaciation in the central Loess Plateau, China. (Paper #2)

4.1 Introduction..... 69
4.2 Methods..... 73
4.3 Modern Climate..... 74
4.4 North to South transect..... 75
4.5 The effect of local variations in the rate of dust accretion along the continua on high-resolution palaeoclimate interpretations..... 78
4.6 Conclusions..... 79
4.7 References..... 81

Chapter 5 High resolution architecture and stratification of the Malan loess (last glacial) in the central Loess Plateau, China. (Paper #3)

5.1 Introduction..... 85
5.2 Methods..... 89
5.3 Dust deposition and the source of loess..... 90
5.4 Stratigraphy of the Malan formation..... 91
5.5 Higher Resolution Correlations..... 95
5.6 Discussion..... 97
5.7 Conclusions..... 100
5.8 References..... 101

Chapter 6 Hydrologic and geologic processes causing spatial variations in loess deposition in China during the last interglacial-glacial cycle: results from proxy climate and GCM analyses. (Paper #4)

6.1 Introduction..... 107
6.2 Methods..... 110
6.3 Comparison of loess and susceptibility records with global ice volume and insolation variations during the last glacial-interglacial cycle..... 111
6.4 Loess Depositional Model..... 114
6.5 Modern Dust Deposition..... 122
6.6 Soil moisture content during the last glaciation..... 123
6.7 Discussion..... 126
6.8 Conclusion..... 127
6.9 References..... 129

Chapter 7 Summary and Conclusion

7.1 Introduction..... 137

7.2 Final Conclusions..... 137
7.3 Future Research..... 140
7.4 Reference..... 143

Appendix..... 144

List of Tables

Chapter 3

Table 3.1. Minimum accumulation rates..... 48

Chapter 4

Table 4.1 Variations in grain size and weight percent sand (>63 μm)..... 77

List of Figures

Chapter 1

Figure 1.1 Base map of the Loess Plateau..... 2

Chapter 2

Figure 2.1 Stratigraphy of the Loess Plateau..... 17
Figure 2.2 Map of the Loess Plateau..... 20

Chapter 3

Figure 3.1 Base map of the Loess Plateau..... 31
Figure 3.2 Topography of the Loess Plateau..... 36
Figure 3.3 Stratigraphic cross-section from the central Loess Plateau..... 39
Figure 3.4 Grain size and magnetic susceptibility variations at Yulin..... 42
Figure 3.5 Schematic model of variations in grain size..... 45
Figure 3.6 Thickness of the last glacial unit (L1; MIS 2-4)..... 47
Figure 3.7 Thickness of the last interglacial unit (S1; MIS 5)..... 47
Figure 3.8 Spatial and temporal comparison of accumulation rates in the Loess Plateau..... 53
Figure 3.9 Schematic of variations in thickness along the transect..... 54

Chapter 4

Figure 4.1 Base map of the Loess Plateau..... 70
Figure 4.2 Comparison of litho- and pedostratigraphy at Yulin and Weinan... 71
Figure 4.3 Grain size and magnetic susceptibility variations..... 76

Chapter 5

Figure 5.1 Base map of the Loess Plateau..... 86
Figure 5.2 Stratigraphic cross-section from the central Loess Plateau..... 88
Figure 5.3 The Yulin site in the last glacial desert-loess transition zone. 92
Figure 5.4 Schematic showing undaform-clinoform-fondoform environments..... 94
Figure 5.5 High resolution correlation of grain size along the transect..... 96
Figure 5.6 Actual variations showing merged loess beds..... 98

Chapter 6

Figure 6.1 Map of the Loess Plateau..... 109
Figure 6.2 Comparison of loess and deep-sea $\delta^{18}O$ records 112
Figure 6.3 Stratigraphic cross-section from the central Loess Plateau..... 115
Figure 6.4 The Yulin site in the last glacial desert-loess transition zone..... 116
Figure 6.5 Schematic model of actual variations in grain size..... 118
Figure 6.6 Spatial and temporal comparison of accumulation rates in the Loess Plateau..... 119
Figure 6.7 Scaled schematic diagram showing the distribution of loess..... 121
Figure 6.8a, b, c Results from numerical GCM experiments..... 124

CHAPTER 1

Introduction

1.1 Introduction

Palaeoclimatologists seek to understand the causes of temporal and spatial variability in the Earth's climate system. Two of the main goals of the paleoclimate community are to determine the extent of human influence on climate change, and to forecast climate change by modeling present trends (Houghton et al. 1990; Rutter 1992; Maslin and Berger 1997). In order to achieve these goals it is necessary to:

1) Improve our knowledge of past global and regional climates, their spatial and temporal variations, and the forcing mechanisms responsible for climate change;

2) Assess the evidence for significant trends in global and regional climates at various time scales;

3) Develop physical-mathematical models capable of assessing the predictability of climate change; and,

4) Investigate the sensitivity of climate to natural change (e.g. El Nino), and human influence (e.g. the Greenhouse Effect).

The general objective of this thesis falls under points 1 and 2 above: to increase our understanding of East Asian Quaternary loess deposition and palaeoclimatology (e.g. winter and summer monsoon variations) through a spatial and temporal evaluation of the geology of the Chinese Loess Plateau (Fig. 1.1).

The Loess Plateau is one of the key areas for studying Quaternary climate change from terrestrial deposits for two reasons: 1) loess and palaeosols spanning the past 2.5 Ma

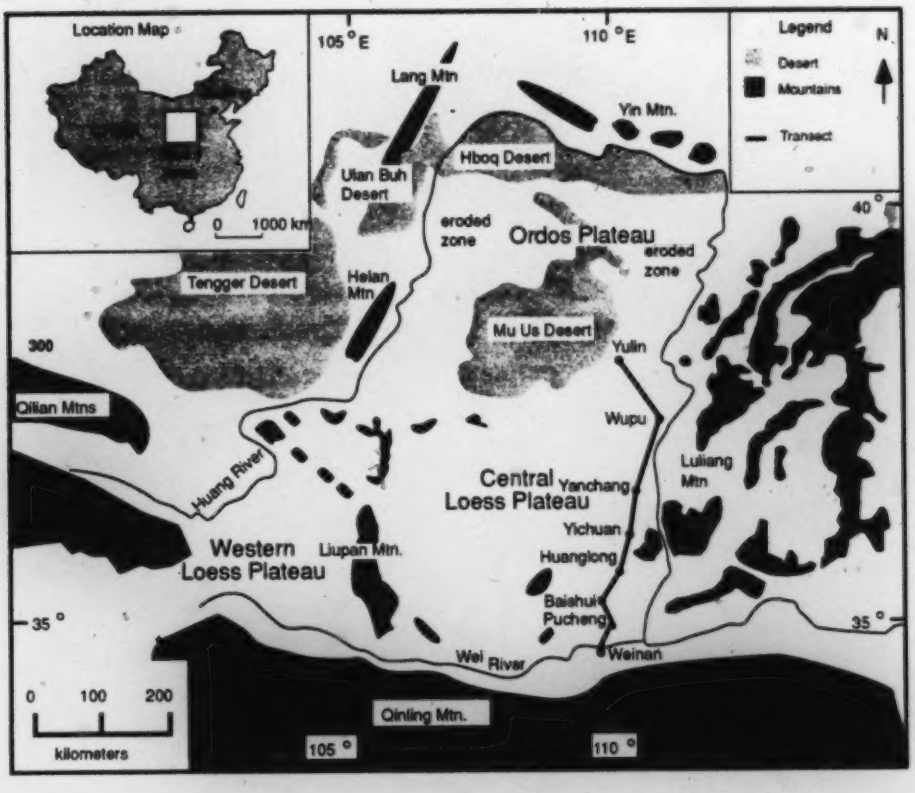

Figure 1.1 Map of the Loess Plateau. The location of the uplands have been modified using US Defense Mapping Agency Aerospace Center, Operational Navigation Chart Series ONC, Sheets F-7, F-8, G-8 and G-9, Edition 4, 1987).

are relatively well preserved (Liu et al., 1985; Rutter *et al.* 1991, 1995, 1996), and 2) the strata appear to be spatially extensive and contiguous at the scale of an interglacial-glacial cycle (Liu et al., 1985). Stratigraphic research in the Loess Plateau over the past 15-20 years has largely concentrated on two time frames: 1) the entire sequence to the base of the Chinese Quaternary at about 2.5 Ma (e.g. Heller and Liu 1982, 1984, 1986; Kukla 1987a, 1987b; Kukla et al. 1988; Ding et al. 1991, 1994; Rutter et. al. 1991; Evans et al. 1992; Bloemendal et al. 1995; Shackleton et al. 1995), and 2) the last interglacial-glacial cycle and/or the Holocene (e.g. Porter and An, 1995, Derbyshire et al., 1995, 1997; Chen et al. 1997; Rutter et al. 1997; Ding et al. 1998; Fang et al. 1998; Sun and Ding 1998).

The primary focus of research involving the last interglacial-glacial cycle has been to evaluate climatic change at high resolutions (i.e. a millennium). The high resolution studies have been correlated to ice core (e.g. Porter and An 1995; Rutter et al. 1997, 1998; Ding et al. 1998; Fang et al. 1998) and deep sea profiles (e.g. An and Porter 1998; Rokosh et al. 1998; Sun and Ding 1998). The result is a dominance of palaeoclimate interpretations based on correlations of loess-palaeosol alternations from one, or a few, sedimentary sections, with the assumption that the interpretations in the Loess Plateau (an area of about 440,00 km^2; Liu et al. 1985) are equally valid regionally.

In the Loess Plateau, however, there are no regional studies that compare loess deposition from the sediment source to the accumulation zone during the last interglacial-glacial cycle. Knowledge of the regional geology of the Loess Plateau during the last interglacial-glacial cycle is important for understanding high resolution loess deposition and interpreting palaeoclimate. Hence, the trend to evaluating palaeoclimate

at high resolutions and the need for a regional study of loess deposition during the last interglacial-glacial cycle signifies a need for a re-evaluation of the stratigraphy of the Loess Plateau. The time frame of the evaluation spans approximately the last 130,000 years. Three scales of observation are used to examine the regional changes in stratigraphy and sedimentology: 1) an interglacial-glacial cycle (~100 ky), 2) the last glaciation (12-74 ky; Liu, J. et al. 1995), and 3) high resolution (a few millennia).

1.2 Geographical Setting

The Loess Plateau covers an area of approximately 440,000 km^2 (roughly the area of the province of Alberta) between about 35°N to 40°N latitude and 100°E to 115°E longitude (Fig. 1.1; Liu et al 1985). Loess distribution forms an arcuate belt, open to the north-northwest, stretching from the northwestern, arid inland basins to the eastern plains (Liu et al. 1985; Ren et al. 1985; Zhao 1986). The Loess Plateau is informally divided into the western, central and eastern regions, with the central region confined by the Huang He (Yellow River), east of the Luipan Mountains. The Qinling Mountains and the Tibetan (Qinghai-Xizang) Plateau border the Loess Plateau on the south (Fig. 1.1). The northwest to southwest trending Qilian Mountains, the north to south trending Helan, Liupan, Luliang and Taihang Mountains average at least 500 meters above the surface of the Loess Plateau (U.S. Defense Mapping Agency Aerospace Center 1987). The Shamoa (sandy) and the Gobi (stoney/rocky) deserts flank the Loess Plateau to the north and west. The Shamoa is further subdivided into regional deserts such as the Tengger, Badain Jaran, Mu Us and Hobq.

1.3 Objective and Rationale

The specific objective of this thesis is to study loess deposition from the sediment source to the accumulation zone during the last interglacial-glacial cycle at a high resolution (e.g. a millennium). The source of loess are largely the deserts of north China as principally indicated by the regional southward decrease in thickness and grain size from the desert margin (von Richthofen 1882; Chamberlin 1897; Barbour 1935, 1965; Bryan 1945; Liu et al. 1985; Sun and Ding 1998). Studying loess deposition at a high resolution should lead to a better understanding of the palaeoclimatic and non-climatic factors that affect loess deposition. The approach to studying loess deposition at a high resolution is to first comprehend loess deposition and palaeoclimatology during an interglacial-glacial cycle (e.g. about 100,000 years; Imbrie et al. 1984). The scale of the observations will change when studying loess deposition and palaeosol development during the last glaciation in China (e.g. Malan Loess; about 12-74 ka; Liu et al. 1995). Finally, after reaching an understanding of the climatic and geologic factors that affect loess deposition at the two larger scales, loess deposition at a millennial scale will then be studied.

In order to meet the objective, approximately 2300 samples were collected along a north to south transect from Yulin in the desert-loess transition zone to Weinan in the southern Loess Plateau (Fig. 1.1). Samples were collected approximately every 5 to 10 centimeters in palaeosols and loess beds (see Appendix 1). All samples were analyzed for grain size, magnetic susceptibility, $CaCO_3$, pedogenic FeO, total Fe, and Total Organic Carbon (TOC) resulting in over 11,000 data points. All analyses were performed in China under the direction of Professor Ding Zhongli.

1.4 Contributions to Quaternary Geology

The contributions to Quaternary geology are:

1) A critical review of the history of loess research in China, prior to the establishment of the People's Republic of China (1949). The purpose is to clearly state the implicit stratigraphical and sedimentological assumptions that were made regarding loess and palaeosols, and outline how these assumptions influenced regional, high-resolution paleoclimate interpretations.

2) Presents the one of the first high-resolution transect studies of loess stratigraphy and loess properties in the Loess Plateau (Fig 1.1).

3) Develops a new, conceptual model of loess deposition from the sediment source to the accumulation zone during the last interglacial-glacial cycle, based on spatial and temporal variations in loess grain size and accumulation rates.

4) Applies the concept of pedofacies (i.e. a balance between the rate of sedimentation and pedogenesis) to regional paleoclimatic and stratigraphical studies of loess and palaeosols in the Loess Plateau.

5) Introduces new ideas on the relationship between palaeoclimatic, hydrologic and geologic factorss that cause spatial variations in loess properties in the Loess Plateau, China.

1.5 Format

This research is presented in four papers; each paper is designed to stand alone. Chapter 2 presents a brief history of loess research in the Loess Plateau prior to the establishment of the People's Republic of China (1949). Chapters 3-6 are separate

papers, although each are related to the central theme of this thesis as outlined in chapter 1. There is some overlap in the discussion of the geography of the Loess Plateau, and the methods used to meet the objectives in each of the papers. Chapter 3 compares regional trends in thickness and grain size variations of loess deposited during the last interglacial period with loess deposited during the last glacial period. The purpose is to examine the role of variations in global ice volume (and related climatic changes) on regional loess deposition. Chapter 4 applies the concept of pedofacies (i.e. the balance between loess accumulation and pedogenic development; Bown and Kraus, 1986, Smith, 1990) to regional loess-palaeosol stratigraphy. Chapter 5 reconstructs high resolution (e.g. millenial scale) regional stratigraphy of the Loess Plateau, and develops a conceptual model of regional, high-resolution loess deposition from the sediment source to the sediment accumulation zone. The climatic, hydrologic and geologic factors that affect palaeo-dust deposition in China are examined in Chapter 6 by integrating the new model of loess deposition (from chapters 3-5), with climatic and hydrologic factors that influence modern loess deposition, and a coupled ocean-atmosphere general circulation model analyses. Chapter 7 presents a summary and conclusions of the entire research project, and the contributions this research has made in improving our understanding of palaeoclimate based upon the interpretation of loess-palaeosol sequences in the Loess Plateau, China. The final section of this chapter covers future research that may continue to improve our understanding of loess deposition, palaeosol development and palaeoclimate

1. 6 References

An, Z. and Porter, S. 1998. Millenial-scale climatic oscillations during the last interglacial in central China. PAGES Newsletter, **6**, 4.

Barbour, G.B. 1935 Recent Observations on the loess of North China: Geographical Journal, **86**(1), 54-64.

Barbour, G.B. 1965. In the field with Teilhard de Chardin. New York, U.S.A., Herder and Herder.

Bloemendal, J., Liu, X.M. and Rolph, T.C. 1995. Correlation of the magnetic susceptibility stratigraphy of Chinese loess and the marine oxygen isotope record: chronological and palaeoclimatic implications. Earth and Planetary Science Letters, **131**, 371-380.

Bryan, K. 1945. Glacial versus desert origin of loess: American Journal of Science, **243**(5), 245-248.

Chamberlin, T.C. 1897. Supplementary hypothesis respecting the origin of the loess of the Mississippi Valley: Journal of Geology, **5**, 795-802.

Chen, F.H., Wang, J.M., and Bloemendal, J. 1998. East Asian monsoon variations during the last interglacial: evidence from the northwest margin of the Chinese Loess Plateau. Past Global Changes (PAGES) Newsletter, **6**: 10.

Derbyshire, E., Keen, D., Kemp, R.A., Rolph, T.A., Shaw, J., and Meng, X.M. 1995. Loess-paleosol sequences as recorders of palaeoclimatic variations during the last glacial-interglacial cycle: some problems of correlation in north-central China. Quaternary Proceedings, **4**, 7-18.

Derbyshire, E., Kemp, R.A., and Meng, X.M. 1997. Climate change, loess and paleosols: proxy measures and resolution in China. Journal of the Geological Society of London, **154**, 793-805.

Ding, Z., Rutter, N.W., Liu, T., Evans, M.E. and Wang, Y. 1991. Climatic correlation between Chinese loess and deep-sea cores: A structural approach. *In* Loess Environment and Global Change. *Edited by* T. Liu. Beijing, Science Press, pp. 168-186.

Ding, Z., Sun, J. Yu, Z. and Liu, T. 1998. Chronology of environmental events over East Asia during the last 130 ka. Chinese Science Bulletin, **43**, 1761-1769.

Ding, Z., Yu, Z., Rutter, N.W. and Liu, T. 1994. Towards an orbital time scale for Chinese Loess. Quaternary Science Reviews, **13**, 39-70.

Evans, M., E., Wang, Y. and Ding, Z. 1992. A detailed study of the Brunhes/ Matuyama boundary in the Baoji loess section, central China. EOS, Transactions, American Geophysical Union, **73**, 104.

Fang, X.-M., Pan, B.-T., Li, J.-J., Ono, Y., Fukusawa, H., Nagatsuka, S. and Torii, M. 1998. High Resolution pedogenic and rock magnetic records of Asian summer monsoon instability during the past 60,000 years from the Chinese western Loess Plateau. PAGES Newsletter, **6**, 7.

Heller, F. and Liu, T. 1982. Magnetostratigraphical dating of loess deposits in China.: Nature, **300**, 431-433.

Heller, F. and Liu, T. 1984. Magnetism of Chinese loess deposits. Geophysical Journal of the Royal Astronomical Society, **77**, 125-141.

Heller, F. and Liu, T. 1986. Palaeoclimatic and sedimentary history from magnetic susceptibility of loess in China. Geophysical Research Letters, **13**, 1169-1172.

Houghton, J.T., Jenkins, G.J. and Ephraums, J.J. 1990. Climate Change; the IPCC scientific assessment. Cambridge and New York, Cambridge University Press. pp. 365

Imbrie, J., Hays, J.D., Martinson, D.G., McIntyre, A., Mix, A.C., Morley, J.J., Pisias, N.G., Prell, W.L., and Shackleton, N.J. 1984. The orbital theory of Pleistocene climate: Support from a revised chronology of the marine $\delta^{18}O$ record. *In* Milankovitch and Climate, Understanding the Response to Astronomical Forcing. *Edited by* A. Berger, J, Imbrie, J. Hays, G. Kukla, and B. Saltzman. NATA ASI Series C: Mathematical and Physical Sciences. Reidel Publishing Company, Boston, pp. 269-305.

Kukla, G. 1987a. Loess stratigraphy in central China and correlation with an extended oxygen isotope time stage scale.: Quaternary Science Reviews, v. 6, p. 191-220.

Kukla, G. 1987b. Correlation of Chinese, European and American loess series with deep-sea sediments., *In* Liu, T.S. (Ed.) Aspects of Loess Research. Beijing, China Ocean Press. pp. 27-38.

Kukla, G., Heller, F., Liu, X.M., Xu, T.C., Liu, T.S. and An, Z.S. 1988. Pleistocene climates in China dated by magnetic susceptibility: Geology, **16**, p. 811-814.

Liu, T., and Chang, T. 1964. The "HuangTu" (loess) of China. Report of the Sixth INQUA Congress, Warsaw 1961, **4**, 503-524.

Liu, T.S. et al. 1985. Loess and the Environment. Beijing, China Ocean Press. pp. 251.

Liu, J., Nie, G., Chen, T., Song, C., Zhu., G., Li, K., Gao, Z., and Qiao, Y. 1995. A preliminary high resolution time scale for the last 130,000 years at Weinan loess section. Sciencia Geologica Sinica (Overseas Edition; Supplementary Issue), Beijing, China, **1**, 9-22.

Maslin, M.A. and Berger, A. 1997. A European view of the future of palaeoclimate research. Quaternary Science Reviews, **16**, 501-504.

Porter, S.C. and An, Z. 1995. Correlation between climate events in the North Atlantic and China during the last glaciation. Nature, **375**,.305-308.

Ren, M., Yang, R. and Bao, H., 1985, An outline of China's Physical Geography. China Knowledge Series.

Rokosh, C.D., Rutter, N.W., Little, E.C., Ding, Z. and Sun, J. 1998. Comparing the stratigraphy of the last glaciation in the Loess Plateau and the Indian and Pacific Oceans. PAGES Newsletter, **6**, 9.

Rutter, N. 1992. Presidential address, XIII INQUA congress 1991; Chinese loess and global change. Quaternary Science Reviews, **11**, 275-281.

Rutter, N.W., Ding, Z., Evans, M.E. and Liu, T. 1991. Baoji-type pedostratigraphic section, Loess Plateau, north-central, China. Quaternary Science Reviews, 10,1-22., 1991, Baoji-type pedostratigraphic section, Loess Plateau, north-central, China. Quaternary Science Reviews, **10**, 1-22.

Rutter, N.W., Ding, Z. and Liu, T. 1995. Reliability of grain size variation as a climate proxy and correlation method for loess-paleosol units, north-central China. International Conference on Geology, Geotechnology and Mineral Resources of Indo-China (Geo-Indo'95), pp. 46-52.

Rutter, N.W., Ding, Z. and Liu, T. 1996. Long Records From China. Geophysica, **32**, 7-34.

Rutter, N.W., Rokosh, D., Ding, Z., Ren, J., Sun, J., and Liu, T. 1997. High resolution paleoclimate records from the Loess Plateau and desert margins, North-Central China. Palaeoecology of Africa, **25**: 321-241.

Rutter, N.W., Rokosh, D., Ding, Z. and Liu, T. 1998. High resolution paleoclimate records from the loess-desert margin: Desert Margin Changes in Africa since 135 ka: Implications for Water, Carbon & Man, IGCP 349/404, Jan 5-12, 1997, pp. 100-102.

Shackleton, N.J., An, Z., Dodonov, A.E., Gavin, J., Kukla, G.J., Ranov, V.A. and Zhuo, L.P. 1995. Accumulation rate of loess in Tadjikistan and China: relationship with global ice volume cycles. *Edited by* E. Derbyshire. *In* Quaternary Proceedings. Cambridge, John Wiley & Sons Ltd., pp. 1-6.

Sun, J. and Ding, Z. 1998. Deposits and soils of the past 130,000 years at the desert-loess transition in northern China. Quaternary Research, **50**,2, 148-156.

U.S. Defense Mapping Agency Aerospace Center, 1987. Operational Navigation Chart, Sheets F-7, F-8, G-8, G-9: U.S. Department of Defense.

von Richthofen, F. 1882. On the mode of origin of the loess. Geological Magazine, **9**, 293-305.

Zhao, S. 1986. Physical Geography of China. Science Press, Beijing, China. John Wiley & Sons, New York, U.S.A.

CHAPTER 2

Prior Research

2.1 Introduction

The purpose of this chapter is to critically review early loess research in China in order to determine the major stratigraphic and sedimentological assumptions that may have a bearing on high-resolution palaeoclimate research, and to determine the extent of knowledge regarding loess research prior to the establishment of the People's Republic of China (ca. 1949). The history of loess research in China is divided into two periods: prior to, and after 1949 (Liu et al. 1985). The first section of this chapter will deal with research prior to 1949.

Prior to 1949 loess research was largely dominated by questions concerning origin, chronostratigraphy, mineralogy and textural properties. Loess research was intimately associated archeological and mammalian biostratigraphical studies during the early 20th century in China (Barbour 1965). The relationship between loess and climate in China was detected during the late 19th and early 20th centuries (von Richthofen 1882; Chamberlin 1897b; Penck 1930) and was later associated "with a distinct set of climatic and physiographic conditions" (i.e. largely glacial conditions, Barber 1930, p. 459).

Palaeoclimate studies of Chinese loess largely began after the work of Emiliani (1955) regarding Pleistocene paleotemperatures using stable isotopes, and after the recognition by Chinese scientists of the potential of the Loess Plateau for palaeoclimate research (Liu and Chang 1964; Liu *et al.* 1985).

2.2 Early loess research in China

2.2.1 Introduction: Pre 1949

During the 19th century loess research concentrated on the critical question of loess genesis. In this case, genesis referred to the mechanism of emplacement (i.e. wind or water), as opposed to the "ultimate origin" or source (Chamberlain, 1897a) of loess (i.e. glacial or deserts). The question of loess emplacement dominated loess research until after the mid-20th century. In many respects the question of loess genesis is still unanswered (Smalley 1975b), in as much as loess is presently regarded as a geologic deposit (i.e. wind blown dust) or, a product of diagenesis and/or pedogenesis after aeolian emplacement (i.e. loessification; Berg 1932; Russell 1944, Pesci 1990; Zhang and Shao 1991; Forman 1996).

2.2.2 Loess History

Lyell's early research (1834, 1847) led him to postulate that loess was an aqueous deposit largely associated with floods. His initial views were based on the distribution of loess near the Rhine River, and the similarity between the mineralogy and fossil content of loess near the Rhine River and the Rhine fluvial sediment. Lyell (1847) later concluded that Mississippi Valley loess was similar in origin to the Rhine Basin loess. Lyell observed the massive (i.e. unstratified) nature of loess, but stated that loess must be deposited gradually (Lyell 1834). Bagnold (1941, p. 119) noted that "steady state" aeolian conditions rarely last long enough to build up homogenous layers more than a few millimeters.

The aeolian hypothesis of loess emplacement was most notably extolled by von Richthofen (1882)[1]. In his own words von Richthofen was a "solitary wanderer" throughout the Loess Plateau (and many other areas of China). Hence, von Richthofen had the opportunity to gather a regional view of loess deposition. His study led him to outline 12 criteria that must be satisfied in order to interpret a deposit as loess. Foremost among the criteria are the homogeneity of composition and structure, the absence of stratification, a dominance of angular quartz grains, the altitudinal variation of loess deposition (from ground level to more than 2500 meters above sea level in China), and the dominance of fossil land snails and terrestrial mammal bones. von Richthofen regarded the source of loess as the deserts of North China since he had first hand experience with dust storms. He believed that the climate during loess deposition was continental, with distinct wet and dry seasons.

Chamberlin (1887a) used multiple working hypotheses to outline the origin of Mississippi Valley loess, and to compare his conception of loess to the Chinese deposits (Chamberlin 1897b). In this case origin refers to the 'ultimate source' of loess, as well as the mechanism of emplacement. In terms of emplacement, Mississippi Valley loess was firstly aqueous and secondly aeolian, while Chinese loess was firstly aeolian and secondly fluvial or lacustrine. The ultimate origin of Mississippi Valley loess was considered to be glacial, while Chinese loess was residuary (i.e. from the desert) (Chamberlin 1897b).

Penck (1930) favored Chinese loess as being produced in a mountainous glacial terrain. He strongly regarded loess deposition in North China as resulting from a

[1]Russell (1944) credits Virlet-d'Aoust (1857) for suggesting an aeolian mechanism for loess emplacement.

complex interaction of glaciers, rivers and wind, in a cold and arid environment. These conditions were present during the Ice Age in North America, according to Penck, but presently occur only in Central Asia. This is a very strong correlation of loess deposition with climatic conditions. By implication, loess deposition in China occurs during both glacials and interglacials. This latter observation was corroborated by Ding *et al.* (1995) when they suggested that loess deposition occurred during both glacials and interglacials, but was more rapid during cold periods.

By the late 1940s loess deposition was associated with the action of anticyclonic winds controlled by glaciers (Hobbs 1942). Obruchev (1945) and Smalley (1975a) stated that the idea fits well with the distribution of European and North American loess ('cold loess'), but not with Chinese loess ('hot loess'). For example, the glaciation of Tibet (and consequently a southerly wind) would result in loess thinning to the north, which is the opposite of published observations (Bryan, 1945). More recently, the scarcity of last glacial moraines, and the high aridity of the Tibetan Plateau suggests that there were few glaciers to produce large volumes of loess during the last glaciation in China (Karlén et al. [Eds.] 1998).

Barbour (1930, 1933) summarized the climatic and geologic history of loess deposition in the Loess Plateau using litho- and biostratigraphic evidence from the previous 10-15 years (See Fig. 2.1). The biostratigraphic data consisted largely of mammalian and molluscan fossils. The stratigraphy was initially divided into four stages of development, each separated by periods of erosion. Barbour (1930) noted that the red clay formation of the Paote stage yielded a typical assemblage of Hipparion fauna, whereas above the red clay Hipparion fauna were rare (Andersson 1923; Teilhard and

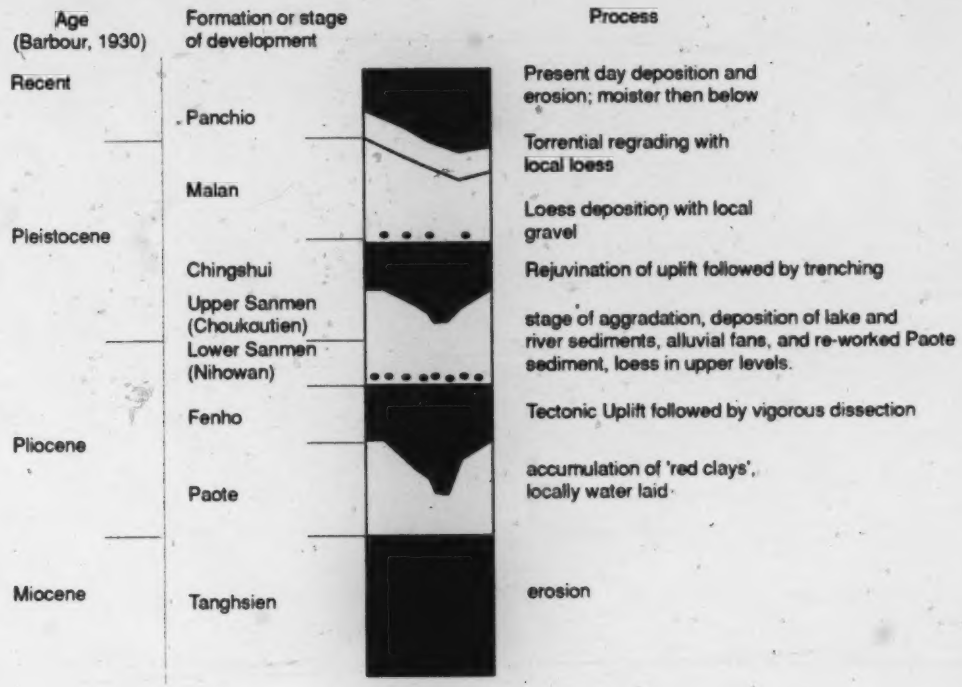

Figure 2.1 Stratigraphy of the Loess Plateau. (Modified after Barbour 1930, 1933). The figure is not to scale. The origin of the term 'Malan' is claimed by J.G. Andersson after a visit (ca. 1920) to the Ma Lan valley (northwest of Beijing) where he observed surficial gravel overlain by loess (Andersson, 1939).

Young 1930). The Sanmen formation was originally thought to be a single stage of development, but was later subdivided into the Choukoutien[2] stage (upper Sanmen) and the Nihowan[3] stage (lower Sanmen). The contact between the two Sanmen stages was initially considered to be conformable (Teilhard and Young 1930; Barbour, 1933) since no unconformities were discernable, and since comparable types of Horse, Hyena, Rhinoceros, Rodents and Molluscs suggested a similar age. However Teilhard de Chardin (1937) suggested that the Fenho period of major gorge cutting should be re-positioned between the upper and lower Sanmen based on palaeontological analysis. Further, Teilhard de Chardin (1937) suggested that a major period of uplift corresponded to the beginning of the Pleistocene. A major period of erosion, the Chingshui stage, was identified beneath the Malan stage. According to Barbour (1930), the Malan forms a veneer or blanket on the Sanmen, but fills up "the small gullies or canyons, rounding out the angularities of the subsurface". The Malan loess is unstratified, except where present in old channels. Mammalian remains in the Malan loess, according to Barbour (1930), were distinctive of an upper Pleistocene cold climate.

Barbour (1930) also suggested that climate at the time of Malan deposition was cold and extremely dry, with the winter monsoon dominating the summer monsoon. Strong winter winds blowing from the northwest, out of the Siberian-Mongolian anticyclone, were proposed as the mechanism of emplacement. Barbour (1935) argued that the regional extent of Chinese loess was due to proximity to the source (deserts), and to the trend of atmospheric pressure gradients. By implication, the source of dust was

---

[2] The Choukoutien stage appears to be named after the archeological sites northwest of Beijing where Peking man was located (from Barbour 1965).

dominantly the Mesozoic and Tertiary deposits of the northern deserts. However, Barbour (1930) also suggests that the aeolian origin of the Malan resulted in the incorporation of locally reworked material into the lower layers of the Malan. This observation may be confirmed by Sun *et al.* (1995) who identified an 'eroded zone' in the Ordos Plateau (Fig. 2.2). The Ordos Plateau is located immediately north (upwind) of the Loess Plateau. In the eroded zone Tertiary and Early Quaternary sediment occur at the surface, and may be capped by the Holocene palaeosol.

The concept of Chinese palaeosols as pedo-complexes was noted by Thorp (1936). He viewed the concept of old soils becoming the parent material of new soils as important for understanding the soils in China. A micromorphology study of the last interglacial palaeosol at Xifeng and Xian by Gou and Fedoroff (1991) confirmed Thorp's view. They suggested that the last interglacial palaeosol was a pedocomplex based on micromorphological and sedimentological evidence. Thorp (1936) noted that the loess parent material was a consistent silty-clay loam or silty clay texture with uniform mechanical properties over a large region. Loess accumulation occurred in stages, largely during cycles of dry weather, while soils developed during moist intervals. Near the desert margin, Thorp (1936) observed a rapid transition from silty loess to fine sands and sandy loams, and finally to coarse sands of the desert. Thorp (1936) concurred with von Richthofen (1882) and Barbour (1930) that the source of loess was the northern deserts, along with dry rivers beds, under a prevailing northwesterly wind. Modern dunes of the Ordos desert were observed as gradually migrating to the southeast.

---

[3] Barbour (1930) credits the Geological Survey of China (of which Teilhard de Chardin was an advisor) for suggesting that the Sanmen be subdivided into conformable stages of aggradation.

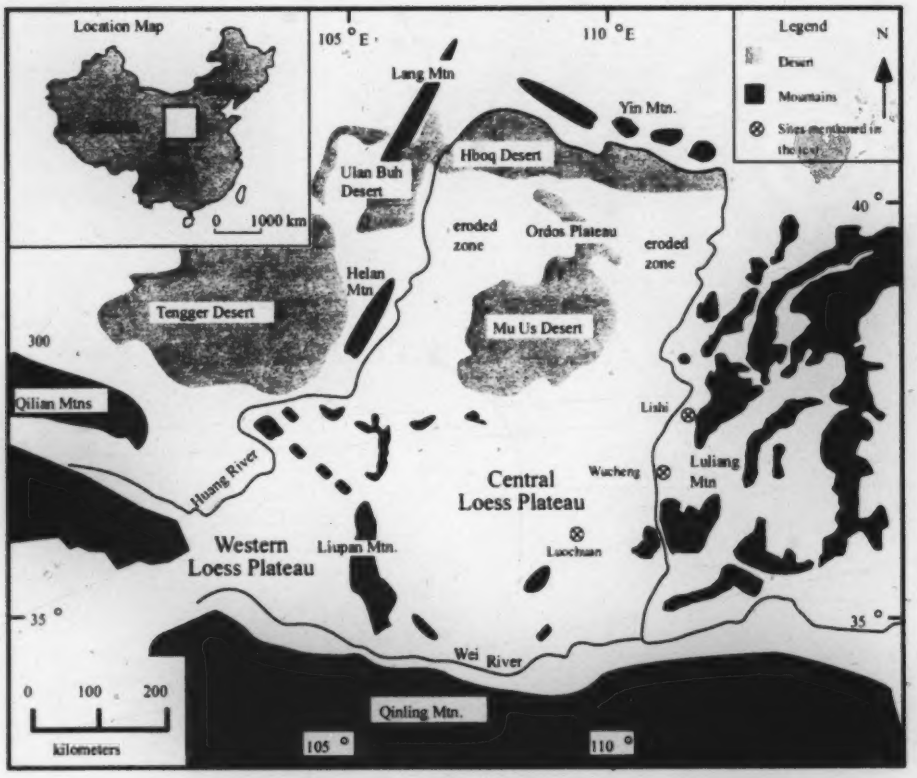

Figure 2.2 Base map of the Loess Plateau showing the location of the eroded zone and the sites mentioned in the text.

Obruchev (1951) summarized loess research in China beginning with the views of von Richthofen (1882). Obruchev was convinced that the origin of loess was polygenetic. While he agreed, in part, with von Richthofen's aeolian origin of loess deposition, Obruchev believed that loess was also deposited by diluvial (i.e. floodplain) and proluvial (i.e. slope) processes. Quite obviously, the scientific community was still debating the definition and origin of loess at this time. Aeolian loess was massive, whereas loess associated with diluvial or proluvial processes was stratified. Similar to Barbour (1930, 1933) loess stratigraphy was divided into stages: 1) red clay with Hipparion fauna; 2) the red loess of the Sanmen formation, and 3) Huangtu (literally 'yellow loess'; also known as the Malan loess). These stages were separated by major periods of erosion, possibly associated with periods of uplift. Both the Sanmen and the Malan loess were subdivided into facies, from bottom to top (Teilhard de Chardin and Licent 1927 *in* Obruchev 1951; Barbour, 1930): a) torrential or conglomerate facies; b) fluvial or fluvio-lacustrine facies, and c) non-stratified loess.

Teilhard and Licent (1927 *in* Barbour 1930) followed the soils of the Sanmen for some 20 kilometers, attesting to their regional continuity. In the middle reaches of the HuangHe, Teilhard and Licent (1927 *in* Barbour, 1930) observed that the loess facies of the Sanmen was widely developed. In these areas, the contact between the Malan and the (upper) Sanmen was so gradual that demarcation was difficult (Barbour, 1930). The climate of the Malan stage was interpreted to be colder and drier than the Sanmen and contained a variety of steppe fauna. Obruchev (1951) and Pavlinov (1959) concurred with the observations of Barbour (1930) that the conglomerate facies of the Malan was only developed in valleys or along mountain fronts, and that Malan loess "filled the

undulations of the pre-Malan surface forming a plain-like surface". Obruchev (1951) summarized Pliocene-Pleistocene climate fluctuations as periods of moist climate (favoring erosion) alternating with dry periods (favoring accumulation) that tend to become colder during the Pleistocene. The dry periods were suggested to correspond to times of glaciation in Tibet and Western Europe (von Richthofen 1882; Loczy 1893 *in* Obruchev 1951). Hence the association of loess deposition with cold and dry glacials, and palaeosol development with a warmer and wetter climate.

By the early 1950s, just prior to the work of Emiliani (1955) and the advent of palaeoclimate studies in China, loess was resolved as a massive (unstratified) sediment that was primarily deposited by winds emanating from the Siberian-Mongolian anticyclone during glacial periods. Winter monsoon winds were thought to be stronger (i.e. higher velocity) than summer monsoon winds. The deserts of China were determined to be the major source of loess because of a decrease in grain size, a decrease in the percentage of sand, and a thinning of loess beds away from the desert margin.

2.2.3 Introduction: Post 1949

The purpose of this section is to determine trends in research that have a bearing on regional loess stratigraphy and sedimentology during the last interglacial-glacial cycle. Palaeoclimate research in China after 1949, concerning the last interglacial-glacial cycle, is reviewed in chapters 3-6. Beginning at about 1965, near the onset of the cultural revolution (Simon 1978), there are few publications concerning loess stratigraphy and palaeoclimatology until ca. 1978. During 1978, the 'Four Moderizations Program' was implemented (Simon 1987; IDRC/SSTC 1997) with the intention of increasing the role

of science and technology in the economic development of China. According to Simon (1987), reforms to China's science and technology organization and management didn't begin until ca. 1982. These reforms culminated in the 1985 Central Committee 'Decision on the Reform of the Science and Technology Management System' (Simon 1987; IDRC/SSTC 1997). Publications in English by Chinese authors, therefore, become more common during the late 1970s, and are especially prevalent after the International Quaternary (INQUA) convention in Xian during 1985. Furthermore, during the 1980's foreign scientists (e.g. T. Péwé, E. Derbyshire, F. Heller, G. Kukla, I. Smalley, N. Rutter, M.E. Evans, S. Porter) began to conduct research in China in association with their Chinese colleagues. This appears to represent the first international collaborations (other than with Russian Scientists) since ca. 1949.

2.2.4 Trends in research after 1949

After 1949 loess research initially concentrated on practical applications of geology, soil science, water conservation and engineering properties (Liu et al., 1985). Two significant undertakings were to map the distribution of loess in China (Liu et al. 1985), and to map the texture and mean grain size trends of the Malan Loess (last glacial) throughout the Loess Plateau (Liu and Chang 1964). The mean grain size of loess was observed as coarse in the northwest and finer in the southeast, while loess texture was subdivided into sandy loess, silty loess and clayey loess also from the northwest to southeast. These observations and the correspondence of modern dust storm tracks with the observed grain size trends suggested that the dominant wind trend during the deposition of the Malan Loess may be from northwest to southeast (Liu et al. 1985).

Palaeoclimate studies evolved from the work of Liu (1958 *in* Derbyshire et al. 1995) and Liu and Chang (1964), after the work of Emiliani (1955). The alternation of loess and palaeosols throughout the Quaternary of the Loess Plateau was suggested to be due to "rhythmic fluctuations of wet and dry climate" (Liu and Chang 1964, p. 503). However, at Wucheng (Fig. 2.2), along the east bank of the Huanghe, erosional surfaces were observed at the base of the major formations of the Quaternary (Malan, Upper Lishi, Lower Lishi and Wucheng) (Liu and Chang 1964). In an effort to search for sites that exhibited less erosion, the exploration for sites returned to the middle reaches of the Huanghe (i.e. away from the river) (Liu et al. 1985). This was a critical turning point of loess and palaeoclimate studies in China, because research began to concentrate on locating and describing thick sections (> 100 meters) of relatively continuous loess and palaeosols (e.g. Luochuan, Liu et al. 1985). Hence, research began to concentrate on temporal evaluations of loess and palaeosol properties and establishing a Quaternary time scale. Research involving spatial evaluations of loess and palaeosol properties were lacking, and for the purpose of this dissertation, there are no regional comparisons of loess properties during the last interglacial-glacial cycle.

2.3 References

Andersson, J.G. 1923. Essays on the Cenozoic of Northern China. Memoirs of the Geological Survey of China, Serial A, **3**.

Bagnold, R.A. 1941. The Physics of Blown Sand and Desert Dunes., 1954 edition: London, Methuen & Co. Ltd..

Barbour, G.B. 1930. The Loess Problem of China. Geological Magazine, **67**, 458-475.

Barbour, G.B. 1933. Pleistocene history of the Huang Ho. Bulletin of the Geological Society of America, **44**, 1143-1160.

Barbour, G.B. 1935. Recent Observations on the loess of North China: Geographical Journal, **86**(1), 54-64.

Barbour, G.B. 1965. In the field with Teilhard de Chardin. New York, U.S.A., Herder and Herder. 160 pp.

Berg, L.S., 1932. The origin of loess. *Edited by* I.J. Smalley. *In* Loess Lithology and genesis: Benchmark Papers in Geology. Stroudsberg, Dowden, Hutchinsin & Ross, Inc., pp. 61-75.

Bryan, K. 1945. Glacial versus desert origin of loess: American Journal of Science, **243**(5), 245-248.

Chamberlin, T.C. 1897a. The method of multiple working hypotheses: Jour. Geol., **39**(2), 155-165.

Chamberlin, T.C. 1897b. Supplementary hypothesis respecting the origin of the loess of the Mississippi Valley: Journal of Geology, **5**, 795-802.

Derbyshire, E., Keen, D., Kemp, R.A., Rolph, T.A., Shaw, J., and Meng, X.M. 1995. Loess-paleosol sequences as recorders of palaeoclimatic variations during the last glacial-interglacial cycle: some problems of correlation in north-central China. Quaternary Proceedings, **4**, 7-18.

Ding, Z.L., Liu, T.S., Rutter, N.W., Z.W., Y., Guo, Z.T., and Zhu, R.X. 1995. Ice-volume forcing of East Asian winter monsoon variations in the past 800,000 years.: Quaternary Research, **44**, 149-159.

Emiliani, C. 1955. Pleistocene Temperatures. Journal of Geology, **63**, 538-578.

Forman, L.R. 1996. Loess studies in the United States: evolution of concepts. Engineering Geology, **45**, 287-304.

Guo, Z. and Fedoroff, N. 1991. Paleoclimatic and stratigraphic implications of the S1 paleosol in the loess sequence in China, *Edited by* T. Liu, Z. Ding and Z. Gou, Z. *In* Loess, Environment and Global Change: Beijing, Science Press, pp. 187-198.

Hobbs, W.H. 1942. Wind-the dominant transportation agent within extramarginal zones to continental glaciers. Journal of Geology, **50**(5), 556-559.

International Development Research Centre (IDRC) and State Science and Technology Committee (1997). A Decade of Reform. International Development Research Centre and State Science and Technology Committee. 160 pp.

Karlén, W., Lundquist, J., Rutter, N.W., Teller, J.T. and Catto, N.R. 1998. Problematic Ice Sheets, Quaternary International: , Pergamon Press, pp.145.

Liu, T.S. 1958. Preliminary investigation on the loess of Shanxi and Shaanxi Provinces in the middle reaches of the Huanghe River. Quaternaria Sinica, **1**, 255-257. (in Chinese)

Liu, T. and Chang, T., 1964. The "HuangTu" (loess) of China.: Report of the Sixth INQUA Congress, Warsaw 1961, **4**, 503-524.

Liu, T.S. et al. 1985. Loess and the Environment. Beijing, China Ocean Press.

Loczy, L. 1893. Beschreibung der geologischen Beobachtungen und deren Resultate. Die, wiss. Ergenbnisse der Reise des Gr. Bela Sechenyi in Ost-Asien 1877-1880. 307-845.

Lyell, C. 1834. Observations On The Loamy Deposit Called "Loess" of the Basin of the Rhine (Excerpts): Edinburgh New Phil. Journal, **17**, 110-113, 118-120.

Lyell, C. 1847. On the delta and alluvial deposits of the Mississippi and other points in the geology of North America, observed in the years 1845, 1846. American Journal Science, **3**(2), 34-37.

Obruchev, V.A. 1945. Loess Types and Their Origin. American Journal of Science, **243**, 256-262.

Obruchev, V.A.,1951, Loess of Northern China. *Edited by* V.V. Popov. *In* Loess of Northern China. Jerusalem, S. Monson. Translated by A. Gourevitch, Israel Program for Scientific Translations (1964).

Pavlinov, V.I. 1959. Some data about the genesis of loess in Northern China. *Edited by* V.V. Popov. *In* Loess of Northern China. Jerusalem, S. Monson. Translated by A. Gourevitch, Israel Program for Scientific Translations (1964).

Penck, A. 1930. Loess of Central Asia., *Edited by* I.J. Smalley, I.J. *In* Loess lithology and genesis: Benchmark papers in Geology. Stroudsberg, Dowden, Hutchinson & Ross, Inc., pp. 51-52.

Pesci, M. 1990. Loess is not just the accumulation of dust. *Edited by* M. Pesci and D. Loczy. *In* Loess and the Environment: Oxford, Pergamon Press, pp. 1-21.

Russell, R.J. 1944. Lower Mississippi Valley Bulletin of the Geological Society of America, **55**, 1-40.

Simon, D.F. 1987. China's Scientists and Technologists in the Post-Mao era: a retrospective and prospective glimpse. In China's Intellectuals and the State. Harvard Contemporary Series 3. Harvard University Press, Cambridge. pp. 129--158.

Smalley, I.J. (Ed) 1975a. Loess: lithology and genesis. Benchmark papers in geology. Stroudsburg, Dowden, Hutchinson & Ross, Inc., p. 429.

Smalley, I.J. 1975b. Introduction, *Edited by* I.J. Smalley. *In* Loess: lithology and genesis: Benchmark Papers in Geology. Stroudsburg, John Wiley & Sons, pp. 1-12.

Smalley, I.J. 1975c. Editor's comments on paper 10, *Edited by* I.J. Smalley, I.J. *In* Loess: lithology and genesis. Benchmark Papers in Geology. Stroudsburg, John Wiley & Sons. pp. 10.

Teilhard de Chardin, P. 1937. The Post-Villafranchian interval in North China. Bulletin of the Geological Society of China., **XVII**, 169-176.

Teilhard de Chardin, P. and Licent, F. 1927. Observations sur les formations Quaternaires et Tertiares superieures du Honan septentrional et du Chansi meridional. Bulletin of the Geological Society of China, **VI**, 129-150.

Teilhard de Chardin, P. and Young, C.C. 1930. Preliminary observations of the preloessic and post-Pontian formations in W. Shansi and N. Shensi. Memoirs of the Geological Survey of China, Series A8.

Thorp, J. 1936. Geography of the soils in China. Geological Survey of China, Nanking, National Geological of China.

U.S. Defense Mapping Agency Aerospace Center. 1987. Operational Navigation Chart, Sheets F-7, F-8, G-8, G-9. U.S. Department of Defense.

Virlet d'Aoust, P.T. 1857. Observations sur un terrain d'orgine meteorique ou de transport aerien qui existe au Mexique, et sur le phenomene des trombes de poussiere auquel il doit principalement son origine. Bulletin of the Geological Societe of France, **2d**(2), 129-139.

von Richthofen, F. 1882. On the mode of origin of the loess. Geological Magazine, **9**, 293-305.

Zhang, Z., 1991 The Quaternary of China. Zhengding, Hebei, China Ocean Press.

CHAPTER 3

Comparison of loess grain size and accumulation rates during the last interglacial and glacial periods in the central Loess Plateau, China: links to climatic forcing

(submitted to the Canadian Journal of Earth Sciences)

Authorship: Rokosh, D., Rutter, N.W., Ding, Z. and Sun, J.

3.1 Introduction

In the Loess Plateau, China (Fig 3.1) the view that loess is largely deposited during glacial periods is a longstanding interpretation (e.g., Chamberlin 1897; Barbour 1930; Bryan 1945 Ding et al., 1995; Shackleton et al., 1995). This interpretation is based on the stratigraphic record of alternating loess beds and palaeosols; where palaeosols develop during a relatively warm and wet interglacial climate, while loess deposition occurs primarily during cold and dry glacial periods. During glacial and interglacial periods, the intensity of the Asian winter and summer monsoons influence loess deposition and palaeosol development, respectively (Liu et al. 1985; An et al. 1991a,b; Ding et al. 1995). Enhanced soil development was favored by a warmer and wetter interglacial climate, dominated by the East Asian summer monsoon, while during glacial periods the northwesterly winter monsoon shifted dust from the inland deserts of northern China to the Loess Plateau (Liu et al. 1985). Dust deposition continued during both interglacial and glacial periods, however interglacial loess deposition occurred at a reduced rate and was characterized by smaller grain sizes relative to glacial deposition (Ding et al., 1995; Shackleton et al., 1995). The basic model of loess deposition would therefore show a lateral decrease in loess grain size (Liu and Chang, 1964) and thickness during both interglacial and glacial periods (Liu et al., 1985). However, during glacial

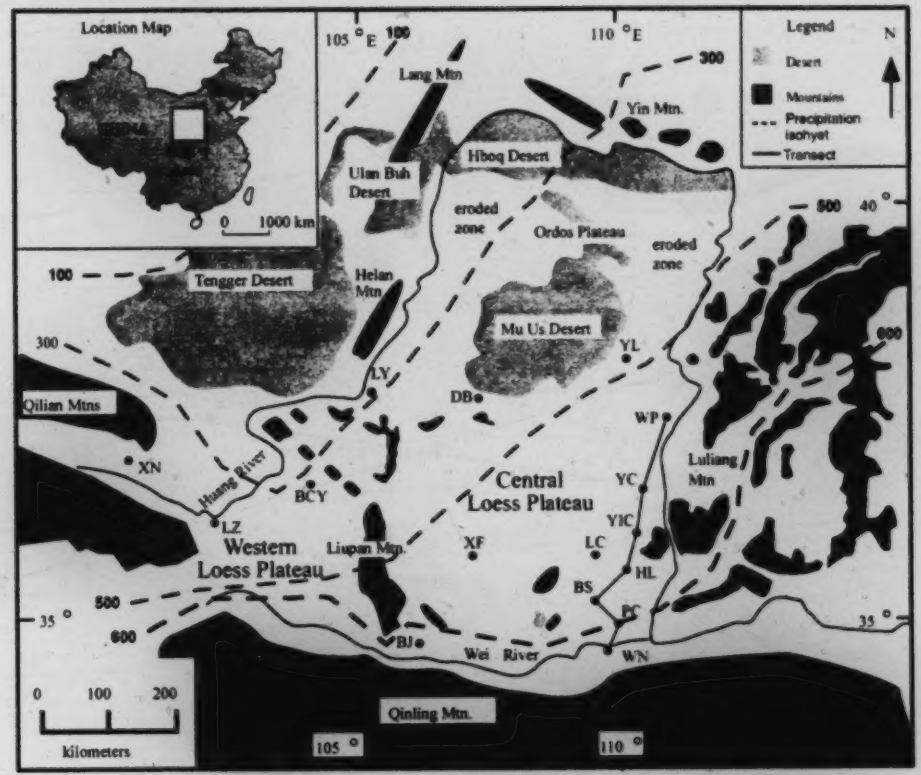

Central Loess Plateau				Western Loess Plateau	
BJ	Baoji	BS	Baishui	BCY	Baicouyuan
DB	Ding Bien	HL	Huanglong	LZJ	Lanzhou (JZT)
LC	Luochuan	LY	Lija Yuan	LZG	Lanzhuo (GLS)
PC	Pucheng	WN	Weinan	XN	Xining
WP	Wupu	XF	Xifeng		
YC	Yanchang	YIC	Yichuan		
YL	Yulin				

Figure 3.1. Map of the Loess Plateau showing the location of the sites along the north-south transect, and other locations mentioned in the text. The isohyets (mean annual precipitation) are from Zhao (1986).(Modified from US Defense Mapping Agency Aerospace Center, Operational Navigation Chart Series ONC, Sheets F-7, F-8, G-8 and G-9, Edition 4, 1987).

periods loess beds would be thicker and contain larger grains than during interglacial periods (Ding et al., 1995; Shackleton et al., 1995).

This model of interglacial to glacial variations in loess properties has been correlated to marine $\delta^{18}O$ ice volume records in order to determine the palaeoclimate processes that force a change in loess grain size (e.g., Ding et al. 1995) and accumulation rates (e.g., Shackleton et al. 1995). For example, Ding et al. (1995) suggest that glacial to interglacial changes in global ice volume control variations in loess grain size at Baoji and Weinan (Fig. 3.1), by changing the strength of the winter monsoon. In their model, downstream cooling of the Siberian Anticyclone during a glaciation led to stronger winter monsoon winds and the deposition of larger grains, while weaker winter monsoon winds during interglacial periods resulted in the deposition of smaller grains. This interpretation suggested that the strength of the winter and summer monsoons were proportionately opposite during glacial and interglacial periods. Strong winter monsoons and weak summer monsoons occurred during glacial periods, while strong summer monsoons and weak winter monsoons occurred during interglacial periods. Chen et al. (1998) suggest that the intensity of the winter and summer monsoons during the last interglacial period were not proportionately opposite, based on their analysis of variations in frequency-dependent magnetic susceptibility and loess texture. They suggest that summer monsoon intensity was driven by changes in Northern Hemisphere insolation, while winter monsoon intensity is linked to global ice volume variations.

Shackleton et al. (1995) interpret global ice volume variations as largely controlling glacial to interglacial variation in loess accumulation rates. Their cross-spectral analysis revealed that loess accumulation rates over the past 2.6 Ma at Xifeng

(China) and Karamaidan (Tadjikistan) are more coherent with a $\delta^{18}O$ ice volume record than with orbital insolation or an orbitally-modeled ice volume record (e.g., SPECMAP, Imbrie et al. 1984). This indicated that glacial to interglacial variability in dust accumulation rates are related more to the growth and decay of terrestrial ice sheets than to changes in insolation forcing. Guo et al. (1998) suggest that a more complex combination of oceanic and atmospheric processes are needed to explain changes in loess and palaeosol properties at Xifeng, Changwu and Weinan (Fig. 3.1). They suggest that a climate extreme indicated by sandy loess or strongly developed palaeosols, between about 0.4-1.2 Ma, are not fully explained by global ice volume variations or orbitally induced insolation changes. Other factors such as variations in atmospheric CO_2 (caused by changes in land biomass or strength of North Atlantic Deep-Water production) are needed to explain the climatic extremes.

In each of the above cases there are two common themes: 1) global ice volume variations play an undetermined role in forcing a change in loess deposition during an interglacial-glacial cycle within the Loess Plateau, and 2) palaeoclimate interpretations are commonly based on variations in loess properties from one or a few sites (i.e., temporal variations), and are assumed to be representative of regional variations (i.e., spatial). However, the assumption that temporal variations in loess deposition are representative of spatial variations has led to an oversimplification of the regional geology of the Loess Plateau. In turn, this has resulted in simplified or erroneous interpretations of climate change or climate forcing. Here, regional variations in loess properties are examined at a different temporal and spatial scale than has previously been done. We compare regional stratigraphy of the last glacial period (L1) to the last

interglacial period (S1), with attention to the variation in loess properties from the sediment source to the accumulation zone. By taking a spatial and temporal approach to studying loess depositional systems, we hope to clarify the climatic controls on loess deposition. Assuming that loess is wind-blown dust (Smalley 1975), this study will establish that global ice volume variations indirectly affect loess deposition by influencing desert expansion and contraction (e.g., the loess source), which results in a re-distribution of loess, rather than directly controlling loess grain size or accumulation rate variations. A model for loess deposition during the last interglacial-glacial cycle is proposed and used to address the connection between loess grain size, wind strength and global ice volume variations. Variations in grain size along a north to south transect are observed, and used to construct a depositional model that demonstrates regional loess grain size variations during the last interglacial-glacial cycle. This is followed by an interpretation of changes in glacial and interglacial accumulation rates and, finally, a discussion of the climatic controls on loess deposition in the Loess Plateau, especially the role of global ice volume variations.

3.2 Geography

The Loess Plateau covers an area of approximately 440,000 km^2 between about 35°N to 40°N latitude and 100°E to 115°E longitude (Fig. 3.1; Liu et al. 1985). The distribution of loess in North China forms an arcuate belt, open to the north-northwest, that stretches from the northwestern, arid inland basins to the eastern plains (Liu et al. 1985; see his fig. 2.1). The Loess Plateau is subdivided into western, central and eastern regions. The central region is bordered by the Huang Ho (Yellow River) to the east, the

Liupan Mountains to the west and the Ordos Plateau to the north. The Qinling Mountains and the Tibetan (Qinghai-Xizang) Plateau border the Loess Plateau to the south. These uplands, along with the NW-SE trending Qilian Mountains, the north-south trending Helan, Liupan, Luliang and Yin Mountains, form barriers against the transport of dust and moisture (Niu 1985, Liu et al. 1985). North of the Loess Plateau, and bordered by the Huang Ho, is the Ordos Plateau consisting of the Mu Us and Hobq (a.k.a. KupuQi) deserts, and an 'eroded zone' (Sun et al. 1995). The Mu Us and Hobq deserts were arid during the last glaciation (Sun et al. 1995) but are presently not in equilibrium with a desert environment in north China (Zhao 1986). At present, the Mu Us and Hobq deserts occur within a temperate, semi-arid steppe environment (Zhao 1986) with a Precipitation/Evaporation (P/E) index of about 1.2-2.0. Modern deserts occur west of the 100 mm precipitation isohyet (Fig. 3.1) where the P/E index is less than 1.0 (Zhao 1986). In the eroded zone, highly weathered, rubified Tertiary terrestrial sediments occur at or near the surface, and are overlain by Early Quaternary sediment, or a veneer of Holocene sediment.

Much of the Ordos and central Loess Plateau lie at an elevation of about 1200-1800 meters above sea level (a.s.l.; Fig. 3.2). The elevation of the southern most portion of the Plateau is influenced by a graben (e.g. WeiHe graben; Zhao 1986) that borders the north flank of the Qinling Mountains. Here the elevation drops to less than 600 m a.s.l. The western Loess Plateau (west of the Liupan Mountains) lies between about 1800-2400 m a.s.l.

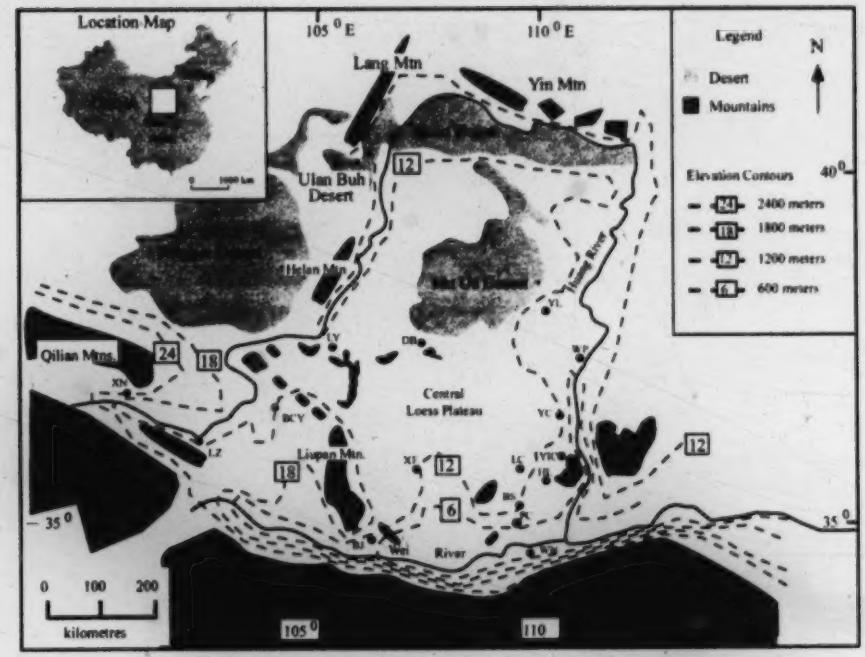

Figure 3.2. Topography of the Loess Plateau and surrounding area. (Modified from US Defense Mapping Agency Aerospace Center, Operational Navigation Chart Series ONC, Sheets F-7, F-8, G-8 and G-9, Edition 4, 1987). See Fig. 3.1 for a summary of the location abbreviations

3.3 Methods

For each section loess beds were sampled every 5-10 cm, while palaeosols were sampled vertically every 2-5 cm. Bulk magnetic susceptibility and grain size were determined on each sample. Grain size analysis was performed on a PRO-700 SK Laser Micron Sizer. An analysis of 20 replicate samples indicated a precision of ±3.5%. Bulk magnetic susceptibility was determined using a Bartington MS-2 susceptibility meter. Magnetic susceptibility values represent one reading on an approximately 50 gram bagged sample. All susceptibility values are calibrated to $CaCO_3$ using the formula:

$$MS = MS \times (100/100 - C)$$

Where MS is Magnetic Susceptibility, and C is the weight percent calcium carbonate (Soil Conservation Service 1972). The magnetic susceptibility values are calibrated to the calcium carbonate content because: 1) the $CaCO_3$ content is generally higher in loess than palaeosols (Liu et al. 1985) due to carbonate dissolution in palaeosols and re-deposition of secondary carbonate in loess, and 2) calcium carbonate has a negative susceptibility (Thompson and Oldfield 1986).

Two age models for the late Pleistocene were considered for calculating accumulation rates: Martinson et al. (1987) and Liu, J. et al. (1995). The age models were generated using independent methods. The Martinson et al. (1987) timescale is a short (~300 ky), high-resolution version of the SPECMAP chronology of Imbrie et al. (1984); while the Liu, J. et al. (1995) chronology spans the last 130 ky and is based on Accelerated Mass Spectrometer (AMS) radiocarbon and Thermoluminescence (TL) measurements on loess and palaeosols from Weinan, at the southern end the transect. The basis of the Martinson et al. (1987), and SPECMAP age models are the theory of

Milankovitch (1930) that the orbital variations of the Earth influence variations in insolation that force or pace (Imbrie et al. 1984) variations in the size of terrestrial ice sheets (Hays et al. 1976; Berger 1978; Imbrie et al. 1984, 1992, 1993). The Martinson et al. (1987) chronology was developed using stacked marine oxygen isotope records and four different tuning approaches. Their chronology represents an average of the four approaches and has an error ranging from about 1 ka to 7 ka. The duration of the last glacial period (Marine Isotope Stages (MIS) 2, 3 and 4) and the last interglacial period (MIS 5) from Martinson et al. (1987) are 61.8 ka and 55.9 ka, respectively and from Liu, J. et al. (1995) are 61.9 ka and 54.9 ka, respectively. The similar duration of the last glacial and interglacial periods in the models indicates that our results are not dependent upon using a particular age model. In this paper, we use the Martinson et al. (1987) chronology to compare regional interglacial and glacial loess accumulation rates.

The nomenclature system of Liu et al. (1985) is used throughout this paper. Loess horizons are designated 'L', while palaeosols are designated 'S'. The youngest palaeosol along the transect, the Holocene soil, is designated S0, while older interglacial soils are given a progressively higher number (e.g. S1, S2, etc.). The last glacial loess bed is labeled L1, with each older glacial loess beds successively labeled L2, L3, etc.

3.4 Stratigraphy along the transect

3.4.1 Methodology

Seven sites along the eastern margin of the central Loess Plateau were used to construct a stratigraphic cross-section (Figs. 3.1 and 3.3). The cross-section datum is the last interglacial-glacial contact (S1/L1). The S1/L1 contact may have been a relatively

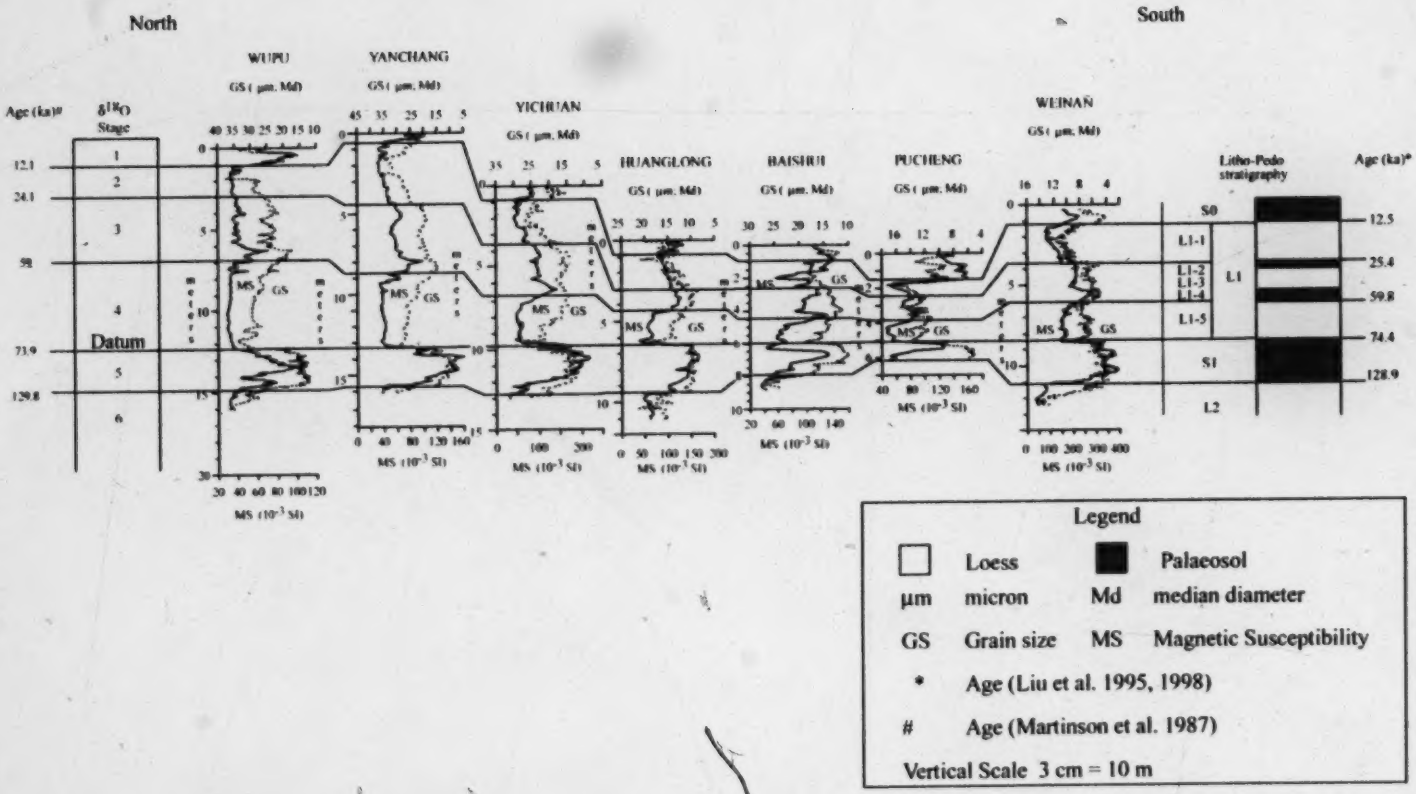

Figure 3.3. Stratigraphic cross-section from the central Loess Plateau showing the continuity of the strata along the north to south transect. All locations use the same vertical scale (1 cm = 3 meters). See Table 3.1 for the approximate distance between locations. All magnetic susceptibility values are carbonate-free.

time-equivalent surface (Sun and Ding, 1998), as is usually required for stratigraphic datums but was not necessarily a horizontal surface. At present, the change in elevation along the transect is up to 600 meters (Fig.3. 2). In this respect, there do not appear to be any surfaces within the last interglacial-glacial cycle that strictly qualify as stratigraphic datums. We use the S1/L1 contact because it is easily identified in the field, and on the grain size and magnetic susceptibility curves as relatively abrupt inflections in the records.

Inflections of the magnetic susceptibility and grain size curves are used, as indicated on Fig. 3.3, to determine glacial and interglacial boundaries. These criteria have been used, in conjunction or separately, in the construction of Quaternary age models (Kukla et al. 1990; Wang et al. 1991; Ding et al. 1994, Liu, J. et al. 1995) and in many other studies comparing loess palaeosol stratigraphy to glacial-interglacial cycles (e.g., Kukla 1987 a, b; Imbrie et al. 1992, 1993; Bloemendal et al. 1995; Ding et al. 1995; Shackleton et al. 1995; Evans et a. 1996; Vandenberghe et al. 1997). At most sites the criteria work quite well. However, palaeosols in the Loess Plateau exhibit some combination of accretion (An et al. 1991b), due to contemporaneous dust input, and overprinting of glacial parent material (e.g., the S0/L1 contact at Bashui on Fig. 3.3). Where a significant amount of overprinting has occurred, the initial inflection of the grain size curve is used to resolve interglacial and glacial contacts (Ding et al. 1995; Vandenberghe et al. 1997). In this manner most of the sediment of the glacial to interglacial transition (~0.5-1.0 m) would be included as interglacial sediment; however, this makes little difference in the regional glacial and interglacial trends.

3.4.2 Temporal and spatial observations of grain size variations along the transect

Within the last glacial unit (L1), each of the temporal grain size profiles along the transect (Fig. 3.3) fine upward from the interglacial-glacial contact (S1/L1) to the top of palaeosol L1-4, and then generally coarsen upwards to near the top of the last glacial period (L1). At the top and base of the last glacial period, the coarsest grains are within a few microns [median diameter(Md)]. The peak grain size of the last glacial period is generally 2-3 times larger than the grain size of the last interglacial (S1) at each of the sites.

The spatial grain size variations in the last glacial unit (L1) generally show a decrease from north to south. From north to south, the peak grain size of L1-1 and L1-5 decrease from about 38 μm median diameter (Md) and 35 μm Md at Wupu, respectively to about 10-12 μm Md and 7-9 μm Md at Weinan, respectively. However, the regional decrease in grain size is not entirely consistent. For example, the grain size within L1-3 (Fig. 3.3) decreases southward to Huanglong, where the grain size is relatively invariant throughout the interval (~10 μm Md). However, the regional decrease in grain size within L1-3 then reverses, and increases from Huanglong toward Pucheng; where three relatively strong peaks are evident. From Pucheng southward to Weinan the grain size again decreases from about 12-14 μm Md to 5-8 μm Md, respectively at the southern end of the transect.

Near the north end of the transect, Sun et al. (1995) and Sun and Ding (1998) published an Md grain size curve (Fig. 3.4) from a site near Yulin in the desert-loess transition zone of the last glaciation (Fig. 3.1; about 120 km northwest of Wupu). The

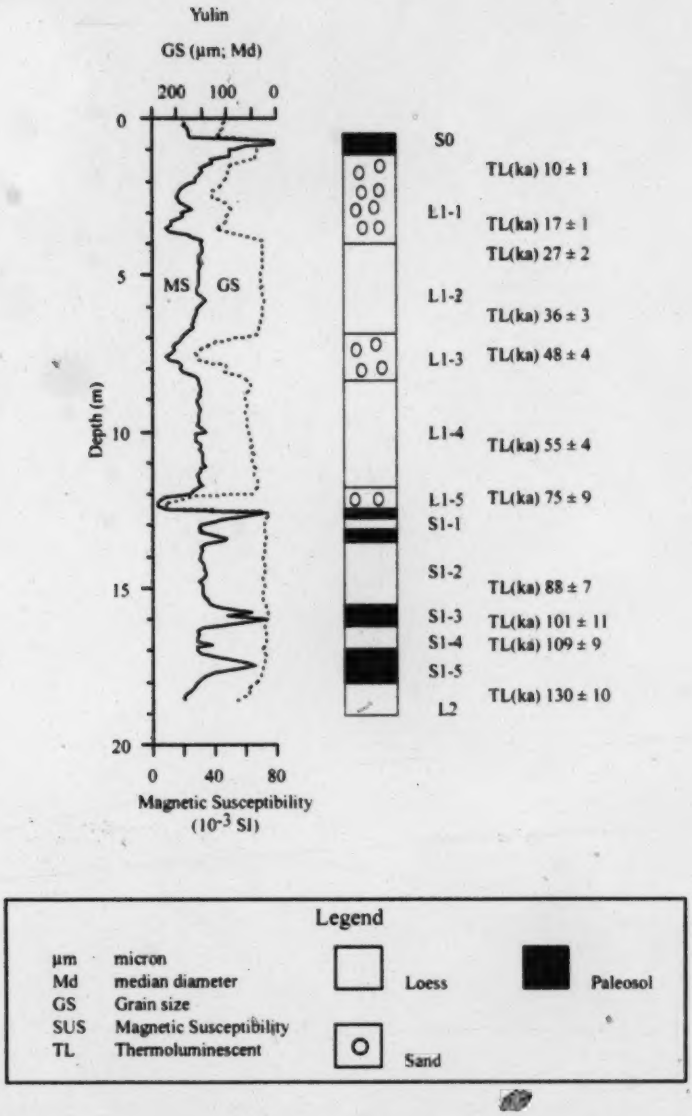

Figure 3.4 The Yulin site near the north end of the transect in the desert-loess transition zone of the last glacil period. (Sun et al. 1995; Sun and Ding, 1998

last glacial unit (L1) consists of three desert sand beds alternating with two loess beds (Sun et al. 1995; Sun and Ding, 1998; Ding et al. 1999). The last interglacial unit (S1) at Yulin consists of three or four soils, alternating with loess beds. Similar loess-palaeosol alternations are seen at Lijia Yuan and Ding Bien (Rutter et al. 1998) indicating regional continuity of last interglacial unit at these three sites (Fig. 3.1).

Along the transect, the median diameter grain size of last interglacial unit (Fig. 3.3) varies, north to south, from about 15-17 μm Md at Wupu to about 4-6 μm Md at Weinan. An analysis of the grain size data set from Yulin indicates that the interglacial loess beds have a relatively invariant grain size of about 20-28 μm Md (lower bed) and 20-26 μm Md (upper bed).

3.4.2.1 Interpretation

At the scale of an interglacial-glacial cycle, the first order interglacial-glacial character of the grain size and magnetic susceptibility curves are quite consistent, suggesting good spatial continuity of the strata. Within the last glacial unit (L1), the general northward increase in grain size reflects proximity to the sediment source (Liu and Chang 1964, Sun et al. 1995; Ding et al. 1999). However, the apparent southward increase in grain size from Huanglong to Pucheng and then decrease to Weinan in L1-3 (a stadial) is difficult to explain. At Huanglong, palaeosols L1-2 and 1-4 (Fig. 3.3) were difficult to identify, so deflation or re-deposition may have occurred. Alternatively, loess deposition may be influenced by local wind variations, or perhaps multiple sources of loess (Zhang et al. 1996; Merrill et al. 1989; Fang et al. 1998). Additional source areas,

in this case, may be east or west of these locations, since the grain size in L1-3 at Weinan is the smallest along the transect.

Along the transect, grain size within the last interglacial unit increases northward from 4-6 μm Md at Weinan to about 20-28 μm Md in the loess beds at Yulin. The increase in interglacial grain size reflects proximity to the source, similar to the last glacial unit. However, north of Yulin no sites containing last interglacial sediment have been located, due to erosion (see Fig. 3.1, "eroded zone") or burial by the last glacial desert expansion, so last interglacial sediment cannot be traced to the source. Thus, a critical assumption is that loess grain size within the last interglacial unit (S1) will continue to increase toward the source; where interglacial loess grains are presumably coarser than the 28 μm Md peak grain size found at Yulin.

A spatial comparison of grain size in the last interglacial and glacial depositional systems is shown in Fig. 3.5. The figure is based, in part, on Pye's (1995) models' of variations in loess deposition along a theoretical transect from a desert source to a loess accumulation zone. In Fig. 3.5 the northern deserts of China are the main source of glacial and interglacial loess (Bryan 1945; Liu et al. 1985). The size of the loess grains and the spatial variation are representative of the sizes observed along the transect. For example, a circle was chosen to represent a 37-38 μm Md grain in the last glacial loess at Wupu. From Wupu to Yichuan the peak diameter in the L1 loess decreases to 27-28 μm Md; thus the grain at Yichuan is about 74% (28 μm Md /38 μm Md) the size of the Wupu grain. Both the last interglacial and glacial depositional systems exhibit a grain size increase toward the sediment source. This spatial change in grain size is reflected, in

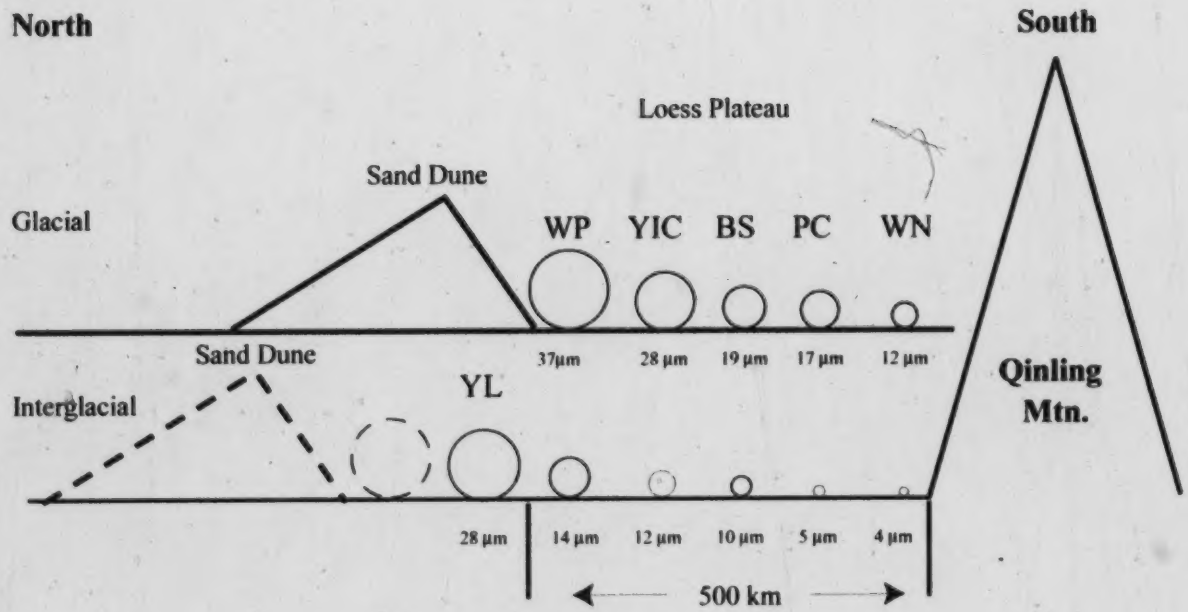

Figure 3.5. Schematic model of variations in grain size. The size of the grains represent actual variations along the transect relative to the peak median diameter at Wupu during the last glacial and interglacial periods. The dashed interglacial grain represents the assumption of grain size increasing northward (upwind) of Yulin toward the source. See Fig. 3.1 for a summary of the location abbreviations.

part, as a function of proximity to the source (Liu and Chang 1964; Pye 1987; Tsoar and Pye 1987; Pye 1995; Ding et al. 1999). This suggests that the original model of larger grains during glacial periods, used to interpret palaeoclimate forcing mechanisms, does not explain the spatial variations. The critical difference between the glacial and interglacial depositional systems is in the spatial distribution of the grains. The distribution of the grains is controlled, in part, by desert expansion and contraction. Desert expansion and contraction in China occurs during interglacial and glacial periods (Sun et al. 1995), respectively, concomitant with variations in global ice volume.

3.4.3 Observations of trends in thickness

Maps of variations in loess thickness (Figs. 3.6 and 3.7; Table 3.1) are constructed for the last interglacial (S1) and glacial periods (L1) in the central Loess Plateau. A few of the more studied sites in the western Loess Plateau are plotted for comparison. In the central Loess Plateau, loess deposited during the last interglacial and glacial periods generally thin southward, and thicken against the flank of the Qinling Mountains (see also Fig. 3.3). However, there does not seem to be any correspondence between present day topography along the transect and regional trends in thickness. For example, Yichuan and Huanglong are at a similar elevation, however Huanglong is 3.1 meters thinner than Yichuan. Additionally, Wupu is northward and at a lower elevation than Yanchang, however the two sites have a similar thickness. The thickest deposits of the last glacial unit (L1) of the central Loess Plateau occur in the northwest at Ding Bien and Lijia Yuan. Southeastward of these sites, there is a noticeable thinning of the last

Figure 3.6. Thickness of the last glacial unit (L1; MIS 2-4). The publications used to estimate the thickness of L1 are listed in Table 3.1. See Fig. 3.1 for a summary of the location abbreviations.

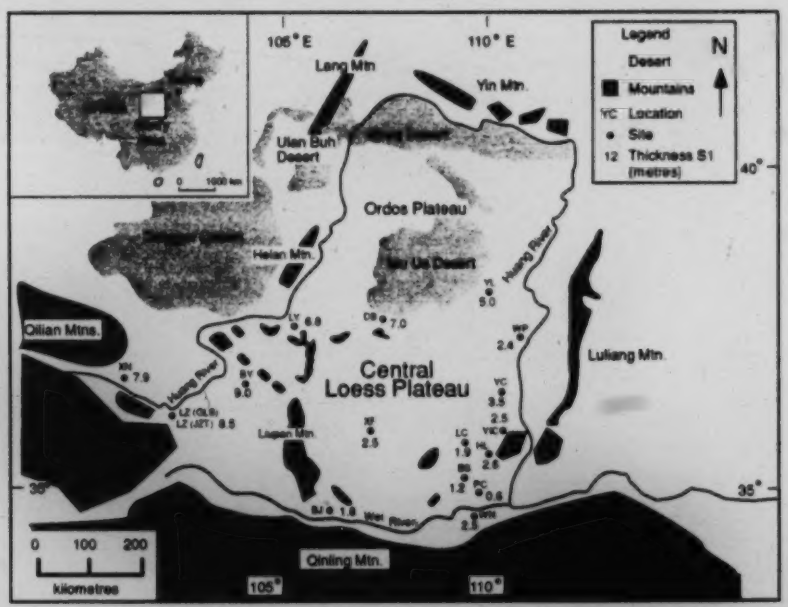

Figure 3.7. Thickness of the last interglacial unit (S1; MIS 5). The publications used to estimate the thickness of S1 are listed in Table 3.1. See Fig 3.1 for a summary of the location abbreviations.

Location	Distance from Yulin	Thickness L1 (m)	Acc. Rate L1 (cm/ky) MIS 2-4	Thickness S1 (m) MIS 5	Acc. Rate S1 (cm/ky) MIS 5
CLP					
Yulin*1	0.0	11.3	18.3	5.0	8.9
Wupu*2	125.0	12.3	19.9	2.4	4.3
Yanchang*2	200.0	12.7	20.6	3.5	6.3
Yichuan*2	295.0	8.9	14.4	2.8	5.0
Luochuan*3	395.0	8.6	13.9	1.9	3.4
Huanglong*2	435.0	5.8	9.4	2.6	4.7
Baishui*2	485.0	5.3	8.6	1.2	2.1
Pucheng*2	510.0	3.7	6.0	0.6	1.1
Weinan*2	560.0	7.2	11.7	2.5	4.5
Baoji*4		5.5	8.9	1.8	3.2
Lija Yuan*5		15.7	25.4	6.8	12.2
Ding Bien*5		29.5	47.7	7.0	12.5
Xifeng*6		10.5	17.0	2.5	4.5
WLP					
Bicaoyuan*7		17.3	28.0	9.3	16.6
Lanzhou (JZT)*8		21.6	35.0	8.5	15.2
Lanzhou (GLS)*9		28.9	46.8	X	X
Xining*10		17.0	27.5	7.9	14.1

Table 3.1. Minimum accumulation rates calculated using the Martinson et al. (1987) age model. CLP = Central Loess Plateau, WLP = Western Loess Plateau. References used at each sites are: 1) Sun et al. 1995; 2) this study 3) Liu et al. 1991; Rousseau and Wu 1997 4) Rutter et al. 1991; 5) Rutter et al. 1998; 6) Liu et al. 1985; Liu, X.M. et al. 1995; 7) Evans and Heller 1994; Hunt et al. 1995; 8) Derbyshire et al. 1995; Fang et al. 1998, JZT = Jiuzhoutai 4 km north of Lanzhou; 9) Derbyshire et al. 1997; GLS = Goulanshan, 10 km SSE of Lanzhou and, 10) Hunt et al. 1995.

glacial unit (L1) along the transect, from Yanchang to Pucheng. From Yanchang to Pucheng the palaeosols and loess beds within L1 (L1-1 to L1- 5; see Fig. 3.3) are preserved (excluding Huanglong), suggesting that the variation in thickness is probably a depositional trait (e.g., bed architecture or variations in wind strength) rather than due to erosion.

The trends in thickness of the last interglacial unit (S1) are similar to the last glacial unit, where interglacial beds thin to the south or southeast. The thickest interglacial and glacial deposits occur at the same sites, although there is less variation in the thickness of interglacial beds at these sites than exhibited by the glacial beds. For example, in the western Loess Plateau at Lanzhou and Bicaoyuan, the last glacial unit has a thickness of 28.9 meters and 15.7 meters, respectively while the interglacial unit is 8.5 meters and 9.0 meters thick, respectively. In the central Loess Plateau at Ding Bien and Lijia Yuan the last glacial unit has a thickness of 29.5 meters and 15.7 meters, respectively while the interglacial unit is 7.0 meters and 6.8 meters thick, respectively.

3.4.3.1 Interpretation of trends in thickness

The interpretation of the maps (Figs. 3.6 and 3.7) will center on two main points: 1) the relationship between loess distribution and passageways for wind between the mountians; and 2) a comparison of loess thickness in the western and central plateaus, especially during the last interglacial period.

In the central Loess Plateau, the Ding Bien (DB) and Lijia Yuan (LY) sites are upwind of an east-west trending upland (Figs. 3.1 and 3.2) that may enhance the thickness of these deposits by blocking the southeastward penetration of dust-bearing

winds. Niu (1985) described three main wind passages, between mountain ranges, into the Yellow River Basin based on landsat imagery of sand dune movement. The trends of the dunes indicated passages between the Lang and Helan Mtns., between the Helan and Qilian Mtns., and south of the Qilian Mtns (Figs. 3.6 and 3.7). These trends suggest a tectonic control of low level wind movement, and dust deposition. A tectonic control of low level wind movement is in general agreement with the interglacial and glacial thickness maps (Figs. 3.6 and 3.7). However, the thickness of the glacial units near the entrance passages (e.g., western Loess Plateau) varies considerably over a relatively short distance suggesting a complex, multi-directional aeolian depositional regime in the Loess Plateau.

The thickest deposits in the central (DB) and western plateaus (LZG) have similar values during the last glacial period (Fig. 3.6). However, during the last interglacial period the deposits in the western Loess Plateau are thicker than all of the sites in the central Loess Plateau. At present, a geologic or climatic reason for this observation is not clear. However, the planetary Westerlies may exert a greater influence on dust deposition in the western Loess Plateau than in the central Loess Plateau. For example, Murakami (1987) observed that during winter the planetary westerlies split into two components (below about 200 millibars), and flow northward and southward around the Tibetan Plateau. The 700 millibar winds to the north flow along the 2-km elevation contour (Murakami 1987). This height matches the present elevation of the western Loess Plateau (about 1800-2400 m a.s.l.; Fig. 3.2), while the central Loess Plateau is some 600-1800 meters lower. Perhaps the planetary Westerlies deposit more dust in the western Loess Plateau than in the central Loess Plateau, especially during interglacials.

However, there are a considerable number of other climatic and non-climatic factors that influence the thickness of a deposit, and whose influence may differ in the central and western plateaus. These factors include changes in accommodation space (due to subsidence or uplift), proximity to the sediment source, changes in wind direction and carrying capacity, multiple sources of loess, topographic variations, types of vegetation, aridity of the sediment source and accumulation zone, and erosion. In addition, the differences in thickness of the western and central Loess Plateau could reflect the scarcity of measurements.

3.4.3.2 Interpretation of variations in accumulation rates

Loess accumulation rates should be regarded as minimum rates because of the difficulty in quantifying the extent of deflation within a loess bed. However, as stated earlier, the grain size variations (Fig. 3.3) show good lateral continuity along the transect over the last ca. 130,000 years. Deflation, or re-deposition, may have occurred within the last interglacial and glacial units, but no unconformities were observed in the field, nor are any unconformities detectable in the transect data. However, soil 'A' horizons that mark the last interglacial-glacial contact (S1/L1) have been eroded according to Bronger and Heinkele (1989) and Guo et al. (1991). Last interglacial sediment, and possible early last glacial material, may be eroded during the transition from a relatively wet interglacial climate to a dry glacial climate.

A temporal comparison of accumulation rates between the last interglacial and glacial periods at each site, shows that the accumulation rate during the last glacial period (L1) is consistently about 2 to 3 times higher than the accumulation rate during

the last interglacial period (S1) (Fig. 3.8). It is this type of comparison that leads to the interpretation that loess accumulates more rapidly during a glacial period than an interglacial period (Liu et al. 1985, Pye and Zhou 1989, Dodonov 1991, Shackleton et al 1995). However, this 'temporal' comparison is intuitively incorrect as far as reflecting regional loess deposition or climate is concerned, because the comparison is between a rate in a thick glacial bed, proximal to the source, against a rate in a thin (i.e., condensed) interglacial bed distal from the source. A more equitable comparison would be to contrast rates along the entire depositional regimes, or at least to compare rates from similar environments within the regime (e.g., proximal, medial or distal).

Figure 3.9 is a schematic of the variations in thickness along the transect during the last interglacial-glacial cycle. The figure is a scaled representation of Fig. 3.3. During the last glacial period, desert expansion has resulted in a southward progression of the proximal, medial and distal loess environments. However, the distal environment (e.g. a condensed section of loess) of the last glacial period is not present at the south end of the Loess Plateau. In contrast, the distal environment of the last interglacial period is present throughout the Loess Plateau. Furthermore, at the north end of the Loess Plateau (e.g. Yulin) the last interglacial unit thickens from about 2-3 meters of loess, overprinted by palaeosols, to about 5-7 meters of alternating loess and palaeosols as indicated at Yulin (Fig. 3.9), Lijia Yuan and Ding Bien (Fig. 3.7; Rutter et al. 1998). Northward of these locations loess or desert sand of the last interglacial period has never been found, although sediment of this age may be preserved in a depression underlying the Mu Us desert (Dong et al. 1989).

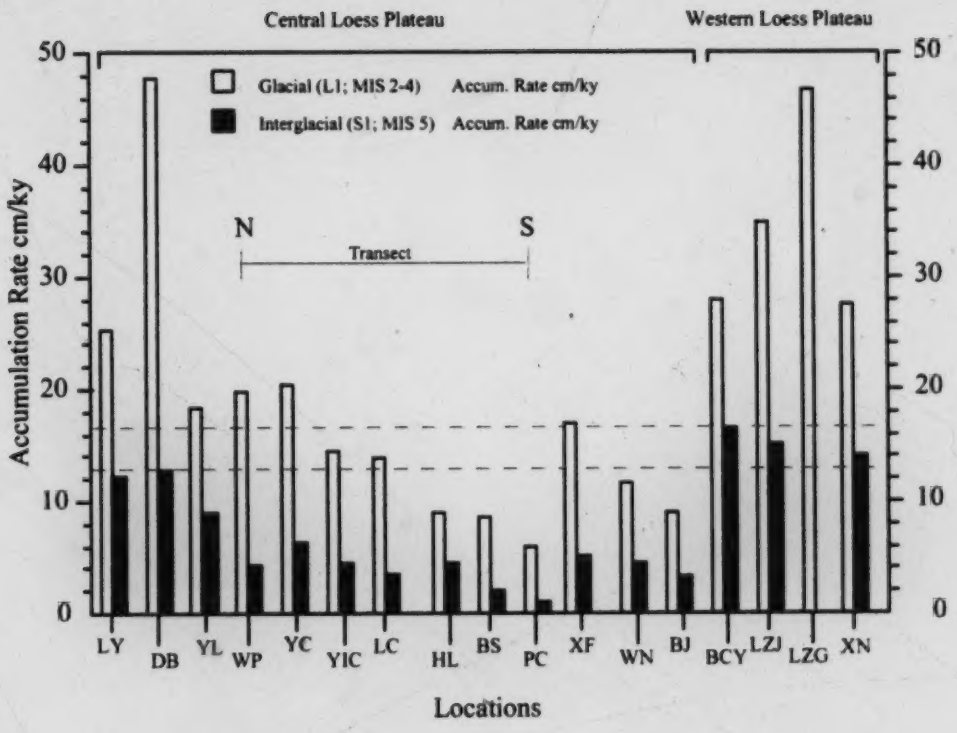

Central Loess Plateau			
BJ	Baoji	BS	Baishui
DB	Ding Bien	HL	Huanglong
LC	Luochuan	LY	Lija Yuan
PC	Pucheng	WN	Weinan
WP	Wupu	XF	Xifeng
YC	Yanchang	YIC	Yichuan
YL	Yulin		

Western Loess Plateau	
BCY	Baicaoyuan
LZJ	Lanzhou (JZT)
LZG	Lanzhuo (GLS)
XN	Xining

Figure 3.8. Spatial and temporal comparison of accumulation rates in the Central and Western Loess Plateau during last glacial and interglacial periods. The dashed lines have been set at the sites with the maximum interglacial accumulation rates in the Western (BCY) and Central Loess Plateau (DB), respectively. See Table 3.1 for a list of the publications used to estimate bed thickness and Fig. 3.1 for the site distribution.

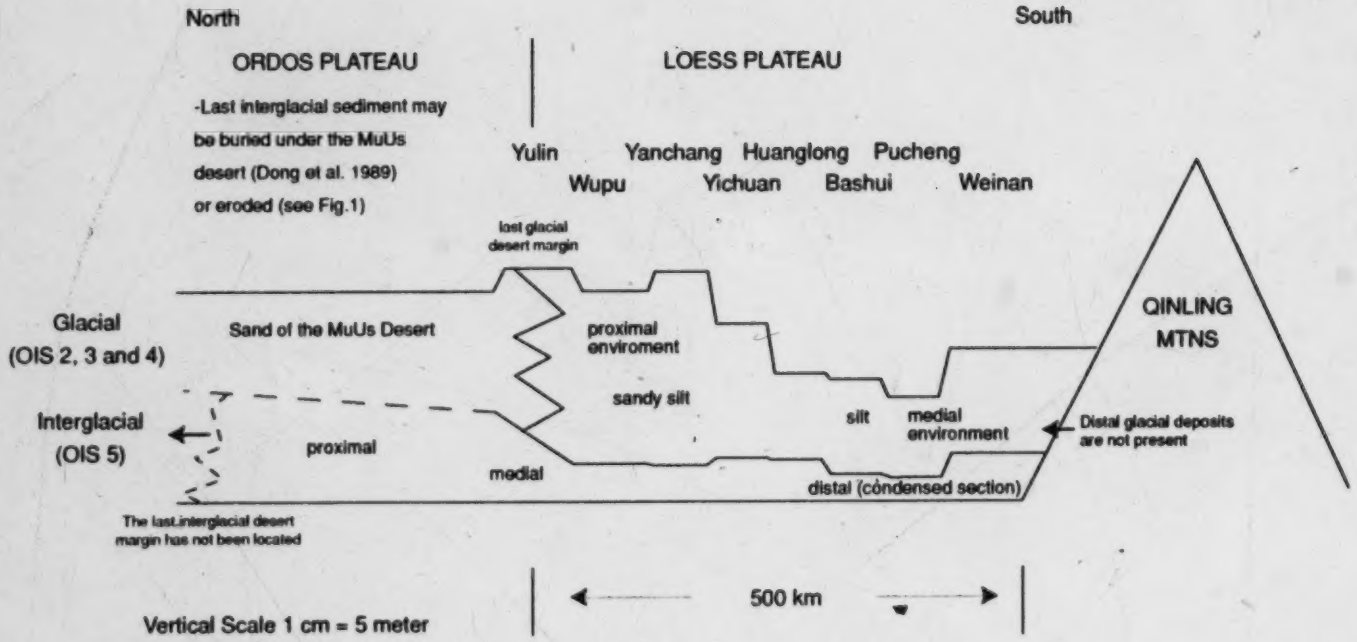

Figure 3.9. Schematic showing the distribution of loess and variations in the position of desert margin during the last interglacial and glacial periods using the correlations from Fig. 3.3. Vertical scale 1 cm = 5 m. Horizontal distance is not to scale. The dashed lines indicate that the last interglacial sediment north of the Loess Plateau have not been located.

A spatial comparison of accumulation rates along the transect (Fig. 3.8) shows that during the last glaciation (L1) accumulation rates generally increase northward from Pucheng to Yanchang, and then flatten out or decrease slightly near the desert source (e.g., Yulin). Similarly, accumulation rates during the last interglacial increase northward as indicated by higher rates at Lijia Yuan, Ding Bien and Yulin. However, since interglacial source rocks and sites proximal to the source rocks have not been located, we cannot be certain that accumulation rates continue to increase toward the source during last interglacial, as they generally do during the last glacial period. However, studies that trace and monitor modern dust storms indicate that dust (i.e. loess) is deposited well north of the geographic extent of the central Loess Plateau (Ing 1972; Deere, 1984; Liu et al. 1985; Merrill et al. 1989; Middleton 1991; Zhang et al. 1992, 1996; Mitsuta et al. 1995). If loess depositional processes and storm paths during the last interglacial are similar to present day processes, then we can at least suggest that loess deposition during the last interglacial may be continuous from the desert source.

During the last interglacial period and the Holocene, the southern edge of the desert margin contracted northward (Yan and Petit-Maire, 1994; Sun et al., 1998a). The contraction of the desert margin during the last interglacial suggests that the areal extent of loess deposition, north of the Qinling Mountains, was much larger than during the last interglacial period than during the last glacial period. A change in the size of the depositional area could have an effect on the thickness (and accumulation rates) of interglacial loess.

3.5 Discussion of results and relationship to global ice volume variations

During the last interglacial and glacial periods, there are some similarities and differences in the loess depositional regimes. Loess grain size increases toward the desert source during the last interglacial and glacial periods. During the last glacial period loess accumulation rates generally increase toward the source rocks. However, during the last interglacial period loess deposition was deposited over a larger area (north of the Qinling Mtns.), relative to the last glacial period and may have been continuous from the source to the accumulation zone. Erosion, or burial of last interglacial loess beneath the Mu Us desert, north of Yulin prevents a comparison of proximal glacial and interglacial deposits. Further, a notable difference between the glacial and interglacial depositional systems is the spatial distribution of the grains. The distribution of the grains is controlled by desert expansion and contraction, during cold and warm periods, respectively.

During the last glacial period, the Chinese deserts expanded northward (Lioubimtseva et al. 1998) and southward (Dong et al., 1989; Yan and Petit-Maire, 1994; Sun et al., 1995, 1998a, 1998b) a few hundred kilometers. As the desert margin expands southward over the underlying loess beds, loess would either be buried or eroded. If eroded and re-deposited in the Loess Plateau, then interglacial loess may be a source of glacial loess. Hence the deserts are, to some degree, a holding zone for interglacial loess (Bowler et al. 1987) which may later be transport to the Loess Plateau.

From the desert source to the accumulation zone, the trends in loess grain size appear to be similar during interglacial and glacial periods. Variations in loess grain size in the Loess Plateau are assumed to reflect the strength of the depositional winds (An et

al. 1991a; Ding et al 1995; Rutter et al. 1997). This assumption is derived in part from observations of a systematic fining in loess grain size downwind of the desert source (Liu and Chang 1964; Liu et al. 1985), and from a comparison to factors controlling aeolian grain size variations in the western Pacific Ocean (see An et al. 1991b, and Rae 1994 for summaries). The similarity of glacial and interglacial grain sizes in Fig. 3.5 from sites relatively proximal to the source (e.g. Yulin interglacial and Yichuan glacial) suggests that the wind speed during these periods may also be similar. Phillips et al. (1993) suggest that glacial winds may not be stronger than interglacial winds, but may be more persistent. Winds that persist at a high velocity would certainly aid desert expansion during a relatively dry glacial period.

3.6 Conclusion

Comparisons of interglacial and glacial variations in loess grain size or accumulation rates from a single section (i.e. temporal variations) do not accurately reflect the regional depositional regime, and should not be assumed to reflect regional depositional processes. Regional loess depositional processes are best interpreted by combining the spatial and temporal variations in loess properties from many sections. This regional study has altered the view of the texture of glacial and interglacial loess. Regional variations in grain size and accumulation rates in north China suggest that the last interglacial and glacial depositional systems are similar in terms of the size and trends of loess grains and possibly, the thickness of the beds. However, the difference between the two systems is largely in the distribution of the grains due to desert expansion and contraction during glacial and interglacial periods, respectively.

Regional variations in glacial and interglacial loess grain size and thickness indicate an indirect relationship between loess deposition and global ice volume variations. During glacial and interglacial periods, spatial variations in the texture of loess are controlled, in part, by proximity to the source. The proximity of the central Loess Plateau to the source changes due to advance and retreat cycles of the desert margin during glacial and interglacial periods, respectively. Thus, the effect of changes in global ice volume on deposition in the Loess Plateau is to shift the desert (source)-steppe (accumulation zone) environments resulting in a redistribution of loess, rather than a direct control on loess grain size or accumulation rates.

3.7 References

An, Z.S., Kukla, G., Porter, S.C., and Xiao, J.L. 1991a. Magnetic susceptibility evidence of monsoon variation on the Loess Plateau of central China during the last 130,000 years. Quaternary Research, **36**, 29-36.

An, Z., Wu., X., Wang, P., Wang, S., Dong, G., Sun, X., Zhang, D., Lu, Y., Zheng, S., Zhao, S. 1991. Changes in the monsoon and associated environmental changes in China since the last interglacial. *In* Loess, Environment and Global Change. Edited by Tungsheng Liu, Zhongli Ding and Zhengtang Guo. Science Press, Beijing, pp. 1-29.

Barbour, G.B. 1930. The Loess Problem of China. Geological Magazine, 67: 458-475.

Berger, A.1978. Long-term variations of caloric insolation resulting from the Earth's orbital elements.: Quaternary Research, 9, 139-167.

Bloemendal, J., Liu, X. M., and Rolph, T. C. (1995). Correlation of the magnetic susceptibility stratigraphy of Chinese loess and the marine oxygen isotope record: chronological and palaeoclimatic implications. Earth and Planetary Science Letters, **131**, 371-380.

Bowler, J.M., Chen, K., and Yuan, B. 1989. Systematic variations in loess source areas: evidence from the Qaidam and Qinghai Basins, Western China. *In* Aspects of Loess Research. *Edited by* T. Liu. Ocean Press, Beijing, pp. 39-51.

Bronger, A. and Heinkele, T. 1989. Micromorphology and genesis of paleosols in the Luochuan loess section, China: pedostratigraphic and environmental implications. Geoderma, **45**, 123-143.

Bryan, K., 1945, Glacial versus desert origin of loess. American Journal of Science, **243**, 245-248.

Chamberlin, T.C. 1897. Supplementary hypothesis respecting the origin of the loess of the Mississippi Valley. Journal of Geology, 5: 795-802.

Chen, F.H., Wang, J.M., and Bloemendal, J. 1998. East Asian monsoon variations during the last interglacial: evidence from the northwest margin of the Chinese Loess Plateau. Past Global Changes (PAGES) Newsletter, 6: 10.

Deere, Z. 1984. Synoptic-climatic studies of dust fall in China since Historic times. Scientia Sinica (Series B), **27**, 825-836.

Derbyshire, E., Keen, D., Kemp, R.A., Rolph, T.A., Shaw, J., and Meng, X.M. 1995. Loess-paleosol sequences as recorders of palaeoclimatic variations during the last glacial-interglacial cycle: some problems of correlation in north-central China. Quaternary Proceedings, **4**, 7-18.

Derbyshire, E., Kemp, R.A., and Meng, X.M. 1997. Climate change, loess and paleosols: proxy measures and resolution in China. Journal of the Geological Society of London, **154**, 793-805.

Ding, Z.L., Liu, T.S., Rutter, N.W., Z.W., Yu., Guo, Z.T., and Zhu, R.X. 1995. Ice-volume forcing of East Asian winter monsoon variations in the past 800,000 years. Quaternary Research, **44**, 149-159.

Ding, Z., Rutter, N.W., and Liu, T. 1993. Pedostratigraphy of Chinese Loess Deposits and Climatic Cycles in the last 2.5 Ma. Catena, **20**, 73-91.

Ding, Z., Sun, J., Rutter, N.W., Rokosh, D. and Liu, T. 1999. Changes in the sand content of loess deposits along a north to south transect of the Chinese Loess Plateau and the implications for desert variations. Quaternary Research, **52**, 56-62.

Ding, Z.L., Yu, Z., Rutter, N.W., and Liu, T.S. 1994. Towards an orbital time scale for Chinese loess deposits. Quaternary Science Reviews, **13**, 39-70.

Dodonov, A.E., 1991. Loess of central Asia.: Geojournal, **24**, 185-194.

Dong, G., Gao, S., Jin, J., and Li, B. 1989. The formation, evolution and cause of the Mu Us Desert in China. Scientia Sinica, Series B: Chemical, Biological, Agricultural, Medical & Earth Sciences = Chung-Kuo K'o Hsueh Yuan, Chu Pan., **32**, 859-872.

Evans, M.E. and Heller, F. 1994. Magnetic enhancement and paleoclimate study of a loess/paleosol couplet across the Loess Plateau of China. Geophysical Journal International, **117**, 257-264.

Evans, M.E., Ding, Z. and Rutter, N.W. 1996. A high-resolution magnetic susceptibility study of a loess/palaeosol couplet at Baoji, China. Studia Geophysica et Geodaetica, **10**, 225-233.

Fang, X., Li, J., Banerjee, S., and Van der Woo, R. 1998. Last Interglacial sharp monsoon fluctuations: rock magnetic and paleomagnetic evidence from high resolution loess-paleosol sequence, Lanzhou, China. Past Global Changes (PAGES) Newsletter, **6**, 6.

Guo, Z., Liu, T., Federoff, N., Wei, L., Ding, Z, Wu, N., Jiang, W. and An, Z. 1998. Climate extremes in Loess of China coupled with the strength of deep-water formation in the North Atlantic. Global and Planetary Change, **18**, 113-128.

Guo, Z.. Federoff, N. and An, Z. 1991. Genetic types of the Holocene soil and the Pleistocene palaeosols in the Xifeng loess section in central China. In Loess, Environment and Global Change. Edited by T. Liu. Science Press, Beijing. pp. 93-111.

Hays, J.D., Imbrie, J., and Shackleton, N.J. 1976. Variations in the Earth's orbit: pacemaker of the ice ages. Science, **194**, 1121-1132.

Hunt, C.P., Banerjee, S.K., Han, J.M., Solheid, P.A., Oches, E., Sun, W.W., and Liu, T.S. 1995. Rock-magnetic proxies of climate change in the loess-Palaeosol sequences of the western Loess Plateau of China. Geophysical Journal International, **123**, 232-244.

Imbrie, J., Hays, J.D., Martinson, D.G., McIntyre, A., Mix, A.C., Morley, J.J., Pisias, N.G., Prell, W.L., and Shackleton, N.J. 1984. The orbital theory of Pleistocene climate: Support from a revised chronology of the marine $\delta^{18}O$ record. *In* Milankovitch and Climate, Understanding the Response to Astronomical Forcing. *Edited by* A. Berger, J, Imbrie, J. Hays, G. Kukla, and B. Saltzman. NATA ASI Series C: Mathematical and Physical Sciences. Reidel Publishing Company, Boston, pp. 269-305.

Imbrie, J., Boyle, E.A., Clemens, S.C., Duffy, A., Howard, W.R., Kukla, G., Kutzbach, J., Martinson, D.G., McIntyre, A., Mix, A.C., Molfino, B., Morley, J.J., Peterson, L.C., Pisias, N.G., Prell, W.L., Raymo, M.E., Shackleton, N.J., and Toggweiler, J.R. 1992. On the structure and origin of major glaciation cycles; 1, Linear Responses to Milankovitch Forcing. Paleoceanography, **7**, 701-738.

Imbrie, J., Berger, A., Boyle, E.A., Clemens, S.C., Duffy, A., Howard, W.R., Kukla, G., Kutzbach, J., Martinson, D.G., McIntyre, A., Mix, A.C., Molfino, B., Morley, J.J., Peterson, L.C., Pisias, N.G., Prell, W.L., Raymo, M.E., Shackleton, N.J., and Toggweiler, J.R. 1993. On the structure and origin of major glaciation cycles; 2, The 100,000-year cycle. Paleoceanography, **8**, 698-735.

Ing, G.K.T. 1972. A dust storm over Central Asia, April 1969. Weather, 27: 136-145.

Kukla, G.J., 1987a, Correlation of Chinese, European and American loess series with deep-sea sediments. *In* Aspects of Loess Research. *Edited by* T. Liu. Ocean Press, Beijing, pp. 27-38.

Kukla, G. 1987b. Loess stratigraphy in central China and correlation with an extended oxygen isotope time stage scale. Quaternary Science Review, 6: 191-220.

Kukla, G., An, Z.S., Melice, J.L., Gavin, J., and Xiao, J.L. 1990. Magnetic susceptibility record of Chinese loess. Transactions of the Royal Society of Edinburgh. **81**, 263-288.

Lioubimtseva, E., Simon, B., Faure, H., Faure-Denard, L., Adams, J.M. 1998. Impacts of climatic change on carbon storage in the Sahara-Gobi desert belt since the last glacial maximum. Global and Planetary Change, **16-17**, 95-105.

Liu, J., Nie, G., Chen, T., Song, C., Zhu., G., Li, K., Gao, Z., and Qiao, Y. 1995. A preliminary high resolution time scale for the last 130,000 years at Weinan loess section. Sciencia Geologica Sinica (Overseas Edition; Supplementary Issue), Beijing, China, **1**, 9-22.

Liu, T., and Chang, T. 1964. The "HuangTu" (loess) of China. Report of the Sixth INQUA Congress, Warsaw 1961, **4**, pp. 503-524.

Liu, T.S. 1985. Loess and the Environment. China Ocean Press, Beijing.

Liu, X.M., Liu, T., Shaw, J., Heller, F., Xu, T., and Yuan, B. 1991. Paleomagnetic and paleoclimatic studies of Chinese loess, *In* Loess, Environment and Global Change. *Edited by* T. Liu, Z. Ding, and Z. Guo. Science Press, Beijing. pp. 61-81.

Liu X.M., Rolph, T., Bloemendal, J. Shaw, J. and Liu, T. 1995. Quantitative estimates of palaeoprecipitation at Xifeng, in the Loess Plateau of China. Palaeogeography, Palaeoclimatology, Palaeoecology, **113**, 243-248.

Martinson, D.G., Pisias, N.G., Hays, J.D., Imbrie, J., Moore, T.C.J., and Shackleton, N.J. 1987. Age dating and the orbital theory of the ice ages; development of a high-resolution 0 to 300,000-year chronostratigraphy. Quaternary Research, **27**, 1-29.

Merrill, J.T., Uematsu, M. and Bleck1989. Meteorological analysis of long range transport of mineral aerosols over the North Pacific. Journal of Geophysical Research, **94**, 8584-8598.

Middleton, N.J. 1991. Dust Storms in the Mongolian People's Republic: Journal of Arid Environments, **20**, 287-297.

Milankovitch, M. 1930. Mathematishe Klimalehre und Astronomische Theorie der Klimaschwankungen. Gebruder Borntreger, Berlin. pp. 176.

Mitsuta, Y., Hayashi, T., Takemi, T., Hu, Y., Wang, J., and Chen, M. 1995. Two severe local storms as observed in the arid area of Northwest China. Journal of the Meteorological Society of Japan, **73**, 1269-1284.

Murakami, T. 1987. Effects of the Tibetan Plateau. *In* Monsoon Meteorology. *Edited by* C.-P. Chang and T.N. Krishnamurti Oxford University Press, New York. pp. 235-270.

Niu, Z. 1985. Landsat image interpretation of sand dune movement in the Yellow River Valley. *In* Hydrological Applications of Remote Sensing and Remote Data Transmission (Proceedings of the Hamburg Symposium, August 1983). *Edited by* B.E. Goodison. International Association of Hydrological Sciences Publication No. 145, pp. 677-684.

Phillips, F.M., Zreda, M.G., Ku, T.-L., Lou, S., Huang, Q., Elmore, D., Kubik, P.W., and Sharma, P. 1993. $^{230}Th/^{234}U$ and ^{36}Cl dating of evaporite deposits from the western Qaidam Basin, China: implications for glacial-period dust export from Central Asia. Geological Society of America Bulletin, **105**, 1606-1616.

Pye, K. 1987. Aeolian dust and dust deposits. Academic Press. London.

Pye, K. 1995. The nature, origin and accumulation of loess. Quaternary Science Reviews, **14**, 7-8, 653-667.

Pye, K., and Zhou, L.P. 1989. Late Pleistocene and Holocene aeolian dust deposition in China and Northwest Pacific Ocean. Palaeogeography, Palaeoclimatology, Palaeoecology, **73**, 11-23.

Rae, D. 1994. The paleoclimate record provided by eolian deposition in the deep sea: the geological history of wind. Reviews in Geophysics, **32**, 2, 159-195.

Rousseau, D.-D. and Wu, N. 1997. A new molluscan record of the monsoon variability over the past 130,000 yr. in the Louchuan loess series. Geology, **25**, 275-278.

Rutter, N.W., Ding, Z., Evans, M.E., and Liu, T. 1991. Baoji-type pedostratigraphic section, Loess Plateau, north-central, China. Quaternary Science Reviews, **10**, 1-22.

Rutter, N.W., Ding, Z. and Liu, T. 1997. Reliability of grain size variation as a climatic proxy and correlation method for loess-paleosol units, North-Central China. International Conference on Geology, Geotechnology and Mineral Resources of Indochina (Geo-Indo 95), November 22-25, Khon Kaen, Thailand, 45-52.

Rutter, N.W., Rokosh, D., Ding, Z. and Liu, T., 1998. High resolution paleoclimate records from the loess-desert margin. Desert Margin Changes in Africa since 135 ka: Implications for Water, Carbon & Man. International Geological Correlation Program 349/404, Jan 5-12 1997, pp. 100-102.

Shackleton, N.J., An, Z., Dodonov, A.E., Gavin, J., Kukla, G.J., Ranov, V.A., and Zhuo, L.P. 1995. Accumulation rate of loess in Tadjikistan and China: relationship with global ice volume cycles. Quaternary Proceedings, **4**, 1-6.

Smalley, I. 1975. Introduction, *in* Loess Lithology and Genesis. *Edited by* I. Smalley. Benchmark Papers in Geology, 26. Dowden, Hutchinson & Ross Inc., Stroudsburg. pp. 1-9.

Soil Conservation Service 1972. Soil Survey laboratory methods and Procedures for collecting soil samples. Soil Survey Investigations report No. 1 United States Department of Agriculture, Washington D.C.

Sun, J., and Ding, Z. 1998. Deposits and soils of the past 130,000 years at the desert-loess Transition in Northern China.: Quaternary Research, **50**, 148-156.

Sun, J., Ding, Z., and Liu, T. 1995. The environmental evolution of the desert-loess transition zone over the last glacial-interglacial cycle, *in* Quaternary Geology and Past Environmental changes in China. *Edited by* S. Wang. Science Press, Beijing, pp. 1-8.

Sun, J., Ding, Z., and Liu, T. 1998a. Desert distribution during the glacial maximum and climatic optimum: example of China. Episodes, **21**, 28-30.

Sun, J., Yin, G., Ding, D., Liu, T., and Chen, J. 1998b. Thermoluminescence chronology of sand profiles in the Mu Us Desert, China. Palaeogeography, Palaeoclimatology, Palaeoecology, **144**, 25-233.

Thompson, R. and Oldfield, F. 1986. Environmental Magnetism. Allen & Unwin. Boston, MA, United States. 227 pp.

Tsoar, H. and Pye, K. 1987. Dust transport and the question of desert loess formation. Sedimentology, **34**, 139-153.

U.S.A. Defense Mapping Agency Aerospace Center 1987, Operational Navigation Chart, Sheets F-7, F-8, G-8, G-9. U.S. Department of Defense.

Vandenberghe, J., An, Z.S., Nugteren, G., Lu, H.Y., and Van Huissteden, K. 1997. New absolute time scale for the Quaternary climate in the Chinese loess region by grain-size analysis. Geology, **25**, 35-38.

Wang , Y., Evans, M.E., Xu, T.C., Rutter, N., Ding, Z. and Liu, X.M. 1991. Rescaled range analysis of paleoclimate proxies. Canadian Journal of Earth Science, **29**, 296-300.

Yan, Z., and Petit-Maire, N. 1994. The last 140 ka in the Afro-Asian arid/ semi-arid transitional zone. Palaeogeography, Palaeoclimatology, Palaeoecology, **110**, 217-233.

Zhang, X., An, Z., Liu, D., Chen, T., Zhang, G., Arimoto, R., Zhu, G., and Wang, X. 1992. Study on three dust storms in China-source characterization of atmospheric trace element and transport process of mineral aerosol particles. Chinese Science Bulletin, 37: 940-945.

Zhang, X., Chen, Z., Zhang, G., Chen, T., and Liu, H. 1996. Remote mineral aerosols in Westerlies and their contributions to the Chinese loess. Science in China (Series D), **39**, 134-143.

Zhang, X.Y., Arimoto, R., and An, Z.S. 1999. Glacial and interglacial patterns for Asian dust transport. Quaternary Science reviews, **18**, 811-819.

Zhao, S. 1986. Physical Geography of China. Science Press, Beijing. John Wiley & Sons, New York.

CHAPTER 4

Regional lithofacies and pedofacies variations along a north to south climatic gradient during the last glaciation in the central Loess Plateau, China.

(submitted to Quaternary Science Reviews)

Authorship: Rokosh, D. Rutter, N.W., Ding, Z. and Sun, Z.

4.1 Introduction

In the Loess Plateau, China (Fig. 4.1) stratigraphy has largely been based on palaeosol counting (Liu, T. et al. 1985), because of the lateral persistence of alternating loess and palaeosols (Pavlinov 1959; Liu, T. et al. 1985). The alternation of loess beds and palaeosols in China is, in part, a function of a relative balance between the rate of pedogenesis and the rate of loess deposition (An et al. 1991; Zheng et al. 1994). The top and base of the palaeosols are interpreted as coinciding with palaeoclimate boundaries. Liu, T. et al. (1985), Kukla (1987a,b), and Liu, J. et al. (1995) demonstrated a chronostratigraphic correlation of marine oxygen isotope stages (MIS) 2, 3 and 4 (last glacial) with the Malan loess (L1), and MIS 5 (last interglacial) with palaeosol S1 (Fig. 4.2). In the southern Loess Plateau, high resolution (e.g. 10 cm sample interval or less in this study) correlations of loess and palaeosols with regional palaeoclimate boundaries are complicated by a low dust accretion rate and a relatively high mean annual temperature and precipitation. These factors result in palaeosol welding such as in palaeosol S1 (Guo and Fedoroff, 1991). In the northern Loess Plateau, near the desert margin, loess accumulation rates are higher than in the south, while mean annual temperature and precipitation are lower. The result is a clear stratigraphic alternation

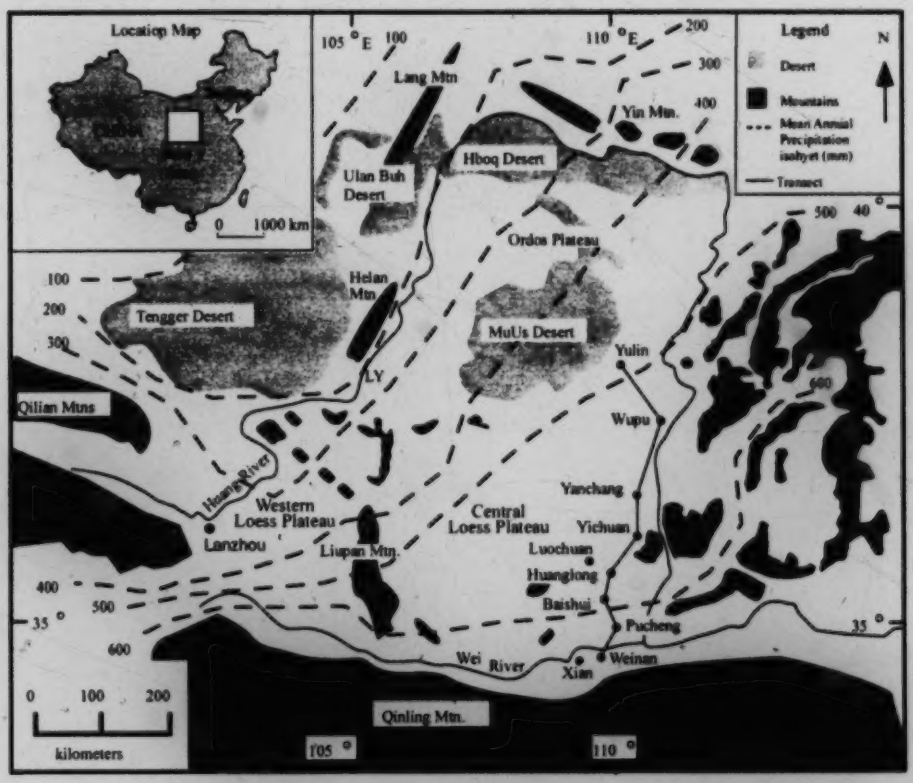

Figure 4.1. Base map of the Loess Plateau showing the location of the sites along the north to south transect in the central Loess Plateau, and other locations mentioned in the text. The isohyets (mean annual precipitation) are from Zhao (1986). (Modified from US Defense Mapping Agency Aerospace Center, Operational Navigation Chart Series ONC, Sheets F-7, F-8, G-8 and G-9, Edition 4, 1987).

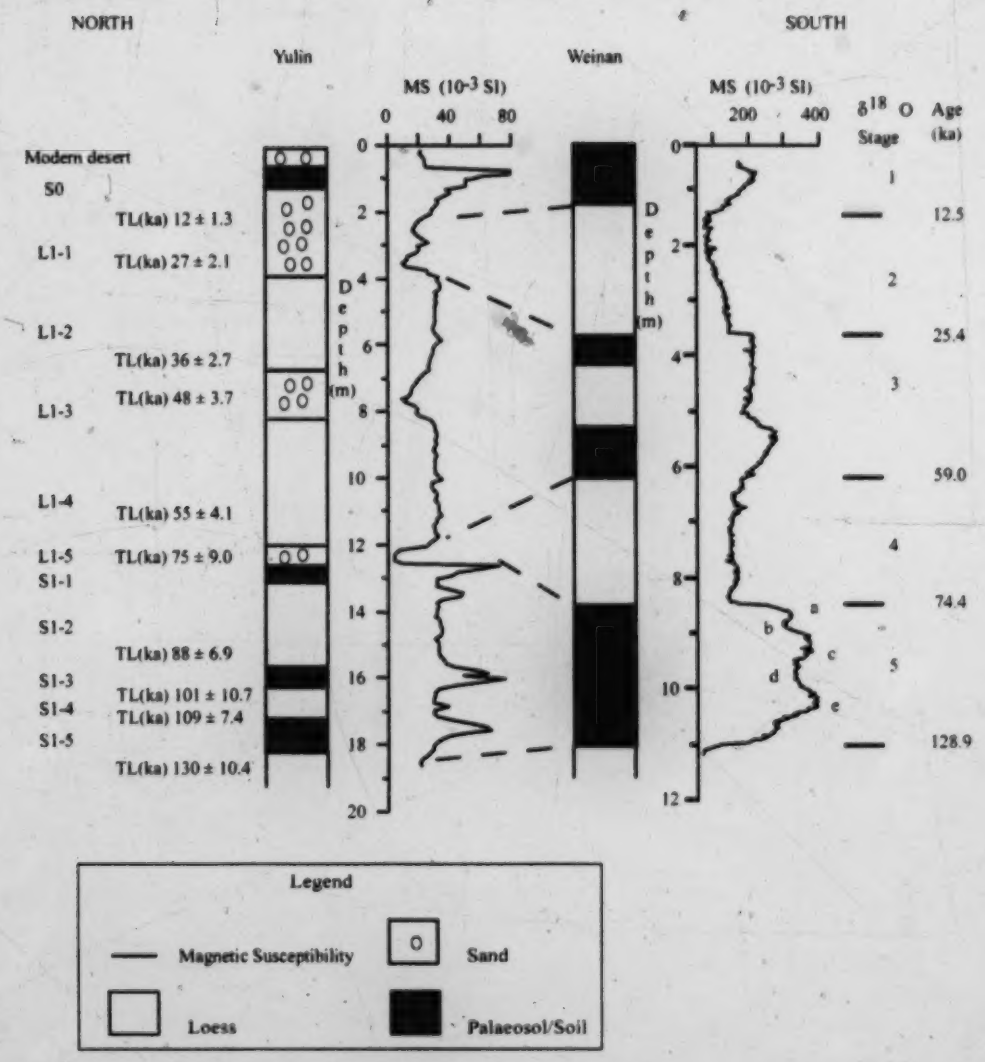

Figure 4.2. Comparison of litho- and pedostratigraphy at the north and south ends of the transect Age control is provided by the age models of Liu, J. et al (1995, 1998) at Weinan at the southern end of the transect, and thermoluminescence (TL) measurements at Yulin at the north end of the transect (Sun et al. 1995, 1998b; Sun and Ding 1998).

of loess beds and palaeosols, such as in palaeosol S1 at Yulin (Fig. 4.2), where soils developed during periods of reduced dust input and more favorable climate (Pye and Tsoar 1987; Pye 1987; An et al. 1991). According to Pye (1987), changes in the dust accretion rate or the rate of rainfall through time, along a theoretical transect, will cause a shift in the point where the rate of weathering equals the rate of dust accretion, and produce a stratigraphic sequence of alternating weathered loess (or soil) and relatively unweathered loess (Pye and Tsoar 1987; Pye 1987). Hence, in the Loess Plateau there is a change in dust accretion rates along a climatic gradient that drive the stratigraphic changes.

Similar observations on the relationship between dust accretion rates and soil development have been made in other areas. Along the bluffs of the Illinois River in central Illinois, Smith (1941, 1942) and Thorp (1945) observed $CaCO_3$-rich loess and weak soils, while farther from the source area, and within the same stratigraphic interval, relatively mature soils were developed. In the Matanuska Valley of Alaska Reiger and Juve (1961) interpret loess deposition, sourced from the Matanuska River floodplain, as continuous during warm and cold periods. Close to the river, Regosols developed where the rate of loess deposition was high, while in areas distal from the source (~35 km) podzolization dominates when the rate of loess deposition was low. In the Columbia Plateau, northwest U.S.A., Busacca and McDonald (1994) suggest that loess deposition occurs during the spring and fall when the winds are most intense. Palaeosols development is dominantly a function of the rate of loess deposition. Changes in climate and vegetation may have played a secondary role (McDonald and Busacca (1990). Bown and Kraus, (1986) and Smith (1990) applied the term 'pedofacies' to lateral changes in

soil properties due to changes in the rate of sediment accumulation. In each of the above cases the lateral changes occur over a few kilometers, or a few tens of kilometers, and under similar climatic conditions.

In this paper, the relationship between dust accretion rates and palaeosol development during the last glacial cycle is examined along a 500-km north to south climatic gradient in the central Loess Plateau, China. Eight sites were sampled along the eastern margin of the central Loess Plateau (Fig. 4.1) that provide the opportunity, for the first time in China, to identify loess and palaeosol alternations at high resolution time intervals along a regional transect. The relatively close spacing of the sites allows a focus on two main objectives. These are: 1) examination of lithofacies and pedofacies variations along the climatic gradient, and 2) analysis of the use of high-resolution variations in loess-palaeosol stratigraphy as indicators of regional palaeoclimate variations. In this respect, the results of this study establish that simple stratigraphic models that correlate loess beds to loess beds, and palaeosols to palaeosols may not apply in regional high resolution studies.

4.2 Methods

Grain size and magnetic susceptibility were determined for samples collected from three sections along the north to south transect (Fig. 4.1) of the central Loess Plateau. Palaeosols were sampled vertically every 2-5 cm, while loess beds were sampled every 5-10 cm. Grain size analysis was performed on a PRO-700 SK Laser Micron Sizer. An analysis of 20 replicate samples indicated a precision of ±3.5%. Bulk

magnetic susceptibility was determined using a Bartington MS-II susceptibility meter. Susceptibility values represent one reading on an approximately 50 gram bagged sample.

The nomenclature scheme of Liu, T. et al. (1985) is adopted in this paper. Loess horizons are designated 'L', while palaeosols are designated 'S'. The youngest palaeosol along the transect, the Holocene soil, is designated S0, while older interglacial soils are given a progressively higher number (e.g., S1, S2, etc.). The last glacial loess bed is labeled L1, with succeeding glacial loess beds successively labeled L2, L3, etc.

Time control is provided by the age models of Liu, J. et al. (1995, 1998) at Weinan at the southern end of the transect, and thermoluminescence (TL) measurements at Yulin at the north end of the transect (Sun and Ding 1998; Sun et al. 1995, 1998a). The chronology of the Liu, J. et al. (1995, 1998) model spans approximately the last 130 ky and is based on Accelerated Mass Spectrometer (AMS) radiocarbon and TL measurements on loess and palaeosols. Liu, J. et al. (1998) revised age of the L1-4/L1-5 contact from 59 ka in the 1995 model to 50 ka based on additional TL and AMS dates.

4.3 Modern Climate

Modern climate in the Loess Plateau is highly seasonal and dominated by winter and summer monsoons (Zhao, 1986). During winter, cold and dry winds emanate from the Siberian-Mongolian anticyclone, located west-southwest of Lake Baikal at about 90°E-105°E longitude (Zhao, 1986; Middleton, 1991). During summer, differential heating between the Asian continent and the surrounding South and East China Seas results in the flow of the moist southeasterly Asian monsoon onto the Asian continent.

Along the transect (Fig. 4.1) mean annual temperature increases from about 8°C in the north near Yulin to about 13°C at Weinan in the southern Loess Plateau (Zhao 1986). Mean annual precipitation varies from about 450 mm at Yulin to about 625 mm at Weinan (Zhao 1986). The decrease in precipitation reflects a northerly decrease in temperature and the progressive northward dissipation of moisture from the East Asian summer monsoon. The modern desert margin, where mean annual precipitation is about 100 mm, lies west of the Helan Mountains (Fig. 4.2) (Zhao 1986; Sun et al. 1998b).

4.4 North to south transect

Along the climatic gradient, the end members of the transect exhibit a contrast in litho- and pedostratigraphy in that part of the succession representing the last glacial period (Fig. 4.2). The lithostratigraphy of last glacial period at Yulin consists of alternating sand (L1-1, L1-3 and L1-5) and loess beds (L1-2 and L1-4, with the sand beds representing three periods of desert expansion (Sun et al. 1995, 1998b). The equivalent interval at Weinan is interpreted as alternating loess beds and palaeosols.

The median diameter grain size and wt. % sand >63 μm (Ding et al. 1999) in L1-1, L1-3 and L1-5 decrease southward from the desert margin at Yulin toward Weinan (Fig. 4.3; Table 4.1). Both L1-1 and L1-5 exhibit a lithofacies change from sand at the desert margin to relatively weakly weathered loess at Weinan. From Yulin to Yanchang the decrease in the median diameter grain size and wt. % sand of L1-3 is greater than either L1-1 or L1-5. From Yanchang to Weinan the grain size in L1-3 decreases further to about 5-8 μm (again lower than L1-1 and L1-5), while the wt. % sand decreases to <1 wt. % (Ding et al. 1999).

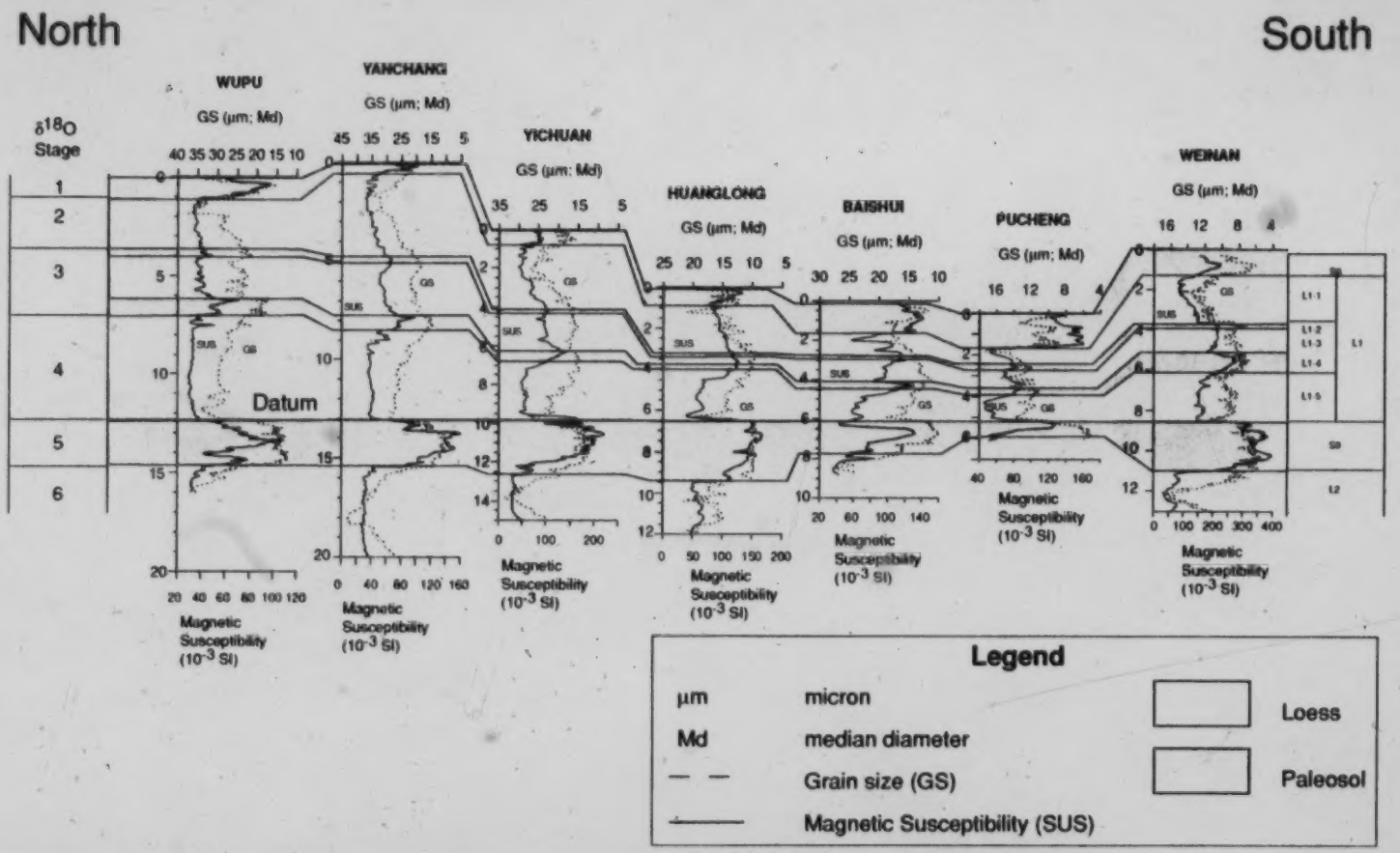

Figure 4.3. Grain size and magnetic susceptibility variations along the north to south transect.

Table 4.1 Variations in median diameter grain size (Md GS) and weight percent sand (> 63 μm) along the transect.

	Yulin (north)		Yanchang		Weinan (south)	
	Md GS (μm)	wt. % sand (> 63 μm)	Md GS (μm)	wt. % sand (> 63 μm)	Md GS (μm)	wt. % sand (> 63 μm)
L1-1	120	85-90	25-35	12-17	8-13	<1
L1-3	160	60-80	20-23	4-8	4-8	<1
L1-5	220	80-85	20-30	8-12	6-10	<1

In the southern Loess Plateau the middle bed (L1-3) is often described and depicted on diagrammatic profiles as either weathered loess or a weakly to moderately developed soil (e.g. at Luochuan, Xiao et al. 1999; at Xian, Wang et al. 1998), based on a slightly higher content of clay and organic matter, and a higher magnetic susceptibility, relative to L1-1 and L1-5. The variety of interpretations of L1-3 in the southern Loess Plateau is in part due to the difficulties inherent in differentiating a weak soil from relatively weathered loess (e.g see Kemp 1998). Differences in sampling strategy may also affect the issue. However, the lateral changes in L1-3 are quite clear. There is a continuum, along a 500 km climatic gradient, from sand at the desert margin to loess in the middle of the transect to weathered loess and, in some interpretations, soils at the southern edge of the transect. Pye's (1987) model of variations in dust accretion versus the rate of weathering, precipitation and pedogenesis predicts the presence of a lateral sand to loess to soil continuum. Hence, our data from L1-3 support Pye's (1987) model.

Palaeosols L1-2 and L1-4 at Weinan are relatively weakly developed soils exhibiting A/Bw profiles, while at Yulin the L1-2 and L1-4 loesses are very weakly weathered (Sun et al 1995). It would appear that the L1-2 and L1-4 palaeosols (Fig. 4.2) in the southern Loess Plateau are laterally equivalent to loess beds near the desert

margin. The lateral change from loess to soil represents a pedofacies change as defined by Bown and Kraus (1986), in which deposition near the loess source is greater than the rate of soil development.

Within the central Loess Plateau only the sand to loess portion of the continua are present during L1-1 and L1-5. At the southern end of the transect, the rate of loess deposition exceeds the rate of pedogenesis, and no soils have developed in L1-1 or L1-5. The continua cannot be traced southward at this time because the Qinling Mountains form the southern boundary of the Loess Plateau, and may block the southerly transfer of dust. During interstadials L1-2 and L1-4, the desert margin migrated northward (Sun et al. 1995), so the continua also migrated northward.

The sand-loess-soil continua appear to shift southward in concert with shifts or steeping of the climatic gradient during periods of maximum cooling (MIS 2 and 4). Conversely, they show a northward shift in those parts of the profiles representing stadials or interstadials (MIS 3) of the last glacial period. Lateral shifts in the sand-loess-soil continua are representative of regional (e.g. East Asia) or global palaeoclimate change.

4.5 The effect of local variations in the rate of dust accretion along the continua on high-resolution palaeoclimate interpretations.

At the north end of the transect the vertical succession of sand and loess beds follows Walther's Law (Middleton, 1973) and translates into regional, lateral lithofacies (sand to loess) sequences. Lateral pedofacies (loess to soil) changes occur in areas distal from the source, where pedogenic development is enhanced due to a warmer and wetter

climate. Derbyshire et al. (1997) suggest that differentiating loess from palaeosols in a vertical profile may be stratigraphically advantageous, but may not be the most useful method of reconstructing high resolution, regional palaeoenvironmental change. Slight variations in the rate of sediment supply along or across the climatic gradient will result in changes in the balance between rates of dust accretion and soil development. Where there are local fluctuations in these factors, especially in the loess to soil portion of the continua, the effect may be that loess and palaeosols (especially weak palaeosols) are chronostratigraphically equivalent. This is similar to the lateral loess to soil observations seen locally in central Illinois (Smith, 1941, 1942; Thorp,, 1945), the Matanuska Valley, Alaska (Regier and Juve, 1961), and the Columbia Plateau (Busacca and McDonald, 1994). In the Loess Plateau pedofacies alternations are most prevalent during intermediate climates (e.g L1-3 interstadial) and climate transitions (e.g. L1-2 and L1-4).

4.6 Conclusion

The high resolution transect from Yulin to Weinan reveals lateral loess-palaeosol variations that are not evident in temporal (i.e. vertical) evaluations of loess and palaeosols. Five lateral sand-loess-soil continua developed in the Loess Plateau during the last glacial cycle, as predicted by Pye's model (1987). The entire continuum is evident along the transect in the L1-3 lithofacies, but the distinction between weak to moderately developed palaeosols versus weathered loess at the southern end of the transect remains subjective. The continua shifted southward during phases of desert expansion (cold periods) and northward during periods of desert retreat (warm periods) and represent regional (e.g. East Asia) or global palaeoclimate change. Spatial and

temporal stratigraphic changes in the Loess Plateau are driven by changes in dust accretion rates along a shifting climatic gradient through time. Variations in the rate of dust accretion (e.g. high near the desert source, low distal from the source) appear to change in concert with shifts in the climatic gradient as suggested in the theoretical model of Tsoar and Pye (1987).

Superimposed on the regional trends are local variations in the balance between rates of dust accretion and soil development. Local fluctuations in either of these factors may result in the temporal equivalence of loess and palaeosols, particularly in the loess to palaeosol portion of the continua. At high resolutions, vertically alternating loess and weak soils may represent local climatic variations and must be correlated regionally in order to assess their validity as indicators of regional or global palaeoclimate change.

References

An, Z.S., Kukla, G., Porter, S.C., and Xiao, J.L. (1991). Late Quaternary dust flow on the Chinese Loess Plateau. *Catena*, 18, 125-132.

Bown, T.M. and Kraus, M.J. (1986). Integration of channel and floodplain suites, I Developmental sequences and lateral relations of alluvial paleosols. *Journal of Sedimentary Petrology*, 57, 587-601.

Busacca, A.J. and McDonald, E.V. (1994). Regional Sedimentation of Late Quaternary loess on the Columbia Plateau. sediment source areas and loess distributions. *Washington Division of Geology and Earth Resources*, 80, 181-190.

Derbyshire, E.D., Kemp, R.A. and Meng, X.M. (1997). Climate change, loess and palaeosols: proxy measures and resolution in North China. *Journal of the Geological Society of London*, 154, 793-805.

Ding, Z., Sun, J., Rutter, N.W., Rokosh, D. and Liu, T. (1999). Changes in the sand content of loess deposits along a north to south transect of the Chinese Loess Plateau and the implications for desert variations. *Quaternary Research*, 52, 56-62.

Guo, Z. and Fedoroff, N. (1991). Paleoclimatic and stratigraphic implications of the S1 paleosol in the Xifeng loess section in central China. In T.S. Liu (Ed.), *Loess, Environment and Global Change*. Beijing: Science Press, 187-198.

Kemp, R.A. (1998). Role of micromorphology in paleopedological research. *Quaternary International*, 51/52, 133-141.

Kukla, G.J., (1987a), Correlation of Chinese, European and American loess series with deep-sea sediments. In T. Liu (Ed.), *Aspects of Loess Research*. Beijing: Ocean Press, 27-38.

Kukla, G. (1987b). Loess stratigraphy in central China and correlation with an extended oxygen isotope time stage scale. *Quaternary Science Reviews*, 6, 191-220.

Liu, J., Nie, G., Chen, T., Song, C., Zhu., G., Li, K., Gao, Z., and Qiao, Y. (1995). A preliminary high resolution time scale for the last 130,000 years at Weinan loess section. *Sciencia Geologica Sinica (Overseas Edition; Supplementary Issue)*, Beijing, China, 1, 9-22.

Liu, J., Liu T. and Chen, T. (1998). Loess dating progress in China. *Past Global Changes (PAGES) Newsletter*, 6, 2.

Liu, T.S. (1985). *Loess and the Environment*. China Ocean Press, Beijing.

McDonald, E.V. and Busacca, A.J. (1990). Interaction between aggrading geomorphic surfaces and the formation of late Pleistocene paleosol in the Palouse loess of a eastern Washington State. *Geomorphology*, 3, 449-470.

Middleton, G.V. (1973). Johannes Walther's Law of the correlation of facies. *Bulletin of the Geological Society of America*. 84, 979-988.

Middleton, N.J. (1991). Dust Storms in the Mongolian People's Republic. *Journal of Arid Environments*, 20, 287-297.

Pavlinov, V.I. (1959). Some data about the genesis of loess in North China, In V.V. Popov, (Ed.)., *Loess in Northern China*, translated by A. Gourevitch, Israeli program for Scientific Translations (1964), Jerusalem: S. Monson, 134 pp.

Pye, K. (1987). *Aeolian dust and dust deposits*. London: Academic Press.

Pye, K. and Tsoar, H. (1987). The mechanics and geological implications of dust transport and deposition in deserts with particular reference to loess formation and dune sand diagenesis in the northern Negev, Israel. In L. Frostick and I. Reid. (Eds.), *Desert Sediments: Ancient and Modern.* Geological Society Special Publications No. 35, 139-156.

Reiger, S. and Juve, R. (1961). Soil development in Recent loess in the Matanuska Valley, Alaska. *Soil Science Society of America Proceedings*, 25, 243-248.

Smith, G.D. (1941). Illinois loess-variations in its properties and distribution. A pedologic interpretation. *Soil Science Society of America Proceedings*, 6, 85.

Smith, G.D. (1942). Illinois loess-variations in its properties and distribution. A pedologic interpretation. *University of Illinois Agri. Exp. Sta. Bull.*, 490, 137-184.

Smith, R.M.H. (1990). Alluvial paleosols and pedofacies sequences in the Permian Lower Beaufort of the southwestern Karoo Basin, South Africa. *Journal of Sedimentary Petrology*, 60, 258-276.

Sun, J., and Ding, Z. (1998). Deposits and soils of the past 130,000 years at the desert-loess Transition in Northern China.: *Quaternary Research*, 50, 148-156.

Sun, J., Ding, Z., and Liu, T. (1995). The environmental evolution of the desert-loess transition zone over the last glacial-interglacial cycle. In S. Wang (Ed.), *Quaternary Geology and Past Environmental changes in China.* Beijing: Science Press, 1-8.

Sun, J., Yin, G., Ding, D., Liu, T., and Chen, J. (1998a). Thermoluminescence chronology of sand profiles in the Mu Us Desert, China. *Palaeogeography, Palaeoclimatology, Palaeoecology*, 144, 25-233.

Sun, J., Ding, Z., and Liu, T. (1998b). Desert distributions during the glacial maximum and climatic optimum: example of China. *Episodes*, 21, 29-30.

Thorp, J. (1945). Significance of loess in classification of soils. American Journal of Science, 423, 263-270.

Wang, H., Liu, C-L and Follmer, L.R. (1998). Climatic trend and habitat variation based on oxygen and carbon isotopes from Liujiapo, Shaanxi, China. *Quaternary International*, 51/52, 52-53.

Xiao, J.L., An, Z.S., Liu, T.S., Inouchi, Y., Yoshikawa, S., and Kondo, Y. (1999). East Asian monsoon variation during the last 130,000 years; evidence from the Loess Plateau of central China and Lake Biwa of Japan *Quaternary Science Reviews*,18; 147-157.

Zheng, H., Theng, B.K.G. and Whitton, J.S. (1994). Mineral composition of loess-paleosol samples from the Loess Plateau of China and its environmental significance. *Chinese Journal of Geochemistry*, 13, 61-72.

Zhao, S. 1986, *Physical Geography of China*. Beijing: Science Press, Beijing and New York: John Wiley & Sons.

CHAPTER 5

High resolution geometry and stratification of loess of the Malan formation in the central Loess Plateau, China (submitted to Sedimentology)

Authorship: Rokosh, D., Rutter, N.W., Ding, Z. and Sun. J.

5.1 Introduction

Over the past 5-10 years, palaeoclimate studies in the Loess Plateau have been evaluating climate change at relatively high resolutions within the last interglacial-glacial cycle (e.g. Porter and An 1995, Derbyshire et al. 1995, 1997; Kemp et al. 1995; Chen et al. 1997, 1998; An and Porter 1998; Ding et al. 1998; Fang et al. 1998a, 1998b, 1999; Rutter et al. 1998). For example, Porter and An (1995) observed that the timing of variations in loess grain size at Luochuan (Fig. 5.1) were similar to the timing of Heinrich events indicated by $\delta^{18}O$ variations in Greenland ice core during the last glacial period. This suggested that a hemispherical climate connection, via the westerlies, existed between Greenland and the Loess Plateau over the last 75,000 years. Other studies have come to similar conclusions using proxy climate parameters from Lanzhou and Linxia in the western Loess Plateau (Chen et al. 1997), and Lijia Yuan and Ding Bien in the central Loess Plateau (Rutter et al. 1998). Hence, there are a number of sites within the central and western Loess Plateau (Fig. 5.1) that have recorded similar palaeoclimate events as observed in the last glacial record in the Greenland ice core. If millennial scale climate fluctuations, indicated at these sites, also represent regional climate change, then millennial scale variations should be regionally traceable in the Loess Plateau. However, the testing of this concept had never been undertaken. High

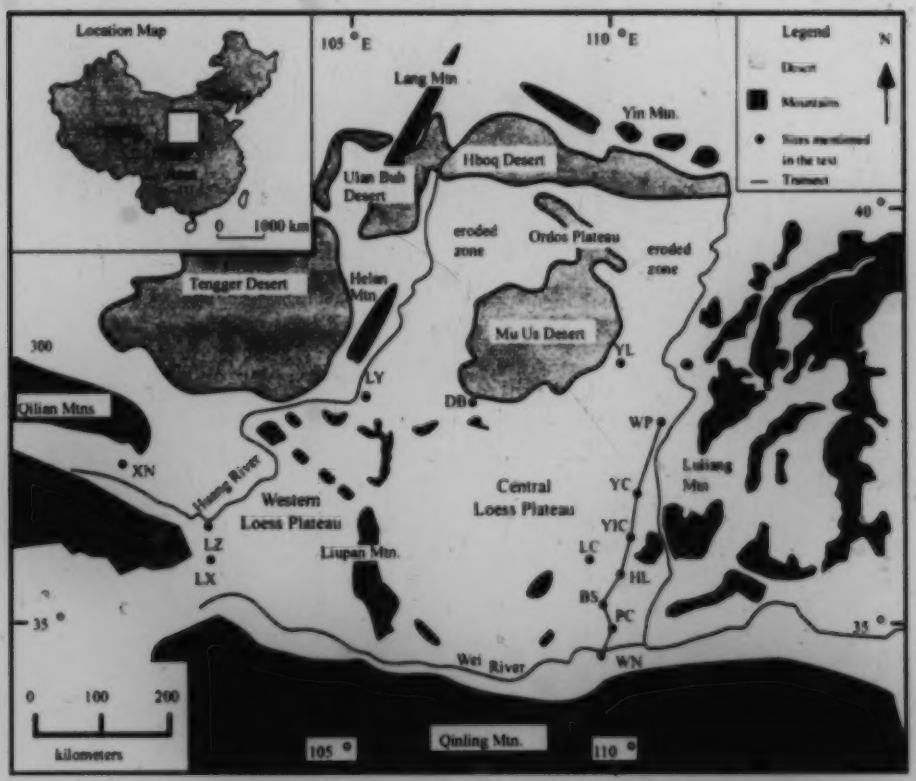

Central Loess Plateau				Western Loess Plateau	
BS	Baishui	DB	Ding Bien	LX	Linxia
HL	Huanglong	LC	Luochuan	LZJ	Lanzhou
LJY	Lija Yuan	PC	Pucheng		
WN	Weinan	WP	Wupu		
YC	Yanchang	YIC	Yichuan		
YL	Yulin				

Figure 5.1. Base map of the Loess Plateau showing the location of the sites along the north to south transect, and other locations mentioned in the text. (Modified from US Defense Mapping Agency Aerospace Center, Operational Navigation Chart Series ONC, Sheets F-7, F-8, G-8 and G-9, Edition 4, 1987).

resolution variations in grain size, for example, have never been regionally correlated, and the geometry of high resolution loess beds has not been studied. It is important to trace millenial-scale variations in order to test the validity of these changes as indicators of regional climatic change, as opposed to local climatic change or non-climatic events.

The concept of tracing regional, high resolution variations in grain size will be tested in the Malan formation (L1; marine oxygen isotope stage (MIS 2-4)]. The Malan formation comprises a contiguous sheet of loess in the central Loess Plateau from the desert margin in the north to the flank of the Qinling Mountains in the south (Fig. 5.1). Vertical variations in grain size of Chinese loess have been used as a stratigraphic tool (Liu et al. 1985; An et al. 1991a, b; Ding et al. 1994; Vandenberghe et al. 1997) for correlation to marine oxygen isotope stratigraphy (Emiliani 1955). Variations in grain size have also been interpreted as indicators of relative wind strength (Liu and Chang 1964; Liu et al. 1985; An et al. 1991; Ding et al.1994; Rutter et al. 1997; Vandenberghe et al. 1997), where large grains near the desert source reflect stronger transporting winds, while smaller grains distal from the source suggest weaker transporting winds.

In this paper, we will observe for the first time the geometry and stratification of high resolution loess beds in China during the last glaciation (i.e. Malan formation; MIS 2-4), principally using variations in loess grain size. Here, three different scales of observation are used. Regional geometry of the Malan formation (L1; Fig 5.2) is examined prior to observing variations within the members of the Malan (L1-1 to L1-5; Fig. 5.2). Lastly, millenial-scale variations in grain size are observed along the transect in order to determine how, or if, high frequency variations in grain size propagate

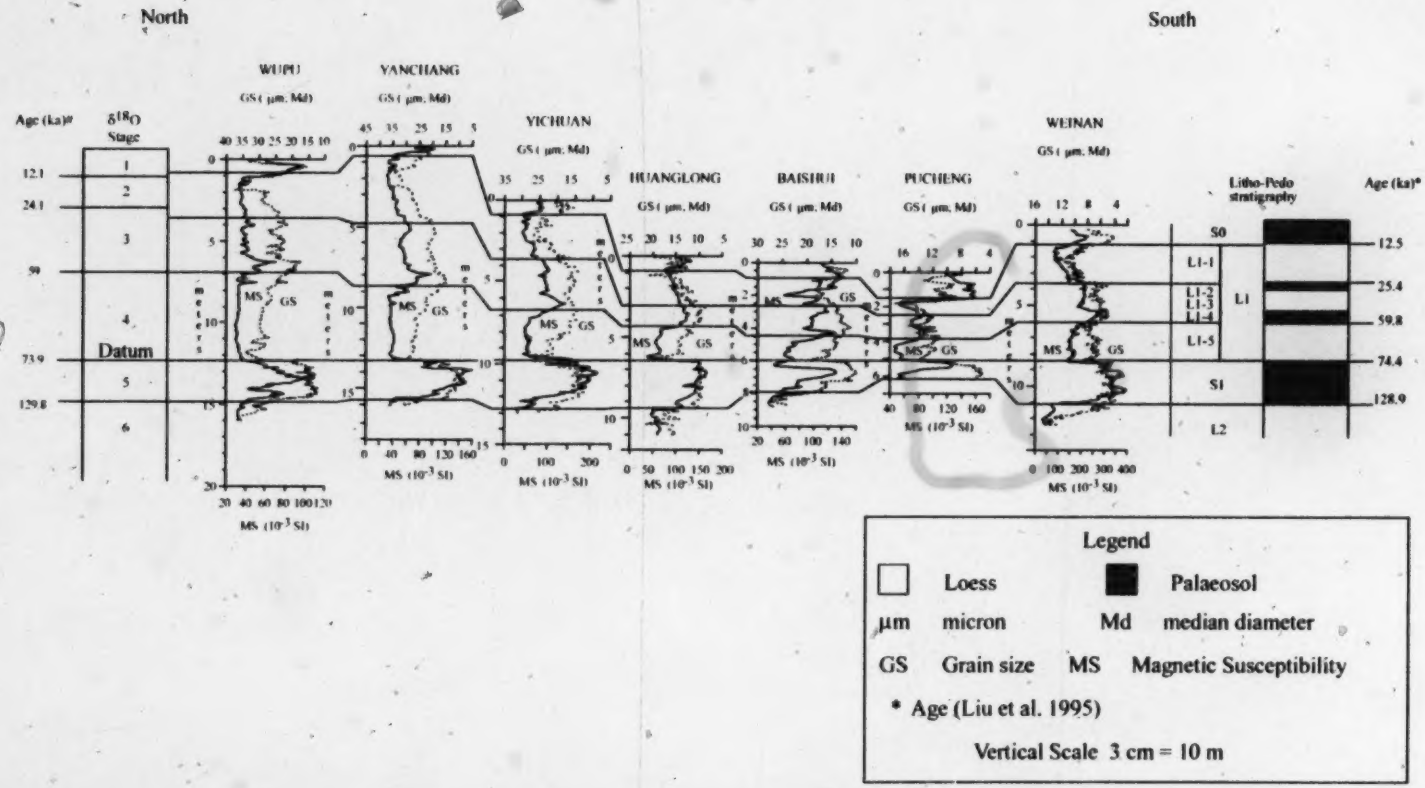

Figure 5. 2. Stratigraphic cross-section from the central Loess Plateau showing the continuity of the strata along the north to south transect. The correlations reflect climostratigraphy. All locations use the same vertical scale (1 cm = 3 meters).

through the central Loess Plateau. It is important in this study to determine both variations in grain size that do, and do not, correlate along the transect. Studying regional, millennial-scale variations in loess grain size is an important step toward discriminating local versus regional climate change, or discriminating variations due to climatic events and non-climatic events.

5.2 Methods

Grain size and magnetic susceptibility were determined on loess and palaeosol samples from seven sites in the central Loess Plateau (Fig. 5.1). Samples were taken every 5-10 cm in the L1 loess bed and 2-5 cm in the S1 palaeosol. A smaller sample interval was taken in thinner loess beds at the southern end of the transect. Bulk magnetic susceptibility and grain size were determined on each sample. Grain size analysis was performed on a PRO-700 SK Laser Micron Sizer. An analysis of 20 replicate samples indicated a precision of 3.5%. Organic material, pedogenic iron and carbonates were removed prior to analysis. Bulk magnetic susceptibility was determined using a Bartington MS II susceptibility meter. Susceptibility values represent one reading on an approximately 50 gram bagged sample. The values are presented as carbonate-free by calibrating each sample to the amount of carbonate present using the formula:

$$A2 = A1 * (100/100\text{-wt.\% C})$$

where A1 and A2 are the measured and resultant magnetic susceptibility, respectively, and C is the weight. % carbonate.

Age control is determined by correlation to the model of Liu, J. et al. (1995) at Weinan at the southern end of the transect (Fig. 5.1). The chronology of the Liu, J. et al.

(1995, 1998) model spans the last ca. 130 ky and is based on Thermoluminescence (TL) measurements and Accelerated Mass Spectrometer (AMS) radiocarbon on loess and palaeosols. Loess-palaeosol alternations have also been correlated to Marine Oxygen Isotope Stages (MIS) (Liu, T. et al. 1985; Kukla 1987a,b; Liu, J. et al. 1995), where MIS 2, 3 and 4 (last glacial period) correspond to the Malan formation (L1), and MIS 5 (last interglacial period) corresponds to palaeosol S1 (Fig.5. 2).

5.3 Dust Deposition and the source of loess

The primary mechanism of dust transport appears to be dust storms and 'calm events' (Ing 1972; Deere 1984; Liu et al. 1985; Merrill et al. 1989; Middleton 1991; Zhang et al. 1992, 1996, 1999; Mitsuta et al. 1995) that largely track northwest to southeast in the central Loess Plateau. Loess is also brought by the mid-latitude westerlies and deposited in the deserts of northwest China and the Loess Plateau primarily during April and early May (Merrill et al., 1989). Fang et al. (1999) suggest that coarse-grained material are also deposited by southerly winds emanating from a winter high pressure zone located above the Tibetan Plateau. However, the primary source of loess during the last glaciation are the deserts of north and northwest China and Mongolia (Bryan 1945; Liu et al., 1985; Middleton, 1991) as principally indicated by the regional decrease in thickness and grain size of loess leeward of the desert margin (Bryan 1945; Liu and Chang, 1964; Liu et al. 1985; Sun et al. 1995; Ding et al. 1999).

5.4 Stratigraphy of the Malan formation

From Wupu to Weinan (Fig. 5.1) the Malan formation (Fig. 5.2) is subdivided into three loess members and two palaeosols, based on field observations. Each of the loess members L1-5, L1-3 and L1-1 generally thin southward along the transect and thicken along the flack of the Qinling Mountains (Fig. 5.2). A southward decrease in grain size is also evident, although the rate of change differs slightly in each of the members (Ding et al. 1999). The lateral variations in grain size during the last glaciation (L1) are related to desert expansion and, in part, reflect proximity to the desert source (Ding et al. 1999). Sun et al. (1995) show that there were three periods of desert expansion and two periods of desert contraction (Fig. 5.3) during the last glaciation. Thus, lateral variations in grain size in the Malan formation are, in part, conjoined to five periods of relative movement of the desert margin.

The vertical grain size profiles also reflect desert expansion and contraction during cold and warm periods, respectively. The grain size profile within L1 (Fig. 5.2) fines upward to the top of palaeosol L1-4, and then generally coarsens upward to the top of L1-1. The fining upward of L1 to the top of palaeosol L1-4 reflects desert contraction, culminating in the development of palaeosol L1-4 during a relatively warm and wet period. The coarsening upward of L1 to the top of L1-1 reflects desert contraction during a cold period (MIS 2).

The architecture of the Malan formation and members also reflects proximity to the source. Sites close to the source exhibit relatively thick beds, while sites distal from the source exhibit relatively thin beds. The architecture of the members, indicated by the lines of correlation (Fig. 5.2), is similar to the architecture of the Malan formation. Thus,

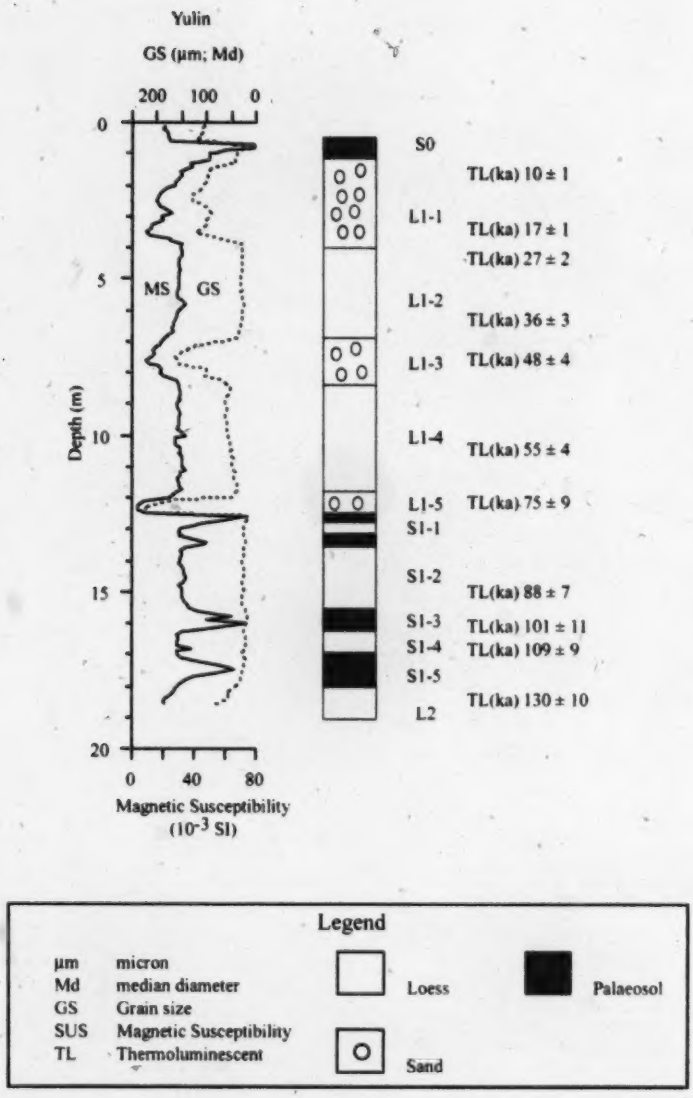

Figure 5.3. The Yulin site in the last glacial desert-loess transition zone near the north end of the transect in the central Loess Plateau (Sun et al. 1995).

at the scale of observation of the members, the internal correlations are regionally consistent, in that the members thin in a manner and direction similar to the Malan formation. This internal consistency is important for determining if the member beds incur the same wind direction(s) as the Malan. This seems to be the case; however, the transect represents a two-dimensional view of deposition (i.e. north-south), and a precise determination of palaeowind directions need to be determined from three-dimensional re-construction, by including an east-west component.

An ideal 2-dimensional representation of the morphology of the desert-loess depositional system may have an analogy in undathem-clinothem-fondothem morphologies (Fig. 5.4a, Rich 1951). These morphologies are typically observed in marine studies; where undathem represents a relatively flat near shore surface, clinothem a marginal marine slope, and fondothem the distal basinal environment. In this case, the undathem-clinothem-fondothem morphologies are analogous to the proximal, medial and distal environments of the desert-loess depositional system (Fig, 5.4b). Both the marine and terrestrial environments have a similar architecture that is related, in part, to proximity to the source. For example, relatively thick sediment of the Malan formation occur proximal to the source, while the distal sediment are relatively thin. Within the Malan the correlations are parallel or sub-parallel to the formation boundary, and converge distal from the source. Both of the lower members of the Malan thicken near the source, while the upper member (L1-1) thins near the source (e.g Yanchang to Wupu, Fig. 5.4b). At present we are not certain if the near-source thinning of the L1-1 member is a depositional trait or is due to erosion. Within the Malan formation, therefore, the vertical grain size profiles reflect desert expansion and contraction during the last

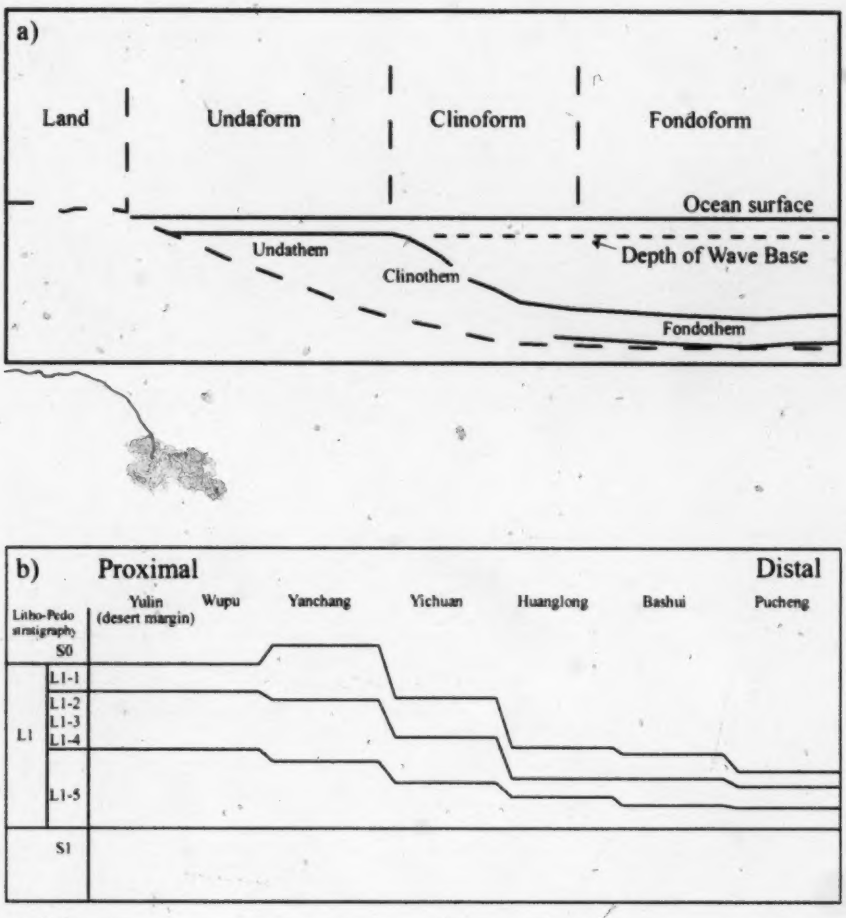

Figure 5.4. a) Schematic showing the undathem-clinothem-fondothem morphologies in a marginal marine setting. (modified after Rich 1951); b) Schematic showing the geometry of the Malan loess and its' members along the transect. The correlations are a scaled representation (vertical only) of Fig. 5.2 (1 cm = 5 m). See Fig. 5.2 for variations in grain size and magnetic susceptibility along the transect.

glaciation (MIS 2-4), while lateral grain size profile and the architecture of the Malan formation generally reflect proximity to the source.

5.5 Higher Resolution Correlations

The key assumption that is applied to the high frequency correlations is that the correlations will reflect desert expansion and contraction, and thinning distal from the source, similar to Malan formation and members. This is a reasonable assumption in stratigraphy, especially sequence and seismic stratigraphy, where the structure of the internal beds may follow the architecture of the formation (Boggs 1995).

In Fig. 5.5 the correlations are accomplished using common inflections in the records, and pattern matching the lithofacies variations along the transect. Correlations involving these criteria are commonly used in subsurface analysis (Cant 1992), although with continuous geophysical measurements rather than using discrete sample points. The correlations in Fig. 5.5 appear to be continuous along the transect. In general, pattern matching is easier near the source, as opposed to correlating in a distal environment where the strata are condensed. Correlation of the top of L1-1 is difficult. This may be due to local variations in deposition during the latter part of L1-1 (MIS 2), or perhaps erosion. Furthermore, the correlation of the middle member (L1-2, 3 and 4) at Huanglong is questionable. In the field, palaeosols L1-4 and L1-2 at Huanglong were not readily identified, so the middle unit (L1-2, 3 and 4) could have been eroded.

In general, the architecture of the high frequency correlations is similar to the Malan formation and members. The correlations are parallel to sub-parallel to the Malan and members, and converge distal from the source. This internal stratigraphic consistency

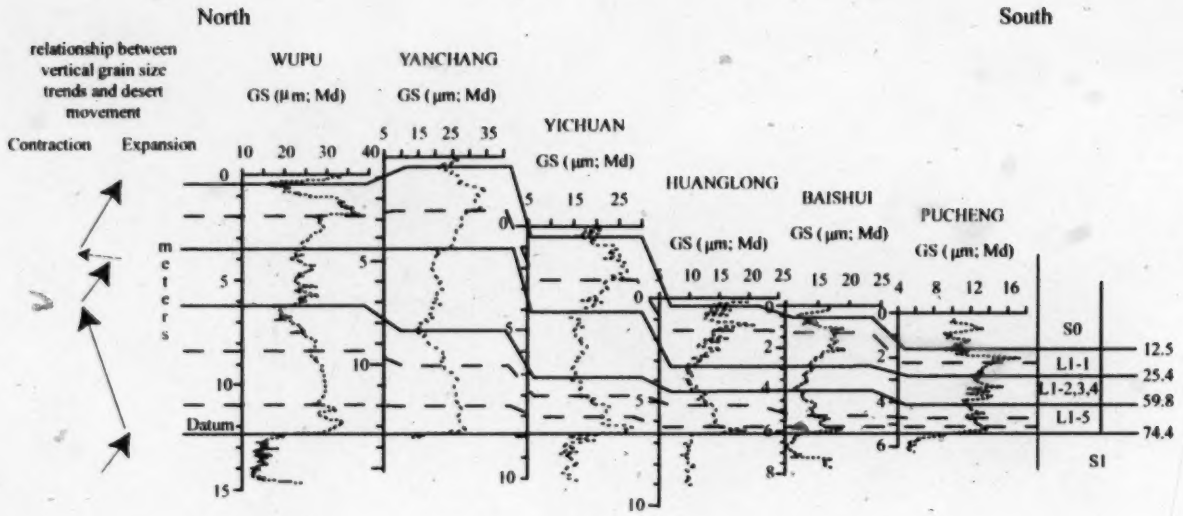

Figure 5.5. High resolution correlation of grain size along the transect. The correlations reflect lithostratigraphy. Note that the grain size scale is the reverse of Fig. 5.2. The dashed lines represent the higher resolution correlations.

may indicate that the wind direction is similar for the high resolution beds and the Malan formation, however the transect needs to be correlated to other locations in the Loess Plateau to confirm this hypothesis. Furthermore, the correlations continue to reflect the movement of the desert margin, where the correlations in the lower Malan reflect a back-stepping desert margin and the correlations in the upper Malan reflect a southward prograding desert margin.

5.6 Discussion

Variations in grain size of the Malan formation are regionally traceable in the central Loess Plateau. The correlations of the Malan and members reflect changes in grain size that are related, in part, to movement of the desert margin. At the three scales of observation the correlations generally follow a geometric pattern of thick proximal deposits and thin distal deposits. Within the desert-loess depositional system the correlations suggest that the Malan formation is regionally stratified, where the stratification is defined by changes in grain size. Bagnold (1941, p. 119) suggested that grain size differences between some aeolian layers are subtle, and may be defined by "a slight shifting in the peak diameter". The correlations within L1 inflections and patterns in the grain size curve that are based on slight shifts in the median diameter of loess. According to Bagnold's (1941) definition, the Malan formation appears to be stratified, where the grain size stratification is partly a function of movement of the desert margin.

Within the Malan formation, multiple peaks of grain size in the relatively thick, loess beds near the source appear to merge into a single peak in thin beds relatively distal from the source (Fig. 5.6). This observation, however, is partly related to the use of

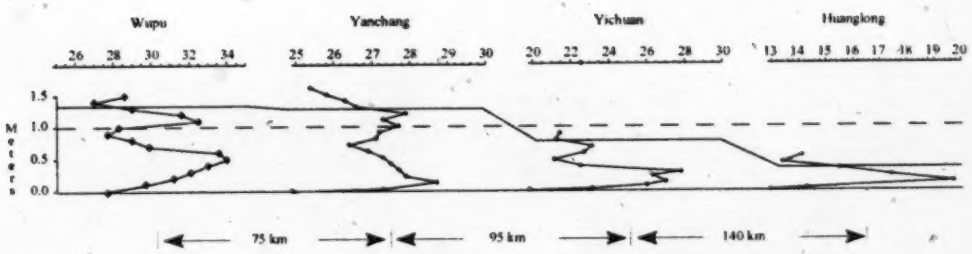

Figure 5.6. Actual variation in grain size at the base of L1-5 (see Fig. 5.2) showing the merging of relatively time-equivalent, high resolution grain size variations along the transect due to variations in accumulation rate and the use of discrete sample points. Vertical scale 1 cm = 1 meter; horizontal is not to scale.

discrete sample points rather than continuous measurements, and partly to the difference in the accumulation rates along the transect. For example, accumulation rates are higher in the northern Loess Plateau, near the source, than the southern Loess Plateau. The thinning of the beds distal from the source and the lateral continuation of the high-resolution correlations suggests that a 'condensed' bed of loess represents distal loess deposition. However, Rokosh et al. (submitted) suggest that the distal environment (i.e. condensed bed) of the Malan formation may not be present north of the Qinling Mountains. The Malan formation thickens against the flank of the Qinling Mtns. (see Fig. 5.2). A better representation of a distal environment, exhibiting a condensed bed of loess, may be the S1 unit (Fig. 5.2), where the associated desert margin is located well north of the Loess Plateau.

In general, the correlations within L1-5 are easier than within L1-1. The patterns and grain size inflections in L1-1 in the upper most Malan are difficult to trace (e.g. L1-1; Yichuan to Pucheng) and could indicate local reworking of the strata. There are, however, no visible deflation surfaces evident in the field at any of the locations, although field detection of deflation surfaces in sequential beds of loess is extremely difficult (Péwé and Liu 1995). An alternative hypothesis is that there was a greater variation in wind directions during L1-1 than L1-5. In this regard, Figure 4 in Ding et al. (1999) shows a southerly decrease in the weight percent sand (>63 μm) from Yulin to Bashui, and a slight increase in the weight percent sand over a few intervals within L1-1 from Bashui to Weinan. This suggests that there may be more variable wind components (e.g. direction(s) and magnitude) recorded in the upper Malan formation than in the lower Malan. Additionally, the difficulty in correlating within L1-1 is compounded by

the use of discrete sample points rather than continuous measurements. The best approach to studying high resolution variations of loess grain size is making continuous measurements in the Malan formation, using geophysical logs and continuous core.

5.7 Conclusions

The desert-loess depositional system of the Malan formation exhibits vertical grain size stratification that is, in part, related to movement of the desert margin. Lateral variations in grain size and the architecture of the Malan and members is related to proximity to the desert source. The relatively high resolution variations in grain size within the Malan appear to propagate regionally, at least along the eastern margin of the central Loess Plateau. These high resolution correlations are compatible with the architecture of the Malan formation and its' members and suggest that it is possible that there was a relatively consistent wind direction during deposition of the Malan. However, an interpretation that all variations in loess grain size are due to regional climate change (by correlation to Greenland ice core, for example) may be incorrect. Some of the peaks and troughs in the upper Malan may not correlate, and this could reflect local climatic variations, multiple wind directions in the upper Malan. Furthermore, some of the variations that do not correlate may be influenced by a non-climate events such as local re-deposition.

5.8 References

An, Z. and Porter, S. 1998. Millenial-scale climatic oscillations during the Last Interglaciation in Central China. Past Global Changes (PAGES) Newsletter, 6, 4.

Bagnold, R.A.1941. The physics of blown sand and desert dunes. Metheun & Co., London. pp. 265.

Boggs, S. Jr. 1995. Principles of Sedimentology and Stratigraphy. Prentice Hall, New Jersey. pp.774.

Bryan, K., 1945, Glacial versus desert origin of loess. American Journal of Science, 243: 245-248.

Cant, D.J. 1992. Subsurface facies analysis. In Facies Models, response to sea level change. Edited by R.G. Walker and N.P. James. Geological Association of Canada, Stittsville. pp. 27-46.

Chen, F.H., Bloemendal, J. Wang, J.M., Li, J.J. and Oldfield, F. 1997. High-resolution multi-proxy climate records from Chinese loess; evidence for rapid climatic changes over the last 75 kyr. Palaeogeography, Palaeoclimatology, Palaeoecology, 130, 1-4. 323-335.

Chen, F.H., Wang, J.M., and Bloemendal, J. 1998. East Asian monsoon variations during the last interglacial: evidence from the northwest margin of the Chinese Loess Plateau. Past Global Changes (PAGES) Newsletter, 6, 10.

Deere, Z. 1984. Synoptic-climatic studies of dust fall in China since Historic times. Scientia Sinica (Series B), 27: 825-836.

Derbyshire, E., Keen, D., Kemp, R.A., Rolph, T.A., Shaw, J., and Meng, X.M. 1995. Loess-paleosol sequences as recorders of palaeoclimatic variations during the last glacial-interglacial cycle: some problems of correlation in north-central China. *In* Wind blown sediments in the Quaternary record. *Edited by* E. Derbyshire. John Wiley & Sons, Chichester, pp. 7-18.

Derbyshire, E., Kemp, R.A., and Meng, X.M. 1997. Climate change, loess and paleosols: proxy measures and resolution in China. Journal of the Geological Society of London, 154, 793-805.

Ding, Z., Sun, J., Rutter, N.W., Rokosh, D. and Liu, T. 1999. Changes in the sand content of loess deposits along a north to south transect of the Chinese Loess Plateau and the implications for desert variations. Quaternary Research, 52, 56-62.

Ding, Z., Sun, J. Yu, Z. and Liu, T. 1998. Chronology of environmental events over East Asia during the last 130 ka. Chinese Science Bulletin, 43, 1761-1769.

Ding, Z.L., Yu, Z., Rutter, N.W., and Liu, T.S. 1994. Towards an orbital time scale for Chinese loess deposits. Quaternary Science Reviews, **13**:39-70.

Emiliani, C. 1955. Pleistocene Temperatures. Journal of Geology, **63**: 6, 538-578.

Fang, X., Li, J., Banerjee, S., and Van der Woo, R. 1998a. Last Interglacial sharp monsoon fluctuations: rock magnetic and paleomagnetic evidence from high resolution loess-paleosol sequence, Lanzhou, China. Past Global Changes (PAGES) Newsletter, 6, 6.

Fang, X.-M., Pan, B.-T., Li, J.-J., Ono, Y., Fukusawa, H., Nagatsuka, S. and Torii, M. 1998b. High Resolution pedogenic and rock magnetic records of Asian summer monsoon instability during the past 60,000 years from the Chinese western Loess Plateau. PAGES Newsletter, 6, 7.

Fang, X., Li, J., and Van der Woo, R. 1999. Rock magnetic and grain size evidence for intensified Asian atmospheric circulation since 800,000 years B.P. related to Tibetan uplift. Earth and planetary Science Letters, 165; 129-144.

Ing, G.K.T. 1972. A dust storm over Central Asia, April 1969. Weather, 27: 136-145.

Kemp, R.A., Derbyshire, E., Meng, X., Chen, F. and Pan, B. 1995. Pedosedimentary reconstruction of a thick loess-Paleosol sequence near Lanzhou in north-central China. Quaternary Research, 43, 30-35.

Kukla, G.J., 1987a. Correlation of Chinese, European and American loess series with deep-sea sediments. *In* Aspects of Loess Research. *Edited by* T. Liu. Ocean Press, Beijing, pp. 27-38.

Kukla, G. 1987b. Loess stratigraphy in central China and correlation with an extended oxygen isotope time stage scale. Quaternary Science Review, 6: 191-220.

Liu , J. Liu, T. and Chen, T. 1998. Loess dating progress in China. Past Global Changes (PAGES) Newsletter, 6, 2.

Liu, J., Nie, G., Chen, T., Song, C., Zhu., G., Li, K., Gao, Z., and Qiao, Y. 1995. A preliminary high resolution time scale for the last 130,000 years at Weinan loess section. Sciencia Geologica Sinica (Overseas Edition; Supplementary Issue), Beijing, China, 1, 9-22.

Liu, T., and Chang, T. 1964. The "HuangTu" (loess) of China. Report of the Sixth INQUA Congress, Warsaw 1961, 4, pp. 503-524.

Liu, T.S. et al. 1985. Loess and the Environment. China Ocean Press. 251 pp.

Merrill, J.T., Uematsu, M. and Bleck, R. 1989. Meteorological analysis of long range transport of mineral aerosols over the North Pacific. Journal of Geophysical Research, 94, 8584-8598.

Middleton, N.J. 1991. Dust Storms in the Mongolian People's Republic: Journal of Arid Environments, 20: 287-297.

Mitsuta, Y., Hayashi, T., Takemi, T., Hu, Y., Wang, J., and Chen, M. 1995. Two severe local storms as observed in the arid area of Northwest China. Journal of the Meteorological Society of Japan, **73**: 1269-1284.

Péwé, T.L., Liu, T., Slatt, R.M., and Li-B. 1995. Origin and character of loesslike silt in the southern Qinghai-Xizang (Tibet) Plateau, China. U.S. Geological Survey Professional Paper, 55 pp.

Porter, S. and An, Z. 1995. Correlation between climate events in the North Atlantic and China during the last glaciation. Nature, 375, 305-308.

Rich, J.L. 1951. Three critical environments of deposition and criteria for recognition of rocks deposited in each of them. Geological Society of America Bulletin, 62, 1-20.

Rokosh, D., Rutter, N.W., Ding, Z. and Sun, J. (submitted). Regional stratigraphy of the central Loess Plateau, China over the last 130,000 years: links to climatic forcing. Canadian Journal of Earth Science.

Rutter, N.W., Ding, Z. and Liu, T. 1997. Reliability of grain size variation as a climatic proxy and correlation method for loess-paleosol units, North-Central China. International Conference on Geology, Geotechnology and Mineral Resources of Indochina (Geo-Indo 95), November 22-25, Khon Kaen, Thailand, 45-52.

Rutter, N.W., Rokosh, D., Ding, Z. and Liu, T. 1998. High resolution paleoclimate records from the loess-desert margin. Desert Margin Changes in Africa since 135 ka: Implications for Water, Carbon & Man. International Geological Correlation Program 349/404, Jan 5-12 1997, pp. 100-102.

Sun, J., Ding, Z., and Liu, T. 1995. The environmental evolution of the desert-loess transition zone over the last glacial-interglacial cycle. *In* Quaternary Geology and Past Environmental changes in China. *Edited by* S. Wang. Science Press, Beijing, pp. 1-8.

U.S. Defense Mapping Agency Aerospace Center 1987, Operational Navigation Chart, Sheets F-7, F-8, G-8, G-9. U.S. Department of Defense.

Vandenberghe, J., An, Z.S., Nugteren, G., Lu, H.Y., and Van Huissteden, K. 1997. New absolute time scale for the Quaternary climate in the Chinese loess region by grain-size analysis. Geology, **25**:35-38.

Zhang, X., An, Z., Liu, D., Chen, T., Zhang, G., Arimoto, R., Zhu, G., and Wang, X. 1992. Study on three dust storms in China-source characterization of atmospheric trace element and transport process of mineral aerosol particles. Chinese Science Bulletin, 37: 940-945.

Zhang, X., Chen, Z., Zhang, G., Chen, T., and Liu, H. 1996. Remote mineral aerosols in Westerlies and their contributions to the Chinese loess. Science in China (Series D), 39: 134-143.

Zhang, X.Y., Arimoto, R., and An, Z.S. 1999. Glacial and interglacial patterns for Asian dust transport. Quaternary Science reviews, 18, 811-819.

Zhao, S. 1986. Physical Geography of China. Science Press, Beijing and John Wiley & Sons, New York. 209 pp.

CHAPTER 6

Hydrologic and geologic factors that influence spatial variations in loess deposition in China during the last interglacial-glacial cycle: results from proxy climate and GCM analyses

(submitted to Palaeogeography, Palaeoclimatology, Palaeoecology)

Authorship: Rokosh, D., Bush, A.B.G., Rutter, N.W., Ding, Z. and Sun, J.

6.1 Introduction

In the Loess Plateau of China, the basic geologic and climatic model explaining loess deposition during cold and warm periods is that loess grains are larger and beds are thicker during glacial periods than interglacial periods (Liu et al. 1985; An et al. 1991a, b; Ding et al. 1995; Shackleton et al. 1995; Vandenberghe et al. 1997). According to this model, loess deposition continues during interglacial periods but at a reduced rate of deposition. Using these observations as a guide, the two main palaeoclimatic mechanisms that affect glacial and interglacial variations in loess deposition have been: 1) variations in insolation received (e.g. An et al. 1991a; Imbrie et al. 1992), and 2) global ice volume variations (e.g. Liu and Ding 1993; Ding et al. 1995; Shackleton et al. 1995). However, these palaeoclimatic forcing mechanisms were interpreted using a simple, geologic model that is based solely on temporal variations in loess grain size and accumulation rates, and assumes that the temporal variations are also representative of spatial variations. More recently, Rokosh et al. (submitted) suggest that temporal variations in loess grain size and accumulation rates are not representative of spatial variations in these properties. They compared loess grain-size, thickness and

accumulation rates in the Loess Plateau during the last interglacial and glacial periods, and developed a new model of loess deposition that contains both spatial and temporal components. According to this model loess deposition is best interpreted as part of a desert-loess depositional system where sediment texture (Ding et al. 1999) and loess distribution are largely controlled by desert expansion and contraction, during cold and warm periods, respectively. In this two-component model, a comparison of the last interglacial and glacial depositional systems shows that there is very little difference between these systems in terms of the size of loess grains, the thickness and geometry of the beds, and loess accumulation rates. However, the principal distinction between the last glacial and interglacial depositional systems is that the distribution of loess is different, owing to desert expansion and contraction during glacial and interglacial periods, respectively. Thus, variations in global ice volume exert a less direct influence on variations in Chinese loess grain size, thickness and accumulation rates than earlier interpretations.

In this paper we use the new model of loess deposition and results from a coupled ocean-atmosphere General Circulation Model (GCM) analysis to determine the influence of hydrologic and geologic factors on glacial to interglacial variations in loess deposition. We take a four-fold approach to our analyses: 1) Review the links between variations in insolation, ice volume and loess deposition during the last interglacial-glacial cycle; 2) Review the new model of loess deposition during the last interglacial-glacial cycle, using results from a north to south transect of the Loess Plateau (Fig. 6.1). The geologic and climatic controls on spatial and temporal variations in loess deposition are outlined. We add additional details to this model by examining variations in

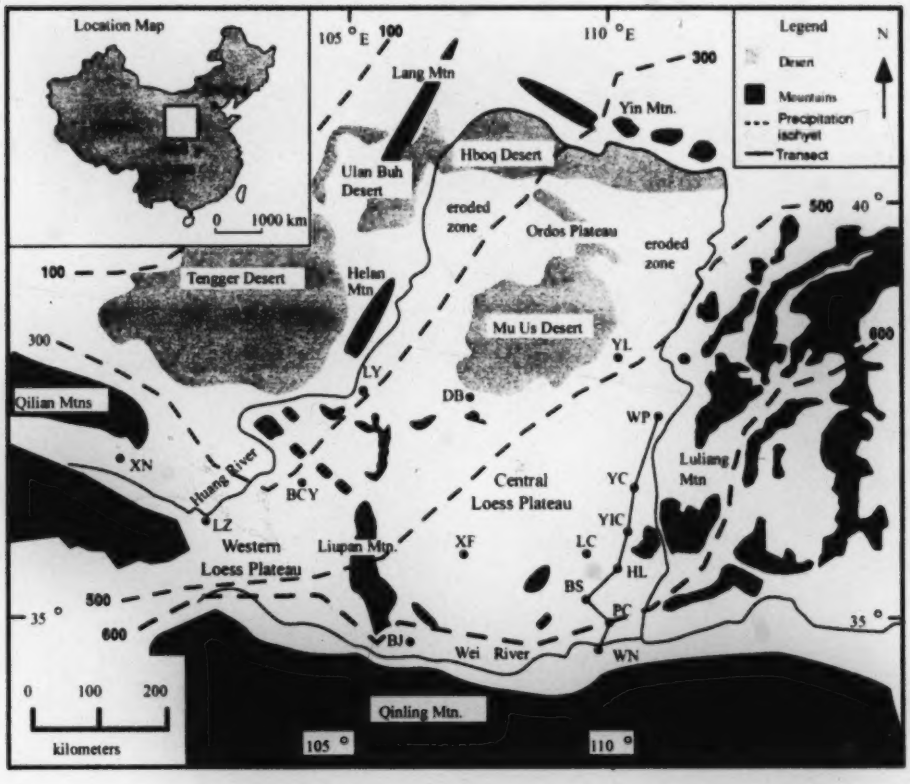

Central Loess Plateau				Western Loess Plateau	
BJ	Baoji	BS	Baishui	BCY	Baicouyuan
DB	Ding Bien	HL	Huanglong	LZJ	Lanzhou (JZT)
LC	Luochuan	LJY	Lija Yuan	LZG	Lanzhuo (GLS)
PC	Pucheng	WN	Weinan	XN	Xining
WP	Wupu	XF	Xifeng		
YC	Yanchang	YIC	Yichuan		
YL	Yulin				

Figure 6.1. Map of the Loess Plateau showing the location of the sites mentioned in the text. The isohyets (mean annual precipitation) are from Zhao (1986).(Modified from US Defense Mapping Agency Aerospace Center, Operational Navigation Chart Series ONC, Sheets F-7, F-8, G-8 and G-9, Edition 4, 1987).

sedimentology and stratigraphy within the last glaciation [i.e. Malan formation, Marine Isotope Stage (MIS 2-4); Liu et al. 1985]; 3) Examine climatic and hydrologic factors that influence modern loess deposition in Northern China in order to gain insight into the controls on dust deposition during the last interglacial period, and possibly, the last glacial period; 4) Generate a numerical simulation of soil moisture during the last glacial maximum (LGM) in East Asia using the coupled GCM of Bush and Philander (1999), and determine factors that may influence interglacial to glacial variations in soil moisture.

6.2 Methods

Grain size and magnetic susceptibility were determined on loess and palaeosol samples from seven sites in the central Loess Plateau (Fig. 6.1). Samples were taken every 5-10 cm in the L1 loess bed and 2-5 cm in the S1 palaeosol. A smaller sample interval was taken in thinner loess beds at the southern end of the transect. Bulk magnetic susceptibility and grain size were determined on each sample. Grain size analysis was performed on a PRO-700 SK Laser Micron Sizer. An analysis of 20 replicate samples indicated a precision of 3.5%. Organic material, pedogenic iron and carbonates were removed prior to analysis. Bulk magnetic susceptibility was determined using a Bartington MS II susceptibility meter. Susceptibility values represent one reading on an approximately 50 gram bagged sample. The values are presented as carbonate-free by calibrating each sample to the amount of carbonate present using the formula:

$$A2 = A1 * (100/100\text{-wt.\% C})$$

where A1 and A2 are the measured and resultant magnetic susceptibility, respectively, and C is the weight. % carbonate.

Age control is determined by correlation to the age model of Liu, J. et al. (1995), developed at Weinan at the south end of the transect (Fig. 6.1). The chronology of the Liu, J. et al. (1995) model spans the last ca. 130 ky and is based on Accelerator Mass Spectrometry (AMS) measurements on radiocarbon and on Thermoluminescence (TL) measurements from loess and palaeosols. Loess-palaeosol alternations have also been correlated to Marine Oxygen Isotope Stages (MIS) (Liu et al. 1985; Kukla 1987a,b; Liu, J. et al. 1995), where MIS 2, 3 and 4 (last glacial period) correspond with the Malan loess (L1), and MIS 5 (last interglacial period) corresponds with palaeosol S1 (Fig. 6.2). The Malan loess is further sub-divided in this paper into members L1-1 to L1-5, where L1-1 corresponds to MIS 2, while L1-2, 3 and 4 correspond with MIS 3, and L1-5 with MIS 4.

6.3 Comparison of loess and susceptibility records with global ice volume and insolation variations during the last interglacial-glacial cycle

In this section we will review the correlation between variations in ice volume and insolation, and temporal variations in loess grain size and accumulation rates. Grain size and susceptibility records from Wupu and Yanchang in the Loess Plateau (Fig. 6.1 and 6.2) are compared with oceanic $\delta^{18}O$ curves and a top-of-the-atmosphere insolation record from Berger and Loutre (1991). The $\delta^{18}O$ records are from the Maldives Ridge (core MD900963; Latitude 05°03.30'N; Longitude 73°52.60'E) of the tropical IndianOcean (Bassinot et al. 1994), and ODP 677 in the eastern equatorial Pacific Ocean

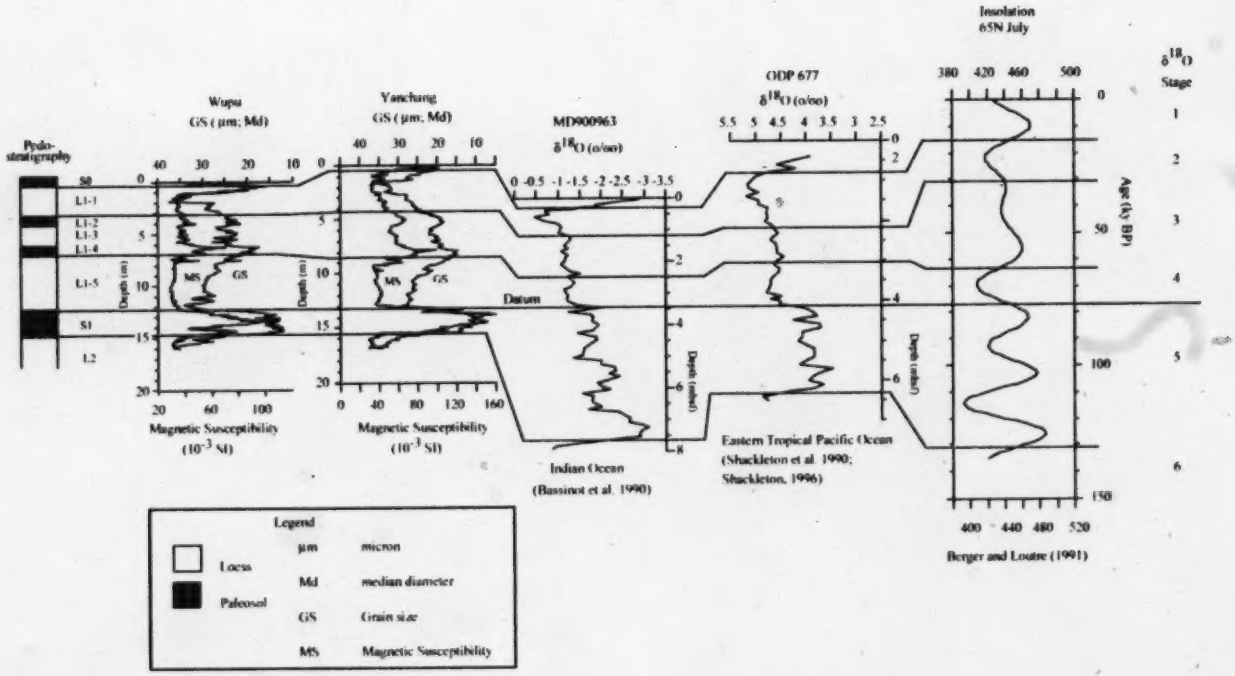

Fiurte 6.2. Comparison of loess-palaeosol stratigraphy with δ18O records from the Indian and Pacific Oceans. The Berger and Loutre (1991) insolation values are calculated relative to the 1950 AD value of 427 W/m2.

(Shackleton et al. 1990; Shackleton 1996; Latitude 1°12'N, Longitude 83°44'E). The glacial to interglacial variation in $\delta^{18}O$ from core MD900963 may be influenced by a local salinity changes, which Bassinot et al. (1994) suggest is most likely controlled by changes in monsoon intensity.

In Fig. 6.2, the stratigraphy during the last glaciation is an alternating series of loess beds (L1-1, L1-3, and L1-5) and palaeosols (L1-2 and L1-4). The insolation curve exhibits three periods of relatively reduced insolation intensity and two periods of increased intensity during the last glaciation (e.g. Berger and Loutre 1991; see also Prell and Kutzbach 1987). Insolation and grain size variations are inversely correlated, while the susceptibility profile is linearly correlated with insolation during this period. The loess-palaeosol variations correspond very well with the curve of Berger and Loutre (1991), showing periods of relatively reduced insolation intensity corresponding to the loess beds and higher insolation intensity corresponding to the palaeosols.

$\delta^{18}O$ curves, including the ones shown in Fig. 6.2, generally show a steady increase in ice volume beginning early in MIS 5, and peak during MIS 2. Most deep sea $\delta^{18}O$ curves show higher ice volumes during MIS 2 than MIS 4 and a slight reduction in global ice volume during interstadial MIS 3. This corresponds very well with the grain size and susceptibility profiles at Wupu and Yanchang. The grain size variations show more abrupt changes during the last glaciation, however differences in sample resolution of the deep-sea and loess records may, in part, explain differences in the magnitude of the changes.

Both $\delta^{18}O$ and insolation variations show a strong correlation with loess grain size and accumulation rate. A temporal comparison of grain size and accumulation rates

clearly shows that loess grains are larger, and beds are thicker during glacial periods than interglacials periods (Liu et al. 1985; An et al. 1991a, b; Ding et al. 1995; Shackleton et al. 1995; Vandenberghe et al. 1997). This is the basic temporal geologic and climatic model relating loess deposition to variations in insolation and global ice volume. In the next section we will examine the two component loess depositional model. In particular, we examine and compare variations in loess grain size and accumulation rates during the last interglacial and glacial periods.

6.4 Loess Depositional Model

Along the transect from Wupu to Weinan (Figs. 6.1 and 6.3) the Malan formation (L1; MIS 2-4) is subdivided into three loess members and two palaeosols, based on field observations. Alternating loess and palaeosols reflect variations in the rate of loess accumulation along a shifting climatic gradient (Pye 1987; Pye and Tsoar 1987). Both the Malan loess and its members generally thin southward along the transect, and then thicken southward along the flank of the Qinling Mountains (Figs. 6.1 and 6.3). The geometry of the correlations within the Malan formation are consistent and suggests a relatively consistent wind direction during deposition of the Malan and its members.

The Malan formation exhibits a southward decrease in grain size (Liu and Chang 1964). Lateral variations in grain size in the Malan reflect proximity to the desert source (Ding et al. 1999). In the desert-loess transition zone near Yulin (Figs. 6.1 and 6.4), Sun et al. (1995) show that there were at least three periods of desert expansion and two periods of desert contraction during the last interglacial-glacial cycle. Thus, lateral

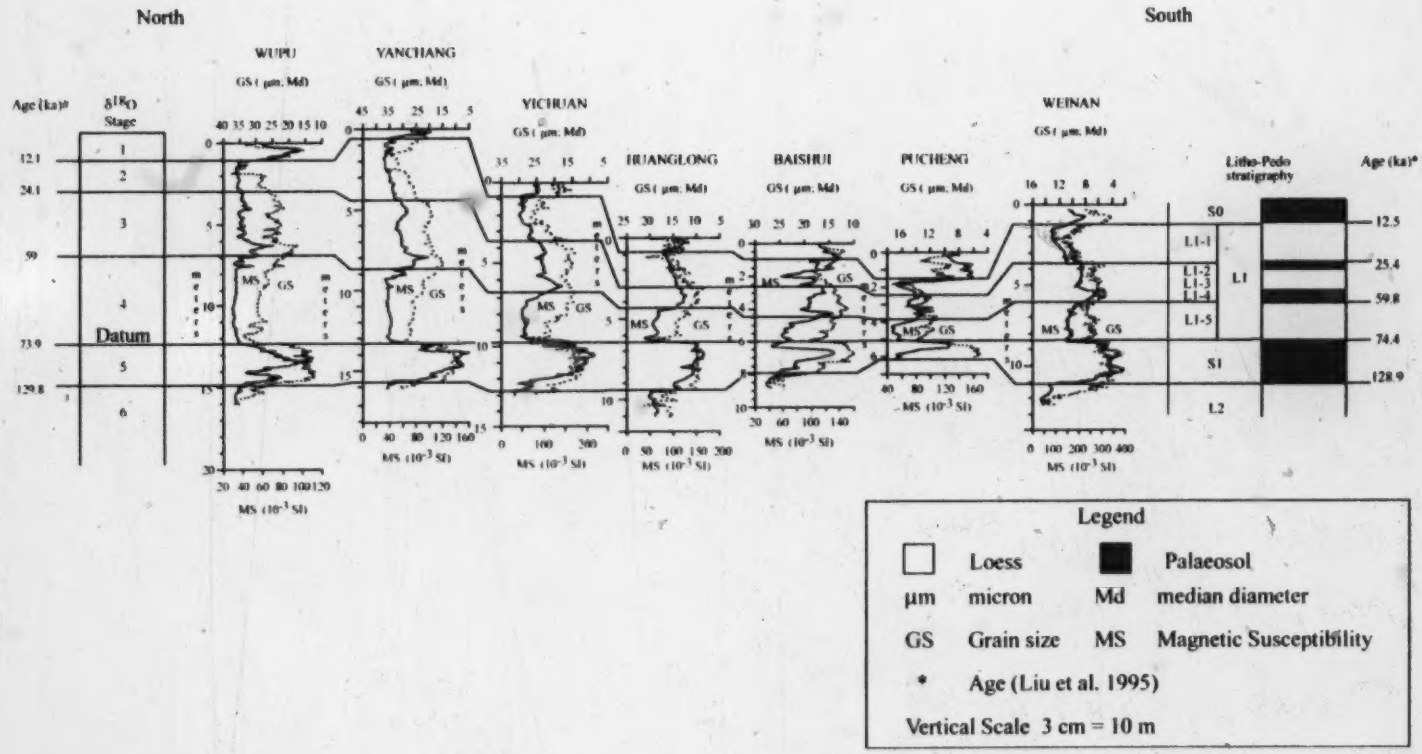

Figure 6.3. Stratigraphic cross-section from the central Loess Plateau showing the continuity of the strata along the north to south transect. All locations use the same vertical scale (1 cm = 3 meters). All magnetic susceptibility values are carbonate-free.

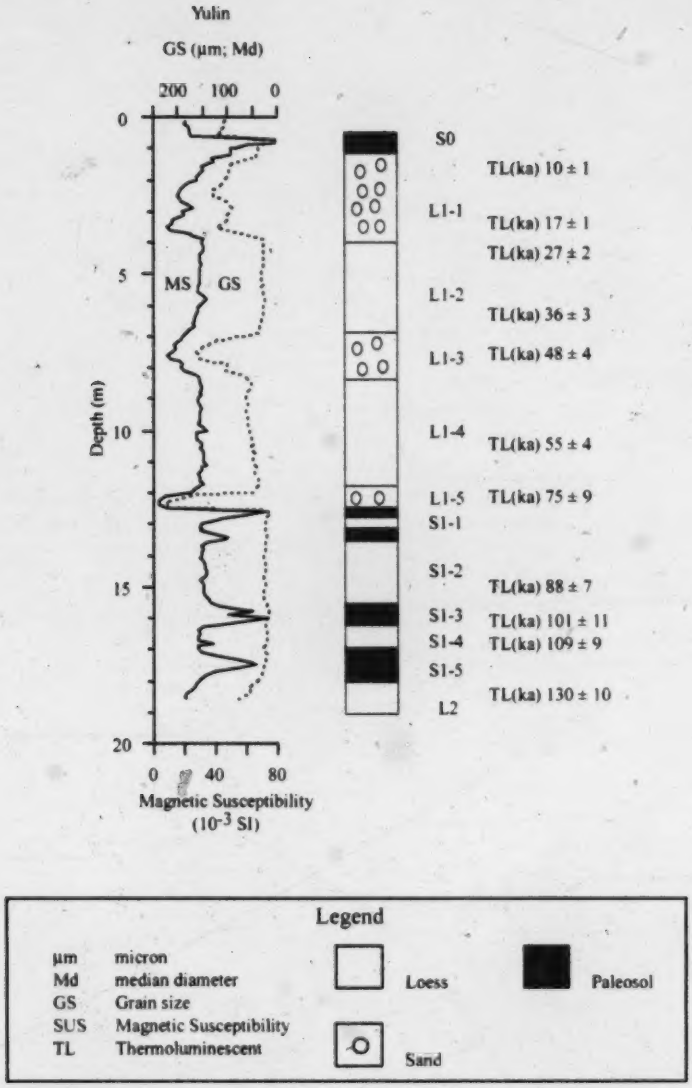

Figure 6.4 The Yulin site near the north end of the transect in the desert-loess transition zone of the last glacil period. (Sun et al. 1995; Sun and Ding, 1998

variations in grain size are, in part, coupled to the movement of the desert margin.

The vertical grain size profiles also reflect desert expansion and contraction during cold and warm periods, respectively. The grain size profile within L1 (Fig. 6.3) fines upward to the top of palaeosol L1-4, and then generally coarsens upward to the top of L1-1. The fining upward trend of L1 to the top of palaeosol L1-4 reflects desert contraction, culminating in the development of palaeosol L1-4 during a relatively stable, warm and wet period. The coarsening upward profile, from L1-4 to the top of L1-1, reflects desert expansion during the last glaciation (MIS 2).

The peak median diameter of loess along the transect displays a relatively steady increase northward toward the source during both the last interglacial and glacial periods (Fig. 6.5). Interglacial and glacial loess grains that are relatively close to the source are similar in size (e.g. Yulin interglacial and Yichuan glacial; Weinan glacial and Yichuan interglacial); however the distribution of the grains was different during the last glacial and interglacial periods, owing to desert expansion and contraction, respectively. The regional distribution of the grains suggests that temporal geologic model of larger grains during glacial periods than interglacial periods does not accurately reflect regional variations. The affect of variations in global ice volume on loess deposition, therefore, is to influence the distribution of loess grains through desert expansion and contraction.

Loess beds are generally thickest and accumulation rates are highest near the source during both the last glacial and interglacial periods (Fig. 6.6). There is no consistent display of glacial loess beds being thicker (Rokosh et al. submitted) or showing higher accumulation rates than interglacial loess beds (Fig. 6.6) as suggested in earlier interpretions (Shackleton et al. 1995). For example, loess accumulation rates

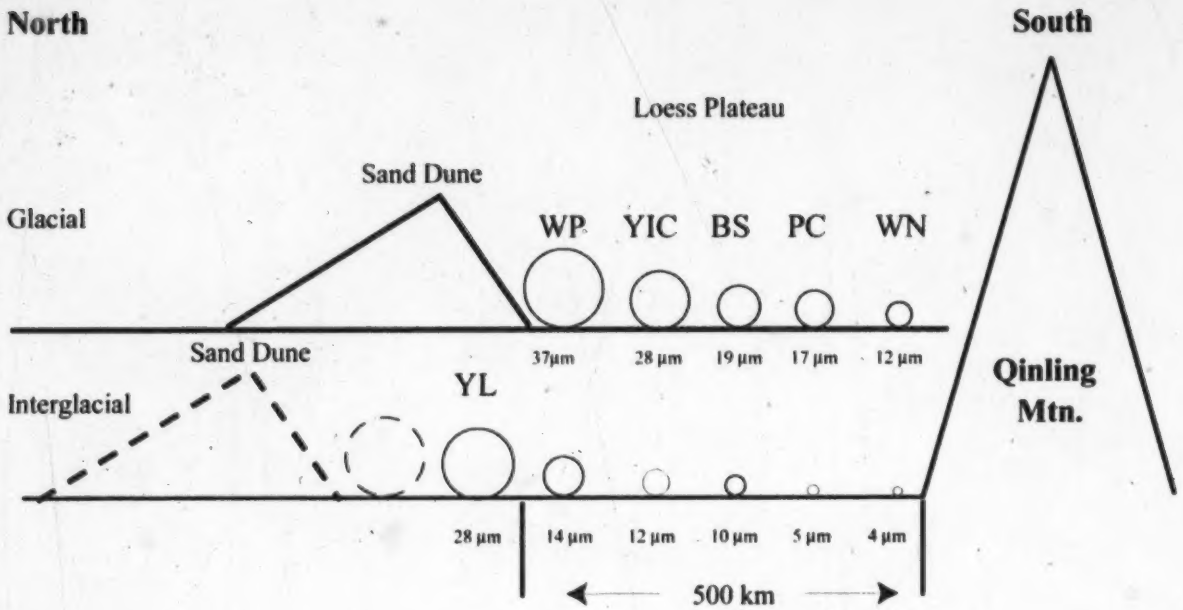

Figure 6.5. Schematic model of variations in grain size. The size of the grains represent actual variations along the transect relative to the peak median diameter at Wupu during the last glacial (Mis 2) and interglacial (MIS 5) periods. The dashed interglacial grain represents the assumption of grain size increasing northward (upwind) of Yulin toward the source. See Fig. 6.1 for a list of the location abbreviations.

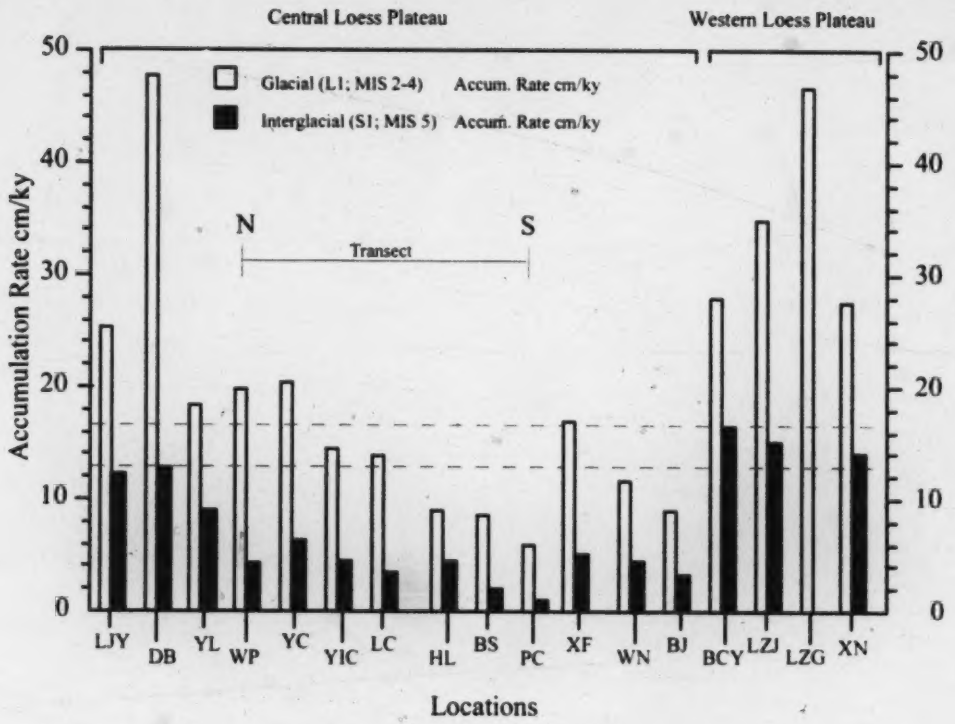

Central Loess Plateau				Western Loess Plateau	
BJ	Baoji	BS	Baishui	BCY	Baicaoyuan
DB	Ding Bien	HL	Huanglong	LZJ	Lanzhou (JZT)
LC	Luochuan	LJY	Lija Yuan	LZG	Lanzhuo (GLS)
PC	Pucheng	WN	Weinan	XN	Xining
WP	Wupu	XF	Xifeng		
YC	Yanchang	YIC	Yichuan		
YL	Yulin				

Figure 6.6. Spatial and temporal comparison of accumulation rates in the Central and Western Loess Plateau during last glacial and interglacial periods. The dashed lines have been set at the sites with the maximum interglacial accumulation rates in the Western (BCY) and Central Loess Plateau (DB), respectively. See Fig. 6.1 for the site abbreviations and distribution of the sites. Publications used to estimate the thickness of the deposits are: YL Sun et al. 1995, 1998; LZ Liu et al. 1991, Rousseau and Wu 1997; BJ Rutter et al. 1991; LY and DB Rutter et al. 1998; XF Liu et al. 1985; Liu, X.M. et al. 1995; BCY Evans and Heller 1994; Hunt et al. 1995; JZT Derbyshire et al. 1995; Fang et al. 1998, JZT = Jiuzhoutai 4 km north of Lanzhou; GLS Derbyshire et al. 1997, GLS = Goulanshan, 10 km SSE of Lanzhou, XN Hunt et al. 1995; all other locations Rokosh et al. in press.

(using the MIS 1/2, 4/5 and 5/6 boundaries of Liu, J. et al. 1995) are higher during the last interglacial period (S1; MIS 5) at Yulin, Ding Bien, Lijia Yuan, Lanzhou, Xining and Baicaoyuan than are most glacial loess beds in the southern Loess Plateau (Figs. 6.1 and 6.6). This suggests that the thickness and accumulation rate of glacial and interglacial loess beds reflect, in part, proximity to the desert source (Fig. 6.7). The geometry and thickness of the loess deposits in the two-component model resemble proximal, medial and distal environments, where the distal environment is a thin, condensed section of loess (Fig. 6.7). The two-component model suggests that there may be little difference, if any, in the regional thickness and accumulation rates of the last glacial and interglacial desert-loess depositional systems. In contrast, the temporal model suggests that loess accumulation rates are higher during glacial periods than interglacial periods. However, this observation is derived by comparing loess accumulation rates from sediments deposited relatively close to the source (during a glacial period) to loess deposited distal from the source (during an interglacial period) (Figs. 6.5, 6.6 and 6.7). Thus temporal depositional model does not accurately reflect regional (i.e. spatial) variations in loess thickness or accumulation rates.

However, the reconstruction of the desert-loess depositional system is incomplete; sediment proximal to the last interglacial desert margin, and sediment distal from the last glacial desert margin have not been located. For this reason, we cannot compare, for example, proximal grain size and accumulation rates during the last interglacial and glacial periods. Nonetheless, the present results suggest that variations in loess accumulation rates, and grain size, during the last interglacial-glacial cycle may be influenced by climatic or non-climatic factors other than, or in addition to, desert

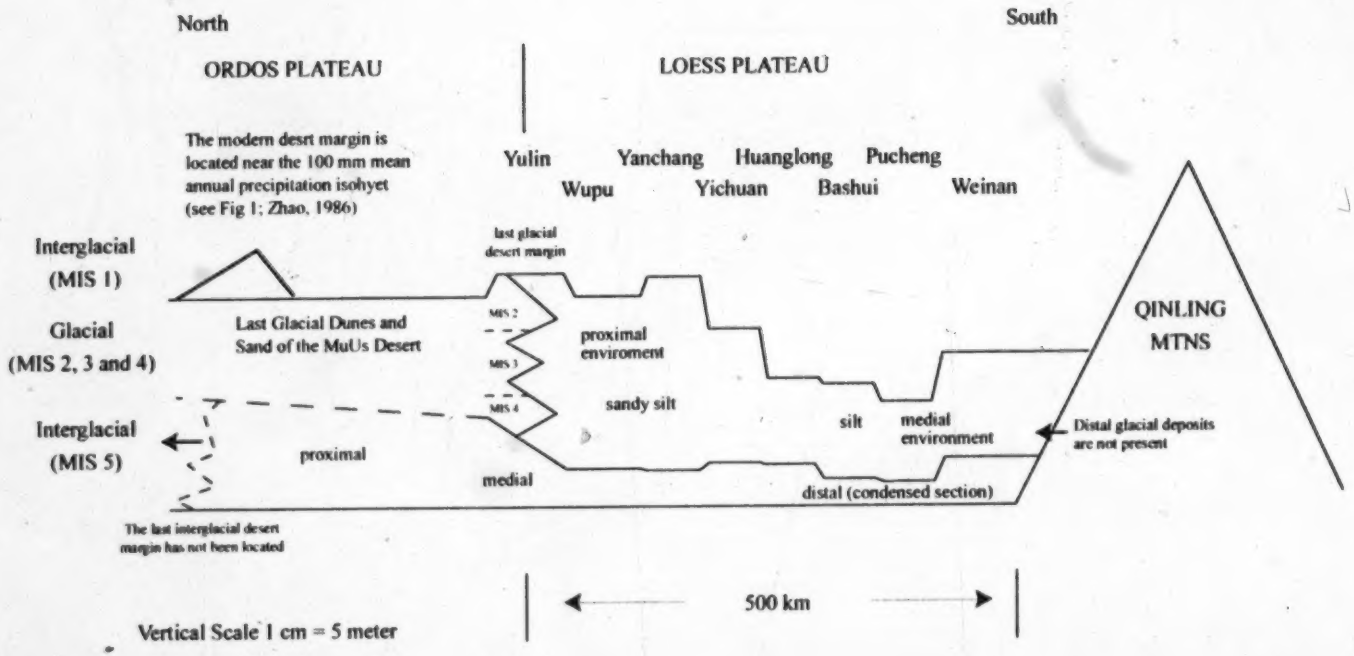

Figure 6.7. Schematic showing the distribution of loess and variations in the position of desert margin during the last interglacial-glacia cycle using the correlations from Fig. 6.3. Vertical scale 1 cm = 5 m. Horizontal distance is not to scale. The dashed lines indicate that the last interglacial sediment north of the Loess Plateau have not been located.

migration and global ice volume variations. In the next section we will examine some of the factors that affect modern loess deposition, in order to gain some insight into past processes that may have operated in the Loess Plateau.

6.5 Modern Dust Deposition

Modern dust accretion in north China occurs largely during dust storms or 'calm' events when a rain of dust occurs with very little surface wind apparent. (Deere, 1984; Zhang et al. 1992, 1999). Dust storms occur most frequently during April and May, and to a lesser extent during autumn (Ing 1972; Deere, 1984; Liu et al. 1985; Littmann 1991, Middleton 1991; Merrill et al. 1989; Zhang et al. 1992; Mitsuta et al. 1995). According to Littmann (1991), dust storms in north China from 1976-86 were associated with cold surges (see also Pye 1987) during the spring, emanating from the high Arctic (Ren et al. 1985; Chang 1987; Murakami 1987). Dust storms are also associated with winter cold surges (Littmann 1991), but at present the winter storms are less frequent than the spring storms in North China (Merrill et al. 1989; Littmann 1991). Hence, at present loess deposition largely occurs after the arid winter monsoon retreats (e.g. late March, Chang 1987), and prior to the onset of the wet summer monsoon (e.g. about mid-July, Tao and Chen 1987) at a time when the Siberian High pressure system is relatively weak or absent (Barry and Chorley 1968; Littmann 1991; Chang 1987).

Three main factors govern the potential for loess deposition (Tsoar and Pye 1987): 1) the availability of silt, 2) the frequency, magnitude and direction of transporting winds, and 3) a suitable sediment trap. In the modern record in China, the dust storm maxima, according to Littmann (1991), correspond to periods of low soil

water storage during the spring, when there is a maximum in evapotranspiration and surface heating (Gillette 1986; Littmann 1991). The spring maxima in dust storm frequency (from 1976-1986; Littmann 1991) shows a very weak correlation with mean monthly temperature ($r = -0.03$), a positive correlation to evaporation ($r = 0.31$), and an inverse correlation with both ground-level atmospheric pressure ($r = -0.46$) (see also Pye 1987), and mean monthly precipitation ($r = -0.26$) (Littmann 1991). Furthermore, there is no correlation between the seasonal strength of winds and dust storm frequency (Littmann 1991). The strongest winds at present occur during the winter in China, while dust storms are most frequent during the dry spring. Thus, at present soil moisture content exerts a strong influence on the availability of dust in China for re-sedimentation in the Loess Plateau.

6.6 Soil moisture content during the last glaciation

Based on a multi-criteria approach (palynologic, pedogenic, palaeocryogenic, palaéoecologic), Velichko (1984) determined that continental Siberia at the LGM was cooler and drier than present, whereas the east Asian coast was wetter. According to Velichko (1984), the Scandinavian Anticyclone (related to the north Eurasian ice sheets), along with the Siberian and Polar Anticyclones "merged" (to a degree), leading to a cooler and drier climate in East Asia. Results from a numerical simulation of the LGM with a coupled atmosphere-ocean GCM (Bush and Philander, 1999) indicate that, according to the soil moisture content, the Asian continental interior is drier at the LGM whereas the east coast tends to be wetter (Figure 6.8a). This pattern of soil moisture difference is in good agreement with that presented by Velichko (1984). Diagnosis of the

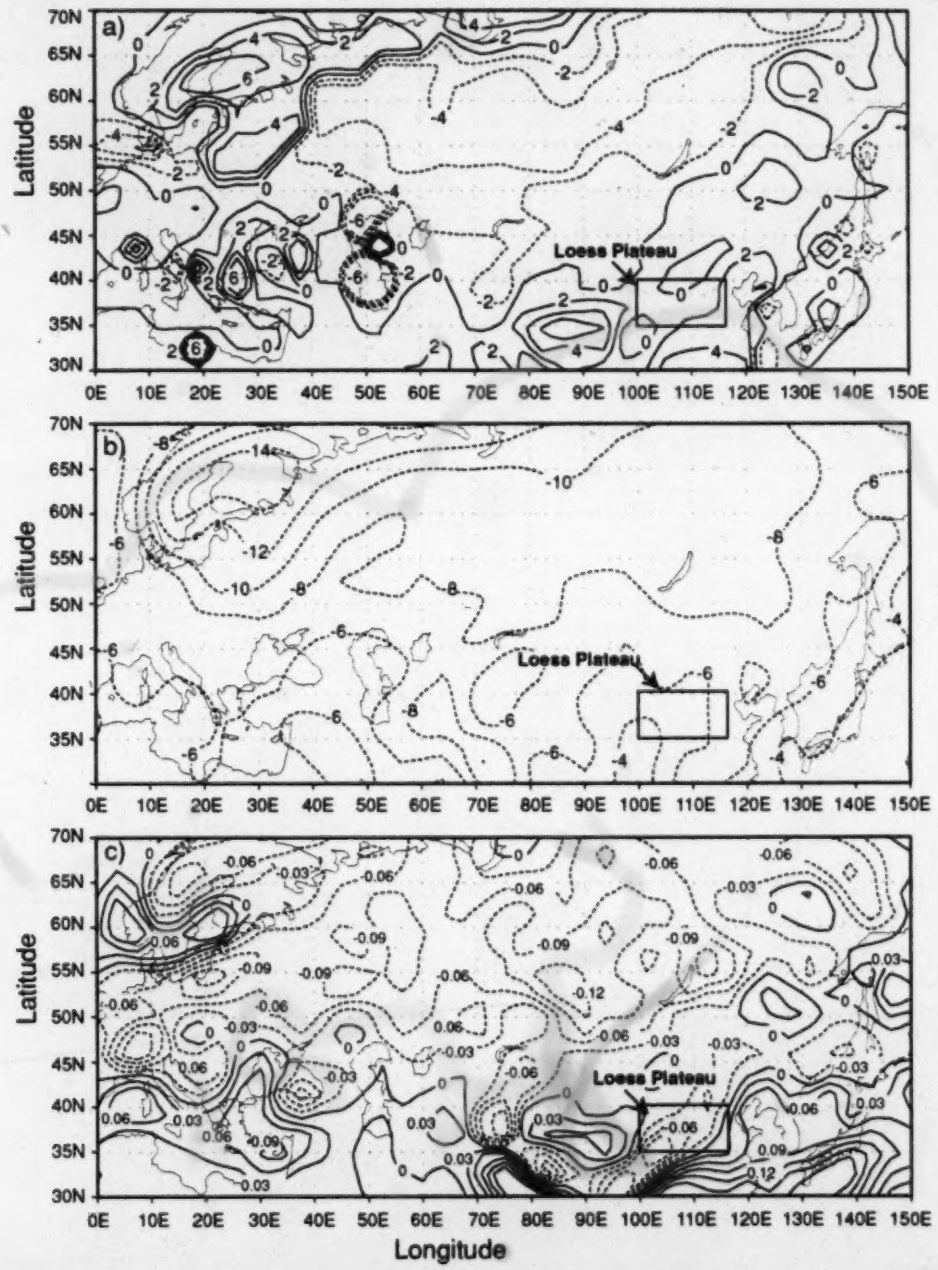

Figure 6.8. Results from numerical general circulation model experiments for the LGM and the present day. Differences are all LGM minus present day. a) Difference in annual mean soil moisture content; values are in cm of water and the field saturation value is 15 cm. b) Difference in annual mean temperature near the surface, in degrees centigrade. c) Difference in annual mean precipitation, in cm/day.

model output indicates that annual mean surface temperatures in the continental interior are colder with respect to today than they are along the east coast (Figure 6.8b). Temperatures are colder in the deep interior both because of downstream cooling induced by the Fennoscandian ice sheet, and because of the large geographical distance to the oceans. A consequence of this pattern of cooling is that the hydrological cycle in the continental interior decreases, leading to less available moisture in the atmosphere. In addition to this, the Fennoscandian ice sheet induces large-scale atmospheric subsidence downstream of itself, thereby suppressing precipitation over a large portion of the continental interior until the winds reach the east coast, where precipitation increases relative to today (Figure 6.8c).

As indicated in Figure 6.8, the Loess Plateau is geographically located along the boundary between drier and wetter regions. The desert margin would be sensitive to these changes in surface hydrology, through dune destabilization or stabilization by vegetation (Bagnold, 1941), as would loess distribution on the Plateau. These results suggest that non-local effects (i.e., the Fennoscandian ice sheet and the atmospheric circulation pattern that it induces downstream) can have an influence on the desert margin and hence on loess deposition in East Asia. The link between ice volume and palaeo-loess deposition in China, therefore, involves desert expansion or contraction, conceivably as a results of changes in soil moisture during relatively dry glacials and wet interglacials.

6.7 Discussion

The interpretation of climate mechanisms that force a change in loess deposition during the last interglacial-glacial cycle must account for, at least, four stratigraphic and sedimentological observations in the Loess Plateau: 1) The stratigraphic alternation of sand, loess and palaeosols involves variations in the rate of sediment accumulation along a shifting climatic gradient (Pye 1987; Pye and Tsoar 1987); 2) Loess beds are thickest and accumulation rates are highest near the desert source during both glacial and interglacial periods. Glacial loess beds are not exclusively thicker with higher accumulation rates than interglacial loess beds. However, we cannot compare the thickness of glacial and interglacial loess beds along the entire desert-loess depositional systems, because of a lack of sites near the interglacial desert source and distal from the last glacial source; 3) Glacial and interglacial beds of loess show similar grain size variations in space, however the distribution of the sizes differ owing to desert expansion and contraction, and 4) Temporal records of loess grain size show larger grains during glacial periods than interglacial periods due to desert expansion and contraction.

Vertical and lateral variations in grain size are related to ice volume variations through desert migration. The lateral variations in loess grain size are, in part, a function of proximity to the desert source (Ding et al. 1999), while vertical grain size trends appear to reflect desert expansion and contraction. Variations in regional accumulation rates are difficult to explain solely by climatic forcing. At present there does not seem to be any consistent relationship between loess accumulation rates, and insolation or global ice volume variations. Other climatic or non-climatic factors that may affect rates of loess deposition must be considered, such as: 1) regional ice volume variations (Benn

and Owens 1998, Svendsen et al. 1999) that reach maximums prior to the last glacial maximum of the Laurentide and Scandinavian ice sheets; 2) variations in the rate and methods of silt production during glacials and interglacials (Reizebos and Van Der Wall 1974; Smalley 1995; Wright et al. 1998); 3) multiple source areas (Fang et al. 1999); 4) The persistence of glacial versus interglacial winds; glacial winds may be more persistent than interglacial winds, but not necessarily higher velocity (Phillips et al. 1993); 5) erosion, especially at warm to cold climate transitions, and 6) variations in soil moisture in the source and depositional areas (Bagnold 1941; Velichko 1984; Rae 1994).

With respect to soil moisture, a low soil moisture content does correlate to an increase in the frequency of dust storms in modern records (Littman 1991). This may infer that there would have been more dust storms during the last glacial period than the last interglacial period. However, we do not know if more dust storms correspond to more dust deposited in the Loess Plateau during the last glacial period.

6.8 Conclusion

Temporal records of loess grain size, thickness and accumulation rates during the last interglacial-glacial cycle do not accurately reflect regional spatial variations in these properties. Specifically, the temporal model of larger grains and thicker loess beds during glacial periods than interglacial periods is not applicable to both spatial and temporal components of loess properties. Interpretations of climatic forcing of the palaeomonsoons have been largely based on observations of temporal changes in grain size and accumulation rates, and do not accurately reflect regional climatic or geologic influences on loess deposition.

Global ice volume variations result in a southward or northward shift in the climatic gradient that influences desert expansion or contraction during cold or warm periods, respectively. However, the movement of the desert margin is due, in part, to variations in the Fennoscandian Ice Sheet that affects East Asian wind patterns (Velichko 1984; Bush and Philander 1999) and induces changes in soil moisture. Thus, loess deposition in China is indirectly influenced by both regional and global ice volume variations.

The expansion and contraction of the desert source results in a change in the distribution of loess. Vertical changes in loess grain size are related to ice volume variations through shifts in the climatic gradient that results in desert expansion and contraction; while lateral variations in grain size, in part, reflect proximity to the source (Ding et al. 1999). At present, variations in the thickness, or accumulation rates of loess are not directly related to variations in insolation or global ice volume variations, and may correspond to other climatic or non-climatic factors.

6.9 References

An, Z.S., Wu, X., Wang, P., Wang, S., Sun, X., and Lu, Y. 1991a. An evolution model for palaeomonsoon of China during the last 130,000 years. *Edited by* L. Tungsheng. *In* Quaternary Geology and Environment in China, pp. 37-244.

An, Z.S., Kukla, G., Porter, S.C., and Xiao, J.L. 1991b. Late Quaternary dust flow on the Chinese Loess Plateau. Catena, **18**, 125-132.

Bagnold, R.A. 1941. The Physics of Blown Sand and Desert Dunes. 1954 edition: London, Methuen & Co. Ltd. pp. 265

Barry, R.G., and Chorley, R.J. 1968. Atmosphere, Weather and Climate. London, Methuen & Co.

Bassinot, F.C., Labeyrie, L.D., Vincent, E., Quidelleur, X., Shackleton, N.J., and Lancelot, Y. 1994. The astronomical theory of climate and the age of the Brunhes-Matuyama magnetic reversal. Earth and Planetary Science Letters, **126**, 91-108.

Benn, D.I. and Owern, L.A. 1998. The role of the Indian summer monsoon and the mid-latitude westerlies in Himalayan glaciation; review and speculative discussion. Journal of the Geological Society of London, 155, Part 2, 3535-363.

Berger, A. and Loutre, M.F. 1991. Insolation values for the climate of the last 10 million years. Quaternary Science Reviews, 10, 297-317.

Bush, A.B.G. and Philander, S.G.H. 1999. The climate of the Last Glacial Maximum: results from a coupled atmosphere-ocean general circulation model. Journal of Geophysical Research, 104, 24,509-24,525.

Chang, B.K. 1987. Short- and long-range monsoon prediction in Southeast Asia. *Edited by* J.S. Fein, and P.L. Stephens. *In* Monsoons. New York, John Wiley & Sons, pp. 579-606.

Deere, Z. 1984. Synoptic-climatic studies of dust fall in China since Historic times. Scientia Sinica (Series B), **XXVII**, 825-836.

Derbyshire, E., Keen, D., Kemp, R.A., Rolph, T.A., Shaw, J., and Meng, X.M. 1995. Loess-paleosol sequences as recorders of palaeoclimatic variations during the last glacial-interglacial cycle: some problems of correlation in north-central China. Quaternary Proceedings, 4, 7-18.

Derbyshire, E., Kemp, R.A., and Meng, X.M. 1997. Climate change, loess and paleosols: proxy measures and resolution in China. Journal of the Geological Society of London, 154, 793-805.

Ding, Z.L., Liu, T.S., Rutter, N.W., Z.W., Yu., Guo, Z.T., and Zhu, R.X. 1995. Ice-volume forcing of East Asian winter monsoon variations in the past 800,000 years. Quaternary Research, 44, 149-159.

Ding, Z., Sun, J., Rutter, N.W., Rokosh, D. and Liu, T. 1999. Changes in the sand content of loess deposits along a north to south transect of the Chinese Loess Plateau and the implications for desert variations. Quaternary Research, 52, 1, 56-62.

Evans, M.E. and Heller, F. 1994. Magnetic enhancement and paleoclimate study of a loess/paleosol couplet across the Loess Plateau of China. Geophysical Journal International, 117: 257-264.

Fang, X., Li, J., Banerjee, S., and Van der Woo, R. 1998. Last Interglacial sharp monsoon fluctuations: rock magnetic and paleomagnetic evidence from high resolution loess-paleosol sequence, Lanzhou, China. Past Global Changes (PAGES) Newsletter, **6**, 6.

Gillette, D.A. 1986. Dust production by wind erosion: necessary conditions and estimates of vertical fluxes of dust and visibility reduction by dust. *Edited by* E-B. Farouk, and M.H.A. Hassan. *In* Physics of desertification., Martinus Nijhoff Publishers, Dordrecht. pp. 361-371.

Hunt, C.P., Banerjee, S.K., Han, J.M., Solheid, P.A., Oches, E., Sun, W.W., and Liu, T.S. 1995. Rock-magnetic proxies of climate change in the loess-Palaeosol sequences of the western Loess Plateau of China. Geophysical Journal International, **123**: 232-244.

Imbrie, J., Boyle, E.A., Clemens, S.C., Duffy, A., Howard, W.R., Kukla, G., Kutzbach, J., Martinson, D.G., McIntyre, A., Mix, A.C., Molfino, B., Morley, J.J., Peterson, L.C., Pisias, N.G., Prell, W.L., Raymo, M.E., Shackleton, N.J., and Toggweiler, J.R. 1992. On the structure and origin of major glaciation cycles; 1, Linear Responses to Milankovitch Forcing. Paleoceanography, **7**, 701-738.

Ing, G.K.T. 1972. A dust storm over Central Asia, April 1969. Weather, **27**, 136-145.

Kukla, G.J., 1987a, Correlation of Chinese, European and American loess series with deep-sea sediments. *Edited by* T. Liu. *In* Aspects of Loess Research.. Ocean Press, Beijing, pp. 27-38.

Kukla, G. 1987b. Loess stratigraphy in central China and correlation with an extended oxygen isotope time stage scale. Quaternary Science Review, 6: 191-220.

Littmann, T. 1991. Dust storm frequency in Asia: climatic control and variability. International Journal of Climatology, **11**, 393-412.

Liu, J., Nie, G., Chen, T., Song, C., Zhu., G., Li, K., Gao, Z., and Qiao, Y. 1995. A preliminary high resolution time scale for the last 130,000 years at Weinan loess section. Sciencia Geologica Sinica (Overseas Edition; Supplementary Issue), Beijing, China, **1**, 9-22.

Liu, T.S. et al. 1985. Loess and the Environment. China Ocean Press, Beijing. pp. 251.

Liu, T., and Chang, T. 1964. The "HuangTu" (loess) of China. Report of the Sixth INQUA Congress, Warsaw 1961, 4, pp. 503-524.

Liu, T. and Ding, Z. 1993. Stepwise coupling of monsoon circulation to global ice volume variations during the Late Cenozoic. Global and Planetary Change, **7**, 119-130.

Liu, X.M., Liu, T., Shaw, J., Heller, F., Xu, T., and Yuan, B. 1991. Paleomagnetic and paleoclimatic studies of Chinese loess. *Edited by* T. Liu, Z. Ding, and Z. Guo, *In* Loess, Environment and Global Change.. Science Press, Beijing. pp. 61-81.

Liu X.M., Rolph, T., Bloemendal, J. Shaw, J. and Liu, T. 1995. Quantitative estimates of palaeoprecipitation at Xifeng, in the Loess Plateau of China. Palaeogeography, Palaeoclimatology, Palaeoecology, **113**, 243-248.

Merrill, J.T., Uematsu, M. and Bleck1989. Meteorological analysis of long range transport of mineral aerosols over the North Pacific. Journal of Geophysical Research, **94**, 8584-8598.

Middleton, N.J. 1986. A geography of dust storms in southwest Asia. Journal of Climatology, **6**, 183-196.

Middleton, N.J. 1991. Dust Storms in the Mongolian People's Republic: Journal of Arid Environments, **20**, 287-297.

Mitsuta, Y., Hayashi, T., Takemi, T., Hu, Y., Wang, J., and Chen, M. 1995. Two severe local storms as observed in the arid area of Northwest China. Journal of the Meteorological Society of Japan, **73**, 1269-1284.

Murakami, T. 1987. Effects of the Tibetan Plateau. *Edited by* C.P. Chang and T.N. Krishnamurti. In Monsoon Meteorology. Oxford University Press, New York. pp. 235-270.

Phillips, F.M., Zreda, M.G., Ku, T.-L., Lou, S., Huang, Q., Elmore, D., Kubik, P.W., and Sharma, P. 1993. $^{230}Th/^{234}U$ and ^{36}Cl dating of evaporite deposits from the western Qaidam Basin, China: implications for glacial-period dust export from Central Asia. Geological Society of America Bulletin, **105**, 1606-1616.

Prell, W.L., and Kutzbach, J.E. 1987. Monsoon variability over the last 150,000 years. Journal of Geophysical Research, **92**, 8411-8425.

Pye, K. 1987. Aeolian dust and dust deposits. Academic Press. pp. 334.

Pye, K. and Tsoar, H. (1987). The mechanics and geological implications of dust transport and deposition in deserts with particular reference to loess formation and dune sand diagenesis in the northern Negev, Israel. In Frostick, L. and Reid., I. (Eds.), Desert Sediments: Ancient and Modern. Geological Society Special Publications, **35**, 139-156.

Rea, D.K. 1994. The paleoclimatic record provided by eolian deposition in the deep sea: The geologic history of wind. Reviews of Geophysics, **32**, 159-195.

Reizebos, A. and Van Der Wall, L. 1974. Silt-sized particles: a proposed source. Sedimentary Geology, **12**: 279-285.

Ren, M., Yang, R. and Bao, H. 1985. An outline of China's Physical Geography. China Knowledge Series. Foreign Languages Press, Beijing. 471 pp.

Rokosh, D., Rutter, N.W., Ding, Z. and Sun, J. (submitted). Regional stratigraphy of the central Loess Plateau, China over the last 130,000 years: links to climatic forcing. Canadian Journal of Earth Science.

Rousseau, D.-D. and Wu, N. 1997. A new molluscan record of the monsoon variability over the past 130,000 yr. in the Louchuan loess series. Geology, **25**, 3, 275-278.

Rutter, N.W., Ding, Z., Evans, M.E., and Liu, T. 1991. Baoji-type pedostratigraphic section, Loess Plateau, north-central, China. Quaternary Science Reviews, **10**, 1-22.

Rutter, N.W., Rokosh, D., Ding, Z. and Liu, T., 1998. High resolution paleoclimate records from the loess-desert margin. Desert Margin Changes in Africa since 135 ka: Implications for Water, Carbon & Man. International Geological Correlation Program 349/404, Jan 5-12 1997, pp. 100-102.

Shackleton, N.J. 1996. Timescale Calibration, ODP 677., International Geosphere Biosphere Program, Past Global Changes World Data Center-A for Paleoclimatology Data Contribution Series #96-018. National Oceanic and Atmospheric Administration /National Geophysical Data Center Paleoclimatology Program, Boulder CO, USA.

Shackleton, N.J., An, Z., Dodonov, A.E., Gavin, J., Kukla, G.J., Ranov, V.A., and Zhuo, L.P. 1995. Accumulation rate of loess in Tadjikistan and China: relationship with global ice volume cycles. Quaternary Proceedings, **4**, 1-6.

Shackleton, N.J., Berger, A., and Peltier, W.R. 1990. An alternative astronomical calibration of the lower Pleistocene timescale based on ODP Site 677. Transactions of the Royal Society of Edinburgh: Earth Sciences, **81**, 251-261.

Smalley, I. 1995. Making the material: the formation of silt-sized primary mineral particles for loess deposits: Quaternary Science Reviews, **14**, 645-657.

Sun, J., Ding, Z., and Liu, T. 1995. The environmental evolution of the desert-loess transition zone over the last glacial-interglacial cycle. *Edited by* S. Wang. *In* Quaternary Geology and Past Environmental changes in China. Science Press, Beijing, pp. 1-8.

Sun, J., Yin, G., Ding, D., Liu, T., and Chen, J. 1998. Thermoluminescence chronology of sand profiles in the Mu Us Desert, China. Palaeogeography, Palaeoclimatology, Palaeoecology, **144**, 25-233.

Svendsen, J.I., Astakov, V.I., Bolshiyanov, D.Y., Demidov, I., Dowdeswell, J.A., Gataullin, V., Hjort, C., Hubberten, H.W., Larsen, E., Mangerud, J., Melles, M., Moller, P. Saarnisto, M., and Siegert, M.J. 1999. Maximum extent of the Eurasian ice sheets in the Barents and Kara Sea region during the Weichselian. *Edited by* E. Larsen, S. Funder, and J. Thiede. *In* Late Quaternary history of northern Russia and adjacent shelves. Boreas, **28**, 234-242.

Tao, S., and Chen, L. 1987. A review of recent research on the East Asian summer monsoon in China., *in* Monsoon Meteorology. *Edited by* C.P. Chang, and T.N. Krishnamurti. *In* Monsoon Meteorology. Oxford University Press, New York. pp. 60-92.

U.S. Defense Mapping Agency Aerospace Center 1987, Operational Navigation Chart, Sheets F-7, F-8, G-8, G-9. U.S. Department of Defense.

Vandenberghe, J., An, Z.S., Nugteren, G., Lu, H.Y., and Van Huissteden, K. 1997. New absolute time scale for the Quaternary climate in the Chinese loess region by grain-size analysis. Geology, **25**, 35-38.

Velichko, A.A. 1984. Late Pleistocene spatial paleoclimate reconstructions. *Edited by* A. A. Velichko, H. E. Wright, Jr. and C. W. Barnosky. *In* Late Quaternary Environments of the Soviet Union. Minneapolis, University of Minnesota,. pp. 35-41.

Wright, J., Smith, B., and Whalley, B. 1998. Mechanisms of loess-sized quartz silt production and their relative effectiveness: laboratory simulations. Geomorphology, **23**, 15-34.

Zhang, X., An, Z., Liu, D., Chen, T., Zhang, G., Arimoto, R., Zhu, G., and Wang, X. 1992. Study on three dust storms in China-source characterization of atmospheric trace element and transport process of mineral aerosol particles. Chinese Science Bulletin, **37**, 940-945.

Zhang, X.Y., Arimoto, R., and An, Z.S. 1999. Glacial and interglacial patterns for Asian dust transport. Quaternary Science Reviews, **18**, 811-819.

CHAPTER 7

Summary and Conclusions

7.1 Introduction

The general objective of this research is to increase our understanding of East Asian Quaternary loess deposition and palaeoclimatology through a spatial and temporal evaluation of the geology of the Chinese Loess Plateau (Chapter 1). The approach to meeting the objective is to study the regional stratigraphy and sedimentology of loess during the last interglacial-glacial cycle at various scales of observation.

7.2 Final Conclusions

The study of the regional stratigraphy of the Loess Plateau, China (Chapter 3) allows a different interpretation of glacial and interglacial loess deposition than is shown by temporal evaluations of loess deposition. Prior to this study, the basic model (i.e. the temporal model) of loess deposition indicated that loess grains are larger and accumulation rates are higher during glacial periods than interglacial periods in the Loess Plateau. However, the temporal model does not accurately reflect regional variations in loess texture, and leads to erroneous or oversimplified palaeoclimate interpretations.

In this study, regional loess deposition in the Loess Plateau, China is best viewed as part of a desert-loess depositional system (Chapter 3). In this system, the desert is the main source of loess and influences loess distribution via desert expansion and contraction during glacial and interglacial periods, respectively. A conceptual model of loess deposition suggests that the proximal, medial and distal environments of both the

last interglacial and glacial desert-loess depositional systems show similarities in the size of loess grains, and possibly even loess accumulation rates downwind of the source. Desert expansion and contraction was forced, in part, by a changes in soil moisture that is influenced by extent of the Fennoscandian ice-sheet and the atmospheric circulation pattern that it induces downstream.

The integration of pedostratigraphy (loess and palaeosols) and lithostratigraphy (sand and loess) during the last glaciation (Chapter 4) shows that vertical and lateral variations in stratigraphy are driven by changes in loess accumulation rates along climatic gradient (from cold and dry near the desert, to warmer and wetter in the southern Loess Plateau). Lateral changes from sand to loess, or loess to soil are driven by variations in the balance between loess accumulation rates and pedogenesis, whereas the vertical alternation of loess and palaeosols is driven by changes in accumulation rates along a climatic gradient that shifts southward during glacial periods and northward during interglacial periods, concomitant with desert expansion and contraction, respectively.

The lithofacies and pedofacies variations are important for understanding high-resolution climate change. In high-resolution studies, vertical profiles of alternating loess and palaeosols (especially weak palaeosols) may not reflect regional or global climatic change. At high resolutions, vertically alternating loess and weak soils may result from local climatic (e.g. local winds from the mountains) or non-climatic variations (changes in topography that induce increased water flowing to an area) that alter the balance between rates of loess accumulation and pedogenesis. These high frequency changes must be correlated regionally in order to assess their validity as indicators of regional or

global palaeoclimate change. Local fluctuations in loess accumulation rates or changes in the factors that influence pedogenesis either of these rates could result in the presence of time equivalent loess and palaeosols at high resolutions. Thus, some high resolution (vertical) loess-palaeosol alternations may reflect local climatic variation rather than global or hemispherical climatic change. It is incumbent upon the scientists involved in high resolution research to prove that temporal variations in loess or palaeosols propagate regionally and represent globally or regional and represent large-scale variations in palaeoclimatic change.

The high resolution correlations of loess grain size along the transect (Chapter 5) suggest that variations in grain size (e.g. millenia scale) propagate through the central Loess Plateau, and represent regional variations in sedimentation. These regional variations are superimposed on a larger desert-loess depositional system that exhibits three periods of desert expansion and two periods of desert contraction during the last interglacial-glacial cycle. The architecture of the high resolution correlations is similar to the architecture of the Malan formation (L1) and its members (L1-1 to L1-5). This observation, along with the lateral trends in grain size, suggests a relatively consistent wind direction during the deposition of the Malan; however, a precise determination of the wind direction should be determined from a regional (i.e. 3-dimensional) reconstruction of the deposits. Furthermore, the lateral variations in grain size and the architecture of the correlations reflect proximity to the source, while the vertical variations in grain size seem to reflect desert expansion and contraction. However, not all high resolution variations in grain size are necessarily related to climate. Some of the peaks and troughs in grain size in the upper Malan are difficult to correlate, and may be

related to local climatic variation or non-climatic events. Finally, the high resolution correlations within the Malan loess suggest that Chinese desert-loess depositional system is stratified; where the stratification of the loess is defined by changes in grain size, as suggested by Bagnold (1941, p. 119).

Results from climate proxy and General Circulation Model (GCM) analyses (Chapter 6) suggest that variations in soil moisture and desert expansion are key hydrologic and geologic factors, respectively in the Loess Plateau, China that cause spatial variations in loess texture and distribution during the last interglacial-glacial cycle. The lateral distribution and texture of loess varies during glacial and interglacial periods with changes in the position of the desert margin. During the last glacial period in East Asia a reduction in soil moisture led to dune de-stabilization and a southward expansion of the desert (the source of loess) toward the Loess Plateau. The desert margin is, therefore, sensitive to changes in surface hydrology. Changes in soil moisture in East Asia may be influenced by the extent of the Fennoscandian Ice Sheet, and the atmospheric circulation pattern that it induces downstream. These results suggest that there are regional environmental factors (i.e. changes in soil moisture and the position of the desert margin) and hemispherical environmental factors (i.e. changes in Eurasian ice sheets)that influence loess deposition in China.

7.3 Future Research

Future research should concentrate on two principle fronts: 1) local and regional stratigraphic and sedimentological research; and 2) integration with other palaeoclimate proxy data.

Stratigraphic research should concentrate on both local and regional mapping. In terms of regional mapping there is a wealth of data from pre-1949 that concentrated on terrace loess associated with the development of the Yellow River (see Fig. 2.1 in Chapter 2). These data, and other important data regarding regional uplift and fluvial history, can be integrated into the known geologic and palaeoclimatic history. Regional geologic and palaeoclimatic history will be more complete by integrating the prior research and finding new sites to study terrace loess and fluvial history.

The regional mapping of the Loess Plateau needs be augmented by linking one or two more transects to the present north to south transect. This may be the only way to ensure that the methods of determining grain size, for example, are the same, and therefore consist of a comparable data set. The continuation of regional mapping over the last glacial and interglacial periods should concentrate on mapping the sub-units within the last glacial period, and perhaps concentrate on mapping near the mountain passages where the thickest sections are evident. Future research must also include locating sites that reveal interglacial sediments proximal to the desert margin. This research can help to verify or refute the models presented in chapters 3-5 by contrasting regional loess and palaeosol properties of the desert-loess depositional systems within the last glacial and interglacial periods.

Local stratigraphic mapping should occur at a number of spatial scales. For example, multiple sites at a single outcrop to examine local high resolution variations in grain size and pedology; and 2) sample sites over a relatively short distance (e.g. 10 sites over one kilometer) in order to examine variations in bed geometry, grain size, and to examine glacial to interglacial (and *vice versa*) loess boundaries. The combined regional

and local stratigraphic mapping should give a much firmer base for palaeoclimate interpretations, especially with respect to differentiating local, regional and global palaeoclimate change.

Lastly, the best method of studying high resolution variations in grain size and pedology is to cut continuous core, and to log the well-bore (or the core) using continuous geophysical measuring devises (such as electrical logs, gamma ray logs, sonic logs, etc.). The core can then be sampled for various laboratory analyses (e.g. geophysical, geological, pedological, palynological).

7.5 Reference

Bagnold, R.A.1941. The physics of blown sand and desert dunes. Metheun & Co., London. pp. 265.

Appendix 1

Grain size and magnetic susceptibility data from the north to south transect

WUPU

Depth (m)	MS (orig) (10-3 SI)	GS (mm)	Coefficient	MS(cal) (10-3 SI)
0.05	56.25	32.9	1.0578	59.50125
0.15	58.82353	33.3	1.0483	61.66471
0.20	62.17949	30	1.0357	64.39929
0.25	70.58823	30.1	1.0189	71.92235
0.30	88.76405	24	1.0294	91.37372
0.35	93.56435	18.2	1.0452	97.79346
0.40	92	16.6	1.0534	96.9128
0.45	88.46153	15.7	1.0629	94.02576
0.50	84.47205	18.2	1.0566	89.25317
0.55	83.80566	17.8	1.0545	88.37306
0.60	79.41177	21.3	1.0503	83.40619
0.65	78.50468	20	1.0482	82.2886
0.70	77.77778	20.2	1.0514	81.77555
0.75	78.7037	20.4	1.0802	85.01573
0.80	65.28302	19.6	1.0908	71.21072
0.85	60.73059	23.3	1.0654	64.70237
0.90	70.7317	22.7	1.0781	76.25584
0.95	66.21622	23.4	1.1002	72.85109
1.00	52.33161	26.7	1.0992	57.52291
1.05	46.2963	25.8	1.1224	51.96297
1.10	37.2549	29.6	1.1203	41.73667
1.15	34.30232	32.6	1.1066	37.95895
1.20	32.39437	32.6	1.1076	35.88
1.25	32.36514	33.1	1.095	35.43983
1.30	36.43123	32.8	1.0992	40.04521
1.35	34.61538	34.2	1.095	37.90384
1.40	34.83607	32.5	1.1055	38.51128
1.45	30.67729	34	1.1023	33.81558
1.50	30.9322	33.5	1.0971	33.93572
1.55	30.88803	36.7	1.1334	35.00849
1.60	30.97345	34.1	1.1197	34.68097
1.65	30.71428	35.5	1.105	33.93928
1.70	30.28846	35.9	1.1218	33.97759
1.75	30.90909	35.6	1.1113	34.34927
1.80	29.88506	36.6	1.1225	33.54598
1.90	30.87248	37.5	1.1171	34.48765
2.00	31.17647	27.1	1.1084	34.556
2.10	31.25	29	1.1127	34.77187
2.20	32.43243	27.9	1.1127	36.08757
2.30	33.241	28.3	1.1095	36.88089
2.40	31.94444	28.4	1.103	35.23472
2.50	30.96774	29.3	1.1062	34.25651
2.60	31.25	29.4	1.1062	34.56875
2.70	30.93525	28.4	1.0976	33.95453
2.80	32.46753	26.5	1.103	35.81169
2.90	34.01361	26.2	1.0965	37.29593
3.00	33.68984	26.4	1.09	36.72192
3.10	36.0215	25.9	1.1062	39.84698
3.20	36.42384	24.4	1.0943	39.85861
3.30	34.45946	24	1.0921	37.63318
3.40	36.04061	24.3	1.0911	39.32391
3.45	35.86207	24.8	1.0921	39.16497
3.50	34.64052	24.1	1.0914	37.80666
3.55	36.53846	23.9	1.0914	39.87807
3.60	37.41007	23.2	1.0849	40.58619
3.65	39.0411	22.7	1.087	42.43768
3.70	38.59649	22.9	1.0936	42.20912
3.75	38.7324	22.4	1.0976	42.51268
3.80	36.47799	24.7	1.1012	40.16956
3.85	35.92814	24.2	1.087	39.05389
3.90	38.50575	23.1	1.0947	42.15224
3.95	40.60913	22	1.0892	44.23146
4.00	43.42105	21.4	1.1153	48.42749

Depth (m)	MS (orig) (10-3 SI)	GS (mm)	Coefficient	MS(cal) (10-3 SI)
4.05	42.19653	23.4	1.111	46.88035
4.10	35.23316	24.1	1.1132	39.22155
4.15	35.39326	23.9	1.1132	39.39978
4.20	31.75676	24.8	1.1142	35.38338
4.25	32.88591	24.8	1.1055	36.35537
4.30	32.55814	26.7	1.1044	35.95721
4.35	31.85185	27.1	1.1023	35.1103
4.40	32.62411	26.4	1.099	35.8539
4.45	33.33333	26.3	1.0979	36.59666
4.50	33.55705	26.7	1.0914	36.62416
4.55	34.28571	25.6	1.0957	37.56685
4.60	36.71875	25.9	1.1066	40.63297
4.65	35.71428	24.6	1.0968	39.17142
4.70	35.21127	23.2	1.0892	38.35212
4.75	35.71429	23.9	1.0925	39.01786
4.80	36.55914	23.2	1.0925	39.94086
4.85	33.57143	24.8	1.0979	36.85807
4.90	34.02778	22.5	1.0936	37.21278
4.95	34	22.8	1.0849	36.8866
5.00	36.56717	22.6	1.0903	39.86918
5.05	38.54166	22.6	1.0936	42.14916
5.10	35.8209	23	1.099	39.36717
5.15	37.5	23	1.0827	40.60125
5.20	32.25806	23.5	1.087	35.06451
5.25	33.61345	25.2	1.0805	36.31933
5.30	36.36364	25.1	1.0849	39.45091
5.35	35.84906	27.5	1.0849	38.89265
5.40	38.14433	23.1	1.0925	41.67268
5.45	38.60759	24.1	1.087	41.96645
5.50	39.0625	22.1	1.0838	42.33594
5.55	39.28571	23.6	1.1044	43.38714
5.60	38.29787	23.3	1.0914	41.7983
5.65	34.57944	26.6	1.0957	37.88869
5.70	32.07547	27.2	1.0903	34.97188
5.75	32.11009	28	1.0805	34.69495
5.80	36.97479	24.5	1.087	40.1916
5.85	36.66667	23.9	1.0762	39.46067
5.90	37.80488	24.6	1.0772	40.72342
5.95	43.29897	23.6	1.0762	46.59835
6.00	41.15226	25.1	1.0685	43.97119
6.05	43.91892	24.5	1.0631	46.6902
6.10	44.60432	23.9	1.0631	47.41885
6.15	47.54099	23.2	1.0609	50.43623
6.20	51.21951	21.4	1.0566	54.11853
6.25	58.11966	19.8	1.0957	63.68171
6.30	65.21739	17.2	1.0849	70.75435
6.35	55.43478	18.5	1.1012	61.04478
6.40	54.79452	18.3	1.1088	60.75617
6.45	49.03846	19.2	1.0881	53.35875
6.50	48.35165	18.8	1.1034	53.35121
6.55	44.92754	18.8	1.0979	49.32595
6.60	43.30709	19.4	1.0892	47.17009
6.65	43.39623	19.2	1.0762	46.70302
6.70	47.01493	20.5	1.0762	50.59747
6.75	49.54129	21.5	1.0827	53.63836
6.80	48.87218	18.9	1.0892	53.23158
6.85	48.88889	19.4	1.1197	54.74089
6.90	50	17.9	1.1186	55.93
6.95	45.20548	21.5	1.1273	50.96014
7.00	34.14634	21.3	1.1044	37.71122
7.05	32.91139	21.3	1.0968	36.09721
7.10	33.80282	22.4	1.0979	37.11211
7.15	34.78261	23.3	1.1066	38.49044
7.20	32.38095	23.2	1.0925	35.37619
7.25	36.79245	23.8	1.1066	40.71453

Depth (m)	MS (orig) (10-3 SI)	GS (mm)	Coefficient	MS(cal) (10-3 SI)
7.30	30.76923	23.7	1.0925	33.61538
7.35	29.09091	24.5	1.0979	31.93891
7.40	28.88889	24.2	1.0631	30.71178
7.45	29.77099	25	1.0794	32.1348
7.50	47.67442	21.2	1.0816	51.56465
7.60	34.67742	25	1.0859	37.65621
7.70	30.17241	25	1.0849	32.73405
7.80	30.40541	26.2	1.087	33.05068
7.90	29.88506	27.4	1.0914	32.61655
8.00	29.62963	26.9	1.087	32.20741
8.10	30.09709	26.8	1.0827	32.58612
8.20	30.53435	27.2	1.0838	33.09313
8.30	29.19708	26.6	1.0783	31.48321
8.40	30.15873	26.4	1.0783	32.52016
8.50	30.37037	26.1	1.0892	33.07941
8.60	29.80132	26.2	1.0827	32.26589
8.70	30.14706	27.4	1.0849	32.70655
8.80	30.58824	27	1.0827	33.11789
8.90	29.82456	27.9	1.0805	32.22544
9.00	29.87013	28.6	1.0783	32.20896
9.10	30.4	29	1.0762	32.71648
9.20	31.09244	29	1.0783	33.52698
9.30	29.87013	28.8	1.0783	32.20896
9.40	29.56522	29.4	1.074	31.75305
9.50	30.15873	29.2	1.0762	32.45683
9.60	29.26829	29.4	1.0718	31.36975
9.70	29.23077	29.3	1.0762	31.45815
9.80	29.05405	29.4	1.0751	31.23601
9.90	28.67133	30.1	1.0729	30.76147
10.00	28.34646	29.8	1.0653	30.19748
10.10	27.27273	29.6	1.0707	29.20091
10.20	27.83505	29.7	1.0696	29.77237
10.30	27.90698	29.6	1.0732	29.94977
10.40	28	29.6	1.0764	30.1392
10.50	27.14286	29.7	1.0677	28.98043
10.60	29.47368	29	1.0677	31.46905
10.70	29.41176	28.4	1.0699	31.46764
10.80	28.23758	28.6	1.0874	30.70554
10.90	28.57143	27	1.0808	30.88
11.00	27.3743	29	1.0786	29.52592
11.10	27.94118	31.6	1.0775	30.10662
11.20	28.46154	32.5	1.0743	30.57623
11.30	29.67742	28.3	1.0764	31.94478
11.40	31.09244	27.7	1.0775	33.5021
11.50	29.11392	29	1.0797	31.4343
11.60	30.82192	29.9	1.0764	33.17672
11.70	30.15873	33.6	1.0764	32.46286
11.80	29.92701	34	1.0743	32.15059
11.90	32.6087	33	1.0764	35.10001
12.00	31.96721	32.1	1.0764	34.40951
12.10	32.67327	31.2	1.0721	35.02901
12.20	34.88372	29.6	1.0764	37.54884
12.30	34.31372	27.6	1.0721	36.78774
12.40	46.49123	18.6	1.0895	50.65219
12.50	48.50299	19.8	1.1136	54.01293
12.60	55.71429	16	1.107	61.67572
12.70	52.17391	15.5	1.1114	57.98608
12.72	56.97674	14.8	1.1136	63.4493
12.74	60.60606	13.9	1.1147	67.55757
12.76	65.38462	13.6	1.1179	73.09347
12.78	59.57447	14.8	1.1092	66.08
12.80	60	15	1.1048	66.288
12.82	60.66667	16.1	1.1322	68.68681
12.84	62.26415	15.4	1.1245	70.01604
12.86	59.77011	14.9	1.1245	67.21149

Depth (m)	MS (orig) (10-3 SI)	GS (mm)	Coefficient	MS(cal) (10-3 SI)
12.88	62.96296	14.1	1.119	70.45555
12.90	64.94846	15.2	1.1245	73.03455
12.92	67.01031	14.6	1.1147	74.69639
12.94	66.88312	15.5	1.1145	74.54124
12.96	68.90756	16.3	1.1134	76.72168
12.98	71.34147	15	1.1069	78.96787
13.00	70.16129	15.7	1.1025	77.35282
13.02	67.54386	14.4	1.0949	73.95377
13.04	64.83516	17.3	1.1014	71.40945
13.06	66.85083	18.3	1.0961	73.27519
13.08	68.70229	15	1.0851	74.54886
13.10	71.07438	14.2	1.0971	77.9757
13.12	72.10884	13	1.0927	78.79333
13.14	74.16666	13.8	1.1003	81.60557
13.16	74.30556	14.1	1.0981	81.59492
13.18	77.93104	13.3	1.0927	85.15524
13.20	76.97369	12.9	1.1014	84.77882
13.22	80.29197	13.2	1.0961	88.00803
13.24	79.16666	14.7	1.0807	85.55541
13.26	78.40909	13.7	1.0654	83.53704
13.28	76	15.9	1.0632	80.8032
13.30	79.38931	16.5	1.072	85.10535
13.32	87.34177	14.1	1.0742	93.82253
13.34	88.99083	12.9	1.0502	93.45817
13.36	90.05848	16.8	1.0523	94.76854
13.38	93.28358	16.9	1.0654	99.38432
13.40	95.65218	13.4	1.0545	100.8652
13.42	94.0594	15.6	1.0436	98.16039
13.44	92.5	14.6	1.0523	97.33775
13.46	89.91597	14.1	1.0622	95.50874
13.48	88.02395	14.1	1.048	92.2491
13.50	87.40157	15.8	1.0436	91.21228
13.52	88.41463	14	1.0469	92.56128
13.54	90.32259	14.2	1.036	93.57421
13.56	87.35632	14.4	1.036	90.50115
13.58	85.21739	14.6	1.0349	88.19147
13.60	84.76821	14.3	1.0305	87.35365
13.62	84.66666	14.2	1.0393	87.99406
13.64	83.68794	13.8	1.0327	86.42453
13.66	81.72043	14.2	1.0382	84.84215
13.68	82	13.6	1.0273	84.2386
13.70	79.14438	14.3	1.0186	80.61646
13.72	73.37663	16	1.0153	74.4993
13.74	68.37607	14.9	1.0131	69.2718
13.76	64	15.4	1.0098	64.6272
13.78	59.2	16	1.0218	60.49056
13.80	58.09524	15.8	1.0524	61.13943
13.82	61.32597	14.6	1.0557	64.74182
13.84	61.22449	14.7	1.0568	64.70204
13.86	61.90476	13.7	1.0972	67.92191
13.88	60	13.2	1.0852	65.112
13.90	57.67196	13.3	1.0983	63.34111
13.92	55.47445	14.1	1.1201	62.13693
13.94	51.03448	13.7	1.1485	58.6131
13.96	47.73869	13.2	1.1638	55.55829
13.98	42.20184	12.9	1.1474	48.42239
14.00	38.46154	12.1	1.1441	44.00385
14.02	40.90909	13	1.1658	47.69181
14.04	37.19008	14.5	1.1494	42.74628
14.06	36.84211	12.9	1.1416	42.05895
14.08	40.35088	13.4	1.1405	46.02018
14.10	39.75155	13.4	1.1298	44.9113
14.12	41.66667	13.5	1.1047	46.02917
14.14	45.37037	12.7	1.096	49.72592
14.16	49.6063	12.4	1.096	54.3685

Depth (m)	MS (orig) (10-3 SI)	GS (mm)	Coefficient	MS(cal) (10-3 SI)
14.18	59	12.8	1.0829	63.8911
14.20	60.91954	12.9	1.0807	65.83575
14.22	62.6087	13	1.0916	68.34365
14.24	66.19718	12.9	1.0829	71.68493
14.26	65.625	12.6	1.0785	70.77657
14.28	70.24793	13.2	1.0796	75.83967
14.30	69.87952	12.6	1.0829	75.67253
14.32	72.12122	12.1	1.0763	77.62408
14.34	70.229	12.3	1.0436	73.29098
14.36	67.32673	12.3	1.0447	70.33624
14.38	75.14451	13.4	1.056	79.3526
14.40	62.12121	15.2	1.0414	64.69302
14.42	65.51724	15.3	1.048	68.66207
14.44	69.62963	13.9	1.0589	73.73082
14.46	68.42105	13.6	1.0458	71.55473
14.48	67.32026	13.6	1.0523	70.84111
14.50	68.75	13.9	1.0436	71.7475
14.52	68.58974	15.1	1.0349	70.98351
14.54	64.08451	15.6	1.0174	65.19958
14.56	63.63636	15.9	1.0109	64.32999
14.58	55	18.7	1.0142	55.781
14.60	53.77358	21.9	1.0131	54.47802
14.62	54.12371	19.5	1.0131	54.83273
14.64	51.48515	21.2	1.0087	51.93307
14.66	49.70414	23	1.0087	50.13657
14.68	43.90244	23.8	1.0044	44.09561
14.70	42.85714	23.9	1.0055	43.09285
14.72	42.85714	25.6	1.0076	43.18285
14.74	41.66667	26	1.0065	41.9375
14.76	41.26984	26.4	1.0098	41.67428
14.78	40.68966	27.2	1.0065	40.95414
14.80	41.29032	25.2	1.0087	41.64955
14.82	39.62264	25.3	1.0087	39.96736
14.84	43.84615	25.8	1.0087	44.22761
14.86	42.85714	27.7	1.0054	43.08857
14.88	42.42424	25.8	1.0044	42.61091
14.90	41.17647	28.3	1.0054	41.39882
14.92	40.17857	27.6	1.0065	40.43973
14.94	37.2549	28.9	1.0044	37.41882
14.96	35.928[illegible]	28.5	1.0054	36.12215
14.98	36.66667	29.4	1.0065	36.90501
15.00	35.31915	30.2	1.0065	35.54873
15.02	34.30232	32.3	1.0065	34.52528
15.04	35.15152	30.7	1.0054	35.34134
15.06	36.29033	29.8	1.0065	36.52621
15.08	35.05155	30.6	1.0065	35.27939
15.10	34.5679	30.6	1.0054	34.75457
15.12	35.2	31.2	1.0065	35.4288
15.14	34.39491	31.5	1.0087	34.69415
15.16	33.96226	31.2	1.1393	38.6932
15.18	34.61539	30	1.1327	39.20885
15.28	28.57143	27.5	1.1436	32.67429
15.38	29.93631	30.7	1.1034	33.03172
15.48	28.65169	30.6	1.0957	31.39366
15.58	29.67742	32.9	1.0936	32.45523
15.68	28.26087	35	1.1001	31.08978
15.78	30.18868	36.3	1.1044	33.34038
15.88	29.28572	36.2	1.1099	32.50422
15.98	28.67133	35.3	1.1012	31.57287
16.08	29.62963	35.1		

Yanchang

Depth (m)	MS (orig) (10-3 SI)	GS (mm)	Coefficient (see thesis)	MS(cal) (10-3 SI)

Depth (m)	MS (orig) (10-3 SI)	GS (mm)	Coefficient	MS(cal) (10-3 SI)
0.05	69.3302	30.4	1.041992	72.24154
0.10	76.28867	25.2	1.045478	79.75816
0.15	85.67416	26.2	1.026799	87.97018
0.20	99.39759	26.5	1.022286	101.6127
0.25	91.72662	25	1.014096	93.01959
0.30	77.98743	24.8	1.014302	79.10278
0.35	93.17803	24.1	1.007658	93.89161
0.40	67.85715	21.6	1.004419	68.15704
0.45	56.69292	22	1.004419	56.94347
0.50	58.72888	21.7	1.004419	58.98843
0.55	42.55319	21	1.004319	42.73696
0.65	49.41177	23.7	1.006543	49.73505
0.75	35.59127	25.1	1.117443	39.77123
0.85	41.02564	24.6	1.184975	48.61434
0.95	28.4951	26.9	1.181893	33.67817
1.05	28.43016	27.2	1.188072	33.77707
1.15	39.02439	27.8	1.151013	44.91758
1.25	39.50104	26.1	1.146657	45.29416
1.35	29.50076	28.9	1.155268	34.08128
1.45	35.62653	30.4	1.164009	41.4696
1.55	29.73978	34	1.136751	33.80673
1.65	30.94556	35.3	1.178967	36.4838
1.75	29.20354	32.6	1.149557	33.57115
1.85	28.34646	32.3	1.117443	31.67556
1.95	28.97196	32.7	1.151013	33.3471
2.05	29.63776	31.9	1.145213	33.94155
2.15	28.70189	31.7	1.138174	32.66776
2.25	28.77193	31.8	1.132631	32.58798
2.35	29.39015	32.1	1.132631	33.2882
2.45	29.28572	33.5	1.135332	33.249
2.55	37.24605		1.116445	41.58318
2.65	32.53425	29.8	1.116445	36.3227
2.75	36.63501	28.3	1.115076	40.85081
2.85	36.57587	27.6	1.116445	40.83495
2.95	36.12903	27.9	1.121957	40.53521
3.05	37.70351	28.1	1.120574	42.24957
3.15	35.2459	28	1.119194	39.447
3.25	35.63636	27.6	1.115076	39.73724
3.35	42.53308	26.9	1.116445	47.48586
3.45	42.11793	26.4	1.119194	47.13814
3.55	39.13406	26.2	1.112347	43.53065
3.65	39.10069	26.4	1.112347	43.49353
3.75	40.5771	26.2	1.117818	45.35781
3.85	39.94674	25.4	1.115076	44.54364
3.95	44.36557	25.8	1.117818	49.59263
4.05	41.46341	24.8	1.119194	46.40561
4.15	41.7981	24.4	1.116445	46.66529
4.25	42.99754	25.3	1.116445	48.00439
4.35	51.43423	24.3	1.116445	57.4235
4.45	51.18484	21.7	1.116445	57.14507
4.55	50.93834	20.8	1.115076	56.80011
4.65	51.22732	21.8	1.117818	57.26282
4.75	55.31296	20.3	1.117818	61.82982
4.85	58.19592	19.4	1.119194	65.13253
4.95	60.21341	18.9	1.116445	67.22497
5.05	57.47127	19.4	1.116445	64.16352
5.15	58.40072	19.2	1.127396	65.84072
5.25	57.67442	18.4	1.127396	65.0219
5.35	53.79747	18.9	1.146395	61.67313
5.45	51.31579	19.5	1.146395	58.82814
5.55	50.47619	19.6	1.147052	57.89882
5.65	45.71429	19.9	1.148501	52.50291
5.75	45.71429	20.9	1.144165	52.30468
5.85	46.21849	21.9	1.137139	52.55685

Depth (m)	MS (orig) (10-3 SI)	GS (mm)	Coefficient	MS(cal) (10-3 SI)
5.95	44.82758	21.7	1.134301	50.84798
6.05	45.83334	21.3	1.138563	52.18415
6.15	44.44444	21.8	1.127396	50.10647
6.25	48.18325	22.2	1.124606	54.18719
6.35	48.74214	22	1.125999	54.88362
6.45	50.16722	20.8	1.124606	56.41838
6.55	51.69629	20.8	1.134301	58.63917
6.65	50.66251	19.7	1.127396	57.1167
6.75	50.98684	20.4	1.121957	57.20502
6.85	52.63158	19.6	1.124606	59.18981
6.95	51.54639	19.4	1.127396	58.11318
7.05	51.02041	21.5	1.121957	57.24269
7.15	51.35135	20.1	1.121957	57.61399
7.25	53.16456	18.9	1.120574	59.57481
7.35	59.50413	18.6	1.119194	66.59667
7.45	55.55556	18.6	1.132888	62.93821
7.55	58.62069	19.8	1.115076	65.36652
7.65	64.28571	18.8	1.116445	71.77148
7.75	68.46847	17.4	1.115076	76.34753
7.85	89.76379	17.6	1.103022	99.01146
7.95	77.93103	14.8	1.117818	87.11271
8.05	67.85715	15.3	1.139991	77.35653
8.15	65.80645	15.8	1.139991	75.01875
8.25	68.21706	14.7	1.139991	77.76682
8.35	66.66666	15.1	1.124606	74.97375
8.45	61.2676	17.1	1.138563	69.75703
8.55	46.07843	16.6	1.161575	53.52356
8.65	39.28571	17	1.201346	47.19571
8.75	55.6962	18	1.11371	62.02941
8.85	50.68493	18	1.125999	57.0712
8.95	57.14285	18.5	1.125999	64.34281
9.05	38.38384	19.6	1.168907	44.86714
9.15	43.75	20.6	1.139991	49.8746
9.25	29.86111	21.7	1.149954	34.3389
9.35	30.39216	22.5	1.144165	34.77364
9.45	30.23256	22.9	1.147052	34.67832
9.55	34.4	23.5	1.130199	38.87885
9.65	38.78788	21.3	1.127396	43.72929
9.75	30.69307	22.1	1.138563	34.946
9.85	33.39191	22	1.135718	37.92381
9.95	32.53012	22.4	1.141422	37.1306
10.05	33.33334	23	1.138563	37.95211
10.15	33.68984	23	1.132888	38.16681
10.25	33.33334	25.3	1.137139	37.90464
10.35	33.77483	25.2	1.134301	38.31083
10.45	32.65306	25.7	1.134301	37.03841
10.55	31.94444	26.1	1.132888	36.18946
10.65	31.25	26.5	1.132888	35.40274
10.75	32.8125	26.5	1.144165	37.54291
10.85	32.07547	26.2	1.131478	36.29268
10.95	34.11765	25.5	1.130199	38.55973
11.05	33.33333	25.7	1.131478	37.71592
11.15	33.78378	26.2	1.127396	38.08769
11.25	35.06493	26	1.128796	39.58114
11.35	35.80247	26.4	1.132888	40.56018
11.45	35.61644	25.4	1.125999	40.10409
11.55	36.70886	25.8	1.127396	41.38541
11.65	38.02817	26.3	1.124101	42.74749
11.75	38.15789	26.6	1.121957	42.8115
11.85	36.91275	27.9	1.119194	41.31253
11.95	38.65546	27.3	1.116445	43.1567
12.05	37.58389	27.7	1.116445	41.96035
12.15	36.84211	27.2	1.116445	41.13219
12.25	35.55556	27.1	1.116445	39.69584
12.35	35.76159	26.4	1.11371	39.82803

Depth (m)	MS (orig) (10-3 SI)	GS (mm)	Coefficient	MS(cal) (10-3 SI)
12.45	35.51402	26.9	1.11371	39.55231
12.55	35.55556	27.3	1.11371	39.59858
12.65	34.09091	27.5	1.11371	37.96738
12.75	32.43243	27.7	1.112347	36.07612
12.85	35	27.9	1.112347	38.93214
12.95	39.32584	28.7	1.104362	43.42997
13.05	52.54237	27.3	1.087429	57.13611
13.15	89.13044	22.1	1.064736	94.90038
13.25	85.71428	15.1	1.075963	92.2254
13.30	100.7874	17.2	1.061008	106.9362
13.35	91.19498	13.6	1.069519	97.53473
13.40	81.70731	14.8	1.077006	87.99927
13.45	85.88235	17.3	1.102779	94.70925
13.50	77.03704	14.6	1.125746	86.72412
13.55	76.8421	15.4	1.093613	84.03555
13.60	95.38461	19	1.092419	104.1999
13.65	131.0345	14.7	1.078283	141.2923
13.70	142.3077	13.6	1.072041	152.5597
13.75	151.4493	11.4	1.05363	159.5715
13.80	140.7407	10.6	1.057306	148.806
13.85	140.3846	11.4	1.057306	148.4295
13.90	139.2857	11.6	1.054852	146.9259
13.95	134.1463	11	1.093613	146.7042
14.00	129.5775	10.7	1.070778	138.7488
14.05	124.3243	10.5	1.125746	139.9576
14.15	124.5454	10.6	1.122965	139.8601
14.20	124.7312	10.6	1.135332	141.6113
14.25	128.5714	10.6	1.134044	145.8056
14.30	131.3953	11.3	1.084599	142.5112
14.35	132.9897	11.9	1.074576	142.9075
14.40	136.7347	10.9	1.100231	150.4398
14.45	133.6207	10.5	1.105461	147.7125
14.50	138.3562	10.3	1.097574	151.8562
14.55	134.9398	10.8	1.100231	148.465
14.60	130.9278	10	1.088495	142.5142
14.65	122.9885	10	1.073307	132.0044
14.70	119.3548	10.6	1.065871	127.2168
14.75	117.1429	11.1	1.054852	123.5685
14.80	114.7287	12.1	1.047669	120.1977
14.85	112.037	11.7	1.050089	117.6488
14.90	110.1695	11.3	1.038314	114.3905
14.95	105.9211	11.1	1.01657	107.6762
15.00	101.1905	13.2	1.017605	102.9719
15.05	101.8692	14.2	1.013171	103.2109
15.15	104.2424	14.4	1.012043	105.4978
15.20	109.8592	13.7	1.009897	110.9465
15.25	98.33333	13.9	1.009897	99.30653
15.30	87.2	13.6	1.014302	88.4471
15.35	82.35294	14.5	1.048878	86.37817
15.40	77.77778	14	1.065871	82.90106
15.45	45.37815	14.1	1.052521	47.76144
15.50	40.18692	20.2	1.033592	41.53687
15.55	40.68966	23.5	1.017605	41.40598
15.60	43.44263	25.3	1.030184	44.75392
15.65	45.37815	26.4	1.030184	46.74786
15.70	37.62376	24.8	1.017605	38.28611
15.75	36.52174	28	1.015435	37.08544
15.80	38.37209	30.4	1.015435	38.96435
15.85	36.11111	29.9	1.023332	36.95366
15.90	34.25926	30.2	1.026694	35.17378
15.95	28.57143	30.4	1.129816	32.28045
16.00	25.21739	30.8	1.209775	30.50737
16.05	24.70588	29.9	1.209775	29.88855
16.10	25.8427	31.9	1.174122	30.34249
16.20	29.16667	32.2	1.136364	33.14394

Depth (m)	MS (orig) (10-3 SI)	GS (mm)	Coefficient	MS(cal) (10-3 SI)
16.30	26.5896	32.3	1.171097	31.13901
16.40	28.22086	33.1	1.18022	33.30681

Yichuan

Depth (m)	MS (orig) (10-3 SI)	GS (mm)	Coefficient (see thesis)	MS(cal) (10-3 SI)
0.05	91.66666	13.4	1.05753	96.9402
0.10	76.4045	21.1	1.055075	80.61247
0.15	72.66187	20.6	1.055075	76.66372
0.20	80.23255	17.6	1.053852	84.55322
0.25	81.30841	17.4	1.05031	85.39902
0.30	78.31325	18.9	1.055075	82.62634
0.35	77.77778	20.4	1.055075	82.06139
0.40	78.37837	17.1	1.05753	82.88744
0.45	84.61538	16.2	1.064849	90.10263
0.50	76.72414	15.6	1.059996	81.32726
0.55	84.09091	18.1	1.052632	88.51675
0.60	83.33334	20.2	1.058761	88.23012
0.65	78.18182	18.8	1.09529	85.63179
0.70	60.60606	18.4	1.147184	69.52628
0.75	53.76344	18.4	1.182592	63.58023
0.80	37.73585	19.5	1.176609	44.40034
0.85	54.13534	19.8	1.150086	62.26031
0.90	65.21739	19.6	1.119319	72.99909
0.95	45.92593	23.5	1.135332	52.14116
1.00	39.13044	24.4	1.158212	45.32133
1.05	43.26923	24.2	1.138174	49.24793
1.10	51.82927	24.6	1.129816	58.55753
1.15	50.28736	23.2	1.116196	56.13055
1.20	49.53271	23.2	1.131222	56.03248
1.25	42.62295	22.7	1.138174	48.51235
1.30	36.64122	23.4	1.146657	42.01493
1.35	36.27451	24.7	1.153802	41.8536
1.40	38.70967	25	1.152339	44.60667
1.45	50	24.9	1.146657	57.33287
1.55	44.0367	21.5	1.143772	50.36795
1.65	43.9394	25.4	1.155268	50.76179
1.75	43.75	26.4	1.16117	50.80121
1.85	41.37931	25.2	1.128413	46.69297
1.95	36.11111	26.8	1.142465	41.2557
2.05	40.84507	26.8	1.142465	46.66408
2.15	41.53846	26.7	1.132631	47.04775
2.25	42.9752	24.8	1.134044	48.73577
2.35	42.06349	23	1.142465	48.05609
2.45	43.29897	23.3	1.132631	49.04176
2.55	48.1132	27.2	1.127015	54.22428
2.65	57.30337	22.2	1.136751	65.13967
2.75	62.29508	21.3	1.121579	69.86887
2.85	61.11111	22.3	1.113462	68.04488
2.95	64.63415	22.5	1.116196	72.14438
3.05	62.5	21.1	1.118819	69.92616
3.15	60.52632	20.9	1.121579	67.88506
3.25	59.57447	20.6	1.114827	66.41524
3.35	56.73077	19.8	1.129816	64.09532
3.45	66.88312	20.1	1.129816	75.56561
3.55	65.11628	16.8	1.121579	73.03307
3.65	75.67567	21.1	1.129816	85.49957
3.75	83.14607	18.8	1.124354	93.48558
3.85	84	16.9	1.118819	93.98076
3.95	88	17.5	1.113462	97.98463
4.05	90	16.7	1.114827	100.3344

Depth (m)	MS (orig) (10-3 SI)	GS (mm)	Coefficient	MS(cal) (10-3 SI)
4.10	86.15385	15.1	1.116071	96.15385
4.20	92.24138	14.4	1.113462	102.7072
4.30	94.84536	14	1.108156	105.1035
4.40	83.75	16.8	1.131222	94.73982
4.50	83.92857	16.7	1.155268	96.96
4.60	63.38028	16.3	1.239157	78.53814
4.70	82.35294	15.8	1.166997	96.10567
4.80	83.45324	17.3	1.142465	95.34245
4.90	82.35294	15.3	1.129816	93.04366
5.00	85.05747	15	1.141032	97.05325
5.10	85.14851	15.9	1.136751	96.79267
5.20	87.7	15.5	1.131222	99.20815
5.30	86.79245	16.6	1.138174	98.78494
5.40	89.47369	15.9	1.132631	101.3407
5.50	90.42554	16.7	1.135332	102.663
5.60	82.87671	16.5	1.136751	94.2102
5.70	73.78641	17.9	1.136751	83.87679
5.80	90.27778	17.8	1.129816	101.9973
5.90	96.72131	16.9	1.110741	107.4323
6.00	101.2821	16.7	1.118819	113.3163
6.10	111.215	17.1	1.113462	123.8336
6.20	116.8539	16.5	1.102779	128.864
6.30	127.451	15.2	1.105461	140.8921
6.40	117.7778	15.7	1.125746	132.5879
6.50	113.0841	15.6	1.113462	125.9148
6.60	105.8824	15.1	1.122965	118.9022
6.70	96.20253	15	1.127015	108.4216
6.80	88.88889	14.8	1.143772	101.6686
6.90	79.33884	15.4	1.138174	90.30144
7.00	71.42857	15.5	1.151013	82.21521
7.10	65	15	1.125746	73.17348
7.20	50	14.7	1.159689	57.98446
7.30	50.63292	14.7	1.16252	58.8618
7.40	50	16.8	1.161036	58.05178
7.50	52.40641	17.3	1.141032	59.79736
7.60	48.78049	17	1.136751	55.45128
7.70	46.59091	16.7	1.129816	52.63915
7.80	43.01075	16.1	1.146657	49.3186
7.90	41.22807	16.5	1.148106	47.33418
8.00	42.85714	16.5	1.159689	49.70096
8.10	42.4	16.5	1.16117	49.23363
8.20	43.52941	19.6	1.16117	50.54507
8.30	42.20184	18.5	1.164009	49.12331
8.40	54.83871	19.4	1.113462	61.06081
8.50	45.61404	19	1.125619	51.34403
8.60	55.73771	23	1.127015	62.81721
8.70	50.53763	21.6	1.136751	57.44871
8.80	51.28205	21.9	1.136751	58.29493
8.90	46.7742	21.9	1.138174	53.2372
9.00	47.31183	21.4	1.146657	54.25046
9.10	45.20548	21.2	1.156738	52.2909
9.20	48.48485	23.1	1.132631	54.91545
9.30	52.34375	22.7	1.118819	58.56316
9.40	38.81579	21.1	1.133787	44.00883
9.50	49.61832	22.5	1.115947	55.37141
9.60	71.42857	27.8	1.089681	77.83434
9.65	126.1682	26.3	1.064509	134.3072
9.75	152.381	27	1.05241	160.3673
9.80	155.2632	26	1.05363	163.5899
9.85	164.9123	23.1	1.04526	172.3762
9.90	162.7119	17.5	1.057194	172.0181
9.95	154.5455	17.3	1.055966	163.1948
10.00	90.36144	14.2	1.07446	97.08976
10.05	130.2632	13.7	1.089681	141.9453
10.10	145	17.3	1.079447	156.5199

Depth (m)	MS (orig) (10-3 SI)	GS (mm)	Coefficient	MS(cal) (10-3 SI)
10.15	155.8559	16.3	1.071926	167.066
10.20	186.9565	19.8	1.071926	200.4036
10.25	173.0769	15.9	1.064509	184.242
10.30	170.5882	14.6	1.047669	178.72
10.35	176.087	13.6	1.059659	186.5921
10.40	189.7872	13.3	1.054741	200.1763
10.45	197.9798	13	1.04526	206.9403
10.50	209.7222	15.4	1.028912	215.7858
10.55	214.6667	14.5	1.02438	219.9003
10.60	215	13.8	1.025536	220.4902
10.65	211.1111	13.3	1.019888	215.3096
10.70	172.2222	12.8	1.040474	179.1928
10.75	189.1473	15.9	1.059659	200.4316
10.80	192.6829	13.2	1.026589	197.8061
10.85	194.9153	12.3	1.038206	202.3622
10.90	195	13.4	1.008776	196.7114
10.95	197.1698	14	1.015435	200.213
11.00	200.9009	13.6	1.00321	201.5459
11.05	194	14.2	1.004319	194.8378
11.10	198.5507	14.6	1.004319	199.4082
11.15	181.982	14.8	1.002205	182.3832
11.20	187.5	15.2	1.013171	189.9696
11.25	170.4082	15.7	1.029442	175.4254
11.30	182.2034	15.7	1.022181	186.2449
11.35	182.6087	15.2	1.05241	192.1792
11.40	168.8073	15.5	1.04526	176.4475
11.45	164.6342	14.1	1.07689	177.2929
11.50	172.2581	13.8	1.102657	189.9417
11.55	160.8333	13.1	1.074229	172.7718
11.60	152.0468	12.8	1.058425	160.9301
11.65	151.6854	13	1.042862	158.1869
11.70	158.9286	12.6	1.039393	165.1893
11.75	130.3483	13.2	1.026589	133.8141
11.80	137.8378	14	1.025536	141.3576
11.85	132.6923	13.8	1.026589	136.2204
11.90	121.2389	13.6	1.033592	125.3115
11.95	122	13.5	1.02438	124.9744
12.00	95.50562	14	1.032418	98.60172
12.05	70.11494	14.5	1.029442	72.17927
12.10	68	14.6	1.022181	69.50833
12.15	65.04855	16.6	1.013171	65.90532
12.20	74.76636	17.6	1.017605	76.08259
12.25	39.13044	17.4	1.006543	39.38645
12.30	46.66667	18.6	1.004319	46.86821
12.35	68.10345	19.6	1.010918	68.84699
12.40	72.79411	21.9	1.012043	73.6708
12.45	70	21.2	1.019888	71.39214
12.50	61.68224	20.4	1.023227	63.11494
12.55	52	20.7	1.067008	55.48442
12.60	45.04504	20	1.124101	50.63516
12.65	53.75	19.5	1.181614	63.51175
12.70	25	19.8	1.140771	28.51928
12.80	26.19048	19.7	1.23533	32.3539
12.90	24.32432	25.9	1.228803	29.8898
13.00	24.375	26.1	1.255493	30.60264
13.10	25.96154	27	1.232286	31.99204
13.20	31.09244	27.2	1.19076	37.02362

Huanglong

Depth (m)	MS (orig) (10-3 SI)	GS (mm)	Coefficient (see thesis)	MS(cal) (10-3 SI)
0.05	105.298	19.8	1.025851	108.0201

Depth (m)	MS (orig) (10-3 SI)	GS (mm)	Coefficient	MS(cal) (10-3 SI)
0.10	100	19.8	1.026905	102.6905
0.15	114.6497	16.3	1.018952	116.8225
0.20	127.451	14.5	1.008776	128.5695
0.25	129.3333	13.9	1.006644	130.1926
0.30	132.7434	13.5	1.004419	133.33
0.35	123.0769	13.4	1.004419	123.6208
0.40	117.2839	15.9	1.008878	118.3251
0.45	111.4286	17	1.016673	113.2864
0.50	110.9756	13.7	1.026905	113.9614
0.55	110.3448	13.8	1.02923	113.5702
0.60	86.07595	12.4	1.149557	98.94921
0.65	76.10619	15	1.165773	88.72255
0.70	94.55782	16.3	1.06519	100.722
0.75	71.76471	12.8	1.165773	83.66136
0.80	68.85246	12.3	1.145213	78.85074
0.85	67.3913	12.9	1.180777	79.57409
0.90	70.27027	13.3	1.180777	82.97352
0.95	69.06078	14	1.155401	79.7929
1.00	82.6087	15.4	1.136751	93.90553
1.10	70.77922	18.7	1.180498	83.55473
1.20	74.64789	21.1	1.165501	87.00219
1.30	75.72816	16	1.155135	87.47625
1.40	76.59575	14.1	1.171372	89.72212
1.50	81.25	13.6	1.159555	94.21384
1.60	80	13.9	1.161036	92.88288
1.70	81.70732	13.9	1.145082	93.56158
1.80	82.90598	16.7	1.139341	94.45818
1.90	84.55882	12.6	1.139341	96.34133
2.00	82.14286	15.2	1.133658	93.12192
2.10	83.5443	12.1	1.133658	94.71066
2.20	88.7931	11.4	1.133658	100.661
2.30	92.43698	14	1.130966	104.5431
2.40	94.17476	15.3	1.133658	106.762
2.50	92.09039	14	1.136493	104.6601
2.60	95.53571	12.3	1.119821	106.9829
2.70	94.23077	13	1.129561	106.4394
2.80	94.89796	10.3	1.152206	109.342
2.90	94.03973	12.2	1.137915	107.0092
3.00	96.55173	10.9	1.143641	110.4205
3.10	97.16312	11.2	1.137656	110.5382
3.20	104.2105	8.5	1.145082	119.3296
3.30	102.381	9.1	1.152206	117.964
3.40	102.459	10.2	1.137656	116.5631
3.50	106.383	9.5	1.133658	120.602
3.60	111.6071	10.9	1.135074	126.6823
3.70	107.3034	9.7	1.149293	123.323
3.80	108.547	9.5	1.137656	123.4891
3.90	109.6154	10.2	1.122586	123.0527
4.00	109.0909	9.5	1.118443	122.0119
4.10	94.25288	11	1.155135	108.8748
4.20	100	11	1.11433	111.433
4.30	96.09375	10.4	1.115698	107.2116
4.40	90.90909	11.1	1.117069	101.5517
4.50	55.9322	12.8	1.186521	66.36473
4.60	59.67742	12	1.172883	69.99464
4.70	56.25	12.3	1.17744	66.231
4.80	59.7015	11.3	1.16252	69.40419
4.90	57.14286	13.1	1.180498	67.45703
5.00	53.46534	13.3	1.180498	63.11573
5.10	53.45912	14.1	1.169727	62.53258
5.20	50.42017	14.4	1.160766	58.52602
5.30	48.27586	14.5	1.146132	55.33051
5.40	48.24562	14.4	1.157809	55.85921
5.50	50	14	1.17426	58.713
5.60	53.125	14.3	1.16523	61.90285

Depth (m)	MS (orig) (10-3 SI)	GS (mm)	Coefficient	MS(cal) (10-3 SI)
5.70	55.6962	14.1	1.151941	64.15874
5.80	58.55856	14.5	1.134687	66.44563
5.90	60.57693	14.1	1.120825	67.89614
6.00	57.57576	13.4	1.118068	64.37361
6.10	45.53571	15.5	1.144951	52.13615
6.20	31.61765	17.4	1.233198	38.99082
6.30	33.6	19.7	1.207001	40.55523
6.40	68.36735	14.3	1.126253	76.99893
6.50	138.4146	10.4	1.054519	145.9608
6.60	142.5	10.1	1.073192	152.9299
6.70	148.2353	10	1.040042	154.1709
6.80	143.3071	10.2	1.048438	150.2486
6.90	142.0561	9.3	1.036484	147.2389
7.00	131.9672	10	1.043623	137.724
7.10	158.6433	9.5	1.041233	165.1846
7.20	160.3053	10	1.038853	166.5336
7.30	156.5789	9.3	1.048438	164.1633
7.40	156.701	9.6	1.049648	164.4809
7.50	143.9252	8.7	1.041233	149.8597
7.60	141.9355	10.1	1.041233	147.7879
7.70	137.5839	10.1	1.055743	145.2532
7.80	137.7953	9.8	1.054519	145.3078
7.90	133.0097	9.7	1.078283	143.4221
8.00	111.2426	11	1.06067	117.9917
8.10	153.7037	9.6	1.023646	157.3382
8.20	135.1145	9.4	1.066894	144.1529
8.30	138.6139	9.7	1.017915	141.0972
8.40	141.3333	9.9	1.015641	143.5439
8.50	137.069	9.8	1.008878	138.2859
8.60	133.0275	10.2	1.002205	133.3208
8.70	123.913	9.5	1.004419	124.4606
8.80	114.6154	9.8	1.009999	115.7614
8.90	110.5263	9.8	1.008878	111.5076
9.00	103.0769	10.8	1.002205	103.3042
9.10	101.2121	11.7	1	101.2121
9.20	111.9658	10.4	1.00553	112.585
9.30	114.7541	10.3	1	114.7541
9.40	106.5089	10.1	1	106.5089
9.50	41.53846	17.8	1.271133	52.8009
9.60	40.13605	14.5	1.267427	50.86951
9.70	41.66667	17.1	1.264063	52.6693
9.80	38.09524	17.5	1.262308	48.08793
9.90	42.36111	17	1.180359	50.00132
10.00	48.86364	15.5	1.239926	60.5873
10.10	46.91358	14.1	1.257071	58.97371
10.20	42.42424	19.3	1.281887	54.38308
10.30	45.45454	17.1	1.243317	56.5144
10.40	50.63291	21.5	1.197461	60.63094
10.50	51.07914	15.7	1.191185	60.8447
10.60	54.65116	16.2	1.246727	68.13508
10.70	57.3913	16.3	1.178828	67.65447
10.80	56.25	15.7	1.197461	67.35719
10.90	49	15.5	1.241619	60.83933
11.00	50	15	1.203804	60.1902
11.10	56.75676	16.4	1.203804	68.32401

Bashui

Depth (m)	MS (orig) (10-3 SI)	GS (mm)	Coefficient (see thesis)	MS(cal) (10-3 SI)
0.10	105.5556	16.9	1.045806	110.3907
0.20	109.4595	16.9	1.038637	113.6887

Depth (m)	MS (orig) (10-3 SI)	GS (mm)	Coefficient	MS(cal) (10-3 SI)
0.30	116.0305	15.1	1.034019	119.9777
0.40	120.9091	12	1.035197	125.1647
0.50	111.4754	11.9	1.041016	116.0477
0.60	131.0345	12.9	1.034019	135.4922
0.70	126	13.6	1.035197	130.4348
0.80	133.3333	12.9	1.024695	136.626
0.90	138.0282	14.7	1.018952	140.6441
1.00	133.7278	15.3	1.015538	135.8057
1.10	130.2158	19.1	1.015538	132.2391
1.20	124.8276	16.8	1.017812	127.051
1.30	126.0116	17.7	1.020096	128.5439
1.40	116.7442	17.6	1.020096	119.0903
1.50	130.4348	17.8	1.020096	133.056
1.60	110.7692	17.1	1.056747	117.055
1.70	69.64286	18.1	1.259446	87.71143
1.80	67.94872	17.8	1.257703	85.45931
1.90	52	16.7	1.259446	65.4912
2.00	44.44444	17.1	1.259446	55.97537
2.10	83.08823	19.4	1.207729	100.3481
2.20	87.5969	15.9	1.196602	104.8186
2.30	86.9281	15.6	1.212562	105.4057
2.40	82.05128	15.9	1.180777	96.88425
2.50	70.37037	14.4	1.193033	83.95417
2.60	93.75	14.5	1.204094	112.8838
2.70	97.29729	14	1.191469	115.9267
2.80	99.01961	13.9	1.168634	115.7177
2.90	98.57143	13.6	1.165773	114.9119
3.00	102.7397	14.1	1.174398	120.6573
3.10	102.439	13.9	1.025851	105.0872
3.20	101.8692	13.2	1.026905	104.61
3.30	96.39175	12.7	1.018952	98.21857
3.40	93.25154	13.4	1.008776	94.06991
3.50	98.58156	12.9	1.006644	99.23653
3.60	98.64865	13.5	1.004419	99.08458
3.70	95.06172	12.6	1.004419	95.4818
3.80	96.73914	12.3	1.008878	97.59799
3.90	95.45454	11.5	1.016673	97.04604
4.00	81.64557	11.2	1.026905	83.84224
4.10	94.17476	12.9	1.02923	96.92749
4.20	106.2937	12.5	1.149557	122.1907
4.30	112.3529	12.6	1.165773	130.978
4.40	102.7778	12.6	1.06519	109.4779
4.50	95.90164	12.9	1.165773	111.7995
4.60	90.42554	14.4	1.145213	103.5565
4.70	82.75862	14.6	1.180777	97.71947
4.80	68.42105	14.6	1.180777	80.79
4.90	59.375	13.8	1.155401	68.60194
5.00	66.01942	14.2	1.136751	75.04765
5.10	61.90476	14.2	1.143249	70.77255
5.20	54.33071	14.3	1.146132	62.27017
5.30	54.08163	14.6	1.151941	62.29884
5.40	57.14286	16.8	1.157809	66.16052
5.50	51.79856	15.4	1.149029	59.51805
5.60	50.45872	15.3	1.149029	57.97853
5.70	51.72414	15.7	1.150483	59.50774
5.80	59.40594	17.1	1.150483	68.34553
5.90	61.70213	18.8	1.149029	70.89754
6.00	54.66667	16.1	1.149029	62.81359
6.10	45.87156	11.6	1.149029	52.70775
6.20	38.09524	11.9	1.143249	43.55235
6.30	38.83495	11.1	1.150483	44.67895
6.40	65.625	11.3	1.163738	76.37031
6.50	104.1958	11.1	1.166725	121.5678
6.60	110.0917	10.4	1.178828	129.7792
6.70	112.2699	10.1	1.184975	133.037

Depth (m)	MS (orig) (10-3 SI)	GS (mm)	Coefficient	MS(cal) (10-3 SI)
6.80	109.8266	10.2	1.16523	127.9733
6.90	101.4815	10.8	1.160766	117.7963
7.00	91.58878	11.2	1.200624	109.9637
7.10	80	12.2	1.177302	94.18416
7.20	65.78947	10.9	1.175779	77.35387
7.30	66.66666	17.3	1.181893	78.79285
7.40	61.90477	15.9	1.218324	75.42007
7.50	62.09678	16.3	1.207001	74.95087
7.60	67.66467	16	1.215067	82.21711
7.70	46.0177	17.2	1.241619	57.13645
7.80	45.13274	16.9	1.274697	57.53057
7.90	39.43662	19.1	1.269358	50.05919
8.00	66.66667	19.6	1.280082	85.33881
8.10	37.89474	23.6	1.241619	47.05083
8.20	34.11765	27	1.283697	43.79672
8.30	33.33333	24	1.223242	40.77473
8.40	32.87671	25.8	1.208605	39.73495
8.50	29.62963	27.8	1.207001	35.76299
8.60	30.18868	25.1	1.208605	36.48619
8.70	30.64516	23.9	1.203804	36.89077
8.80	36.66667		1.200624	44.02288

Pucheng

Depth (m)	MS (orig) (10-3 SI)	GS (mm)	Coefficient (see thesis)	MS(cal) (10-3 SI)
0.10	124.1379	10.2	1.090394	135.3592
0.20	113.5593	9.8	1.087784	123.528
0.30	118.4466	11.9	1.075038	127.3346
0.40	121.1009	12.4	1.067464	129.2708
0.50	124.3243	13.5	1.057642	131.4905
0.60	129.8851	11.4	1.055186	137.053
0.70	148.1481	9	1.073768	159.0767
0.80	136.3095	9.9	1.082603	147.569
0.90	142.2222	9.5	1.093016	155.4511
1.00	119.697	11.9	1.18779	142.1748
1.10	148.7179	11.4	1.062586	158.0256
1.20	148.1481	10.2	1.062586	157.4202
1.30	141.8033	11.1	1.072501	152.0842
1.40	145.3488	8.8	1.090394	158.4874
1.50	151.5152	11.9	1.056412	160.0625
1.60	105.3333	10.5	1.09553	115.3958
1.70	46.46465	11.8	1.268392	58.93538
1.80	43.07692	17.3	1.240849	53.45194
1.90	43.07692	14.5	1.22429	52.73864
2.00	50	14.4	1.201779	60.08893
2.10	57.44681	14.2	1.18779	68.23472
2.20	63.63637	13.3	1.18779	75.58662
2.30	66.27907	13.5	1.1956	79.24326
2.40	65.55556	12.9	1.201779	78.78327
2.50	64.34782	13.3	1.198753	77.13715
2.60	70.19231	11.8	1.211387	85.03005
2.70	61.65413	12.8	1.214034	74.85022
2.80	55.73771	12.4	1.22534	68.29765
2.90	57.89474	12.9	1.226994	71.03649
3.00	55.26316	13.6	1.243472	68.71818
3.10	57.66423	15.5	1.257071	72.48804
3.20	60.75949	11.6	1.257071	76.379
3.30	63.86555	14	1.253761	80.07215
3.40	72.26891	11.6	1.238544	89.50819
3.50	70.17544	14.3	1.246883	87.50054
3.60	73.45132	13.9	1.235178	90.72544
3.70	68.29269	11.1	1.204384	82.25062
3.80	66.01942	11.6	1.213887	80.14011

Depth (m)	MS (orig) (10-3 SI)	GS (mm)	Coefficient	MS(cal) (10-3 SI)
3.90	65.06024	11.3	1.226994	79.82851
4.00	53.67647	12.2	1.270971	68.22124
4.10	46.52778	11.8	1.296176	60.3082
4.20	37.83784	12.6	1.314752	49.74736
4.30	35.15625	13.6	1.299883	45.69901
4.40	39.58333	11.4	1.27275	50.3797
4.50	37.33333	11.6	1.264063	47.19167
4.60	38.59649	12.6	1.240233	47.86864
4.70	44.04762	12.4	1.2108	53.33287
4.80	48.93617	13	1.201346	58.78925
4.90	46.73913	13.1	1.204384	56.29185
5.00	44.18604	13.8	1.226994	54.216
5.10	59.1716	12.1	1.182732	69.98415
5.20	87.5	9	1.329964	116.3719
5.30	88.46153	9.2	1.45624	128.8212
5.40	80.17241	6.2	1.570845	125.9384
5.50	69.89247	6.5	1.770538	123.7473
5.60	49.15254	5.2	1.730403	85.05371
5.70	45.79439	6	1.679825	76.92658
5.80	39.0625	5.2	1.620746	63.31037
5.90	32.75862	5.1	1.560062	51.1055
6.00	30.88235	5.9	1.967729	60.7681
6.10	34.33735	5.8	1.479728	50.80993
6.20	37.00787		1.614987	

Weinan

Depth (m)	Coef	GS (md)	SUS(cal. to GSDepth)	Depth(SUS)	MS (cal) (High Res.)
0.34	1.0126	10.102	154.9	0.34	154.9
0.38	1.0084	9.404	167.4	0.36	167.4
0.42	1.0052	8.642	171.7	0.38	167.4
0.46	1.0126	8.085	171.8	0.4	168.3
0.54	1.0042	9.525	178.8	0.42	171.7
0.58	1.0042	9.189	176.5	0.44	172
0.62	1.0052	8.482	176.7	0.46	171.8
0.66	1.0073	8.305	188.8	0.48	174.1
0.74	1.0021	6.295	226.8	0.5	175.9
0.78	1.0063	6.015	216.2	0.52	178.9
0.82	1	6.095	216.8	0.54	178.8
0.86	1	6.253	219.7	0.56	176.5
0.94	1	7.175	202.8	0.58	176.5
0.98	1.0021	7.247	192.9	0.6	179.7
1.06	1	6.771	181.4	0.62	176.7
1.14	1	7.5	164.7	0.64	188.7
1.18	1	8.202	158.7	0.66	188.8
1.22	1.0073	10.189	153.1	0.68	201.6
1.26	1	9.199	147.8	0.7	209.3
1.34	1.0189	10.734	131.2	0.72	223.3
1.38	1.0283	11.326	134.6	0.74	226.8
1.42	1.1341	10.845	117.9	0.76	218.9
1.46	1.1226	10.289	89.8	0.78	216.2
1.50	1.1541	10.836	94.3	0.8	220.6
1.54	1.0817	11.352	90.7	0.82	216.8
1.58	1.1761	11.988	84.3	0.84	217.1
1.62	1.1352	10.993	86	0.86	219.7
1.66	1.1886	12.247	86.1	0.88	209.1
1.70	1.1844	10.561	80.6	0.9	214.9
1.74	1.1824	11.991	102.9	0.92	203.6
1.78	1.1991	11.779	92.4	0.94	202.8
1.82	1.1782	11.892	94.5	0.96	198.1
1.86	1.1824	11.639	86.6	0.98	192.9
1.90	1.1457	12.685	82.1	1	193.5
1.94	1.2075	12.892	91.6	1.02	185.7
1.98	1.1844	12.406	85.5	1.04	182.2
2.02	1.1932	13.389	86.1	1.06	181.4
2.06	1.1545	11.924	87.5	1.08	176.6
2.10	1.1336	12.314	113	1.1	174.1
2.14	1.1629	14.304	85	1.12	179.4
2.22	1.1775	13.393	98.1	1.14	164.7
2.26	1.1817	13.312	88.1	1.16	160
2.30	1.1618	13.248	93.8	1.18	158.7
2.34	1.1629	13.53	100	1.2	149.1
2.38	1.142	11.801	102.2	1.22	153.1
2.42	1.1503	13.169	104	1.24	142
2.46	1.142	13.023	104.5	1.26	147.8
2.50	1.1295	12.703	114	1.28	141.3
2.54	1.119	12.043	111.8	1.3	151.9
2.58	1.1211	12.651	112.4	1.32	137.8
2.62	1.1253	12.979	114.3	1.34	131.2
2.66	1.1295	12.262	114.3	1.36	132.7
2.70	1.1128	12.613	120.6	1.38	134.6
2.74	1.1545	12.057	117	1.4	128.6
2.78	1.1336	12.225	127.2	1.42	117.9

Depth (m)	Coef	GS (md)	SUS(cal. to GSDepth)	Depth(SUS)	MS (cal) (High Res.)
2.82	1.1221	11.872	130.5	1.44	103.1
2.86	1.1251	11.922	131.9	1.46	89.8
2.90	1.1211	11.007	135.8	1.48	91.8
2.94	1.1044	11.363	137.9	1.5	94.3
2.98	1.1044	12.373	138.5	1.52	88.7
3.02	1.1096	10.882	139.3	1.54	90.7
3.06	1.1086	12.014	139.4	1.56	100.9
3.10	1.1023	12.445	141.1	1.58	84.3
3.14	1.1086	11.094	139.5	1.6	99.1
3.18	1.1232	11.925	148.6	1.62	86
3.22	1.1023	10.543	138.3	1.64	89.5
3.26	1.1013	11.485	133	1.66	86.1
3.30	1.1075	12.474	150	1.68	84.6
3.34	1.1148	11.97	145.7	1.7	80.6
3.38	1.094	11.05	144.5	1.72	77.3
3.42	1.094	11.928	149.5	1.74	102.9
3.46	1.0856	11.391	145.7	1.76	93.2
3.50	1.0919	10.88	148.4	1.78	92.4
3.54	1.0919	11.467	147	1.8	93.3
3.58	1.0992	8.646	148	1.82	94.5
3.62	1.0125	8.715	148	1.84	89.6
3.66	1.0115	10.397	210	1.86	86.6
3.70	1.0104	8.766	213	1.88	88.9
3.74	1	8.708	212	1.9	82.1
3.78	1.0084	8.317	214	1.92	87
3.82	1	7.118	214	1.94	91.6
3.86	1.0167	7.81	220	1.96	90.9
3.90	1.0292	8.519	215	1.98	85.5
3.94	1.0146	9.044	193	2	83.8
3.98	1.0125	9.563	218	2.02	86.1
4.02	1.0125	8.201	212	2.04	84.9
4.06	1.0146	8.882	215	2.06	87.5
4.10	1.0146	8.627	214	2.08	86.5
4.14	1.0188	8.536	214	2.1	113
4.18	1.0104	8.713	211	2.12	86.7
4.22	1.0104	9.192	212	2.14	85
4.26	1.0062	9.563	214	2.16	84.1
4.30	1.0073	9.715	213	2.18	90
4.34	1.0062	8.388	215	2.2	98.1
4.38	1.0187	9.201	215	2.22	87.3
4.42	1.0156	9.911	216	2.24	87.7
4.46	1.0208	9.264	211	2.26	88.1
4.50	1.0385	8.696	211	2.28	90.4
4.54	1.0562	8.559	213	2.3	93.8
4.58	1.05	8.601	210	2.32	94.1
4.62	1.0541	7.95	206	2.34	100
4.66	1.0666	8.276	204	2.36	103.8
4.70	1.0344	9.563	207	2.38	102.2
4.74	1.0677	8.059	211	2.4	104.8
4.78	1.1083	7.464	208	2.42	104
4.82	1.1124	7.605	192	2.44	106.8
4.86	1.1312	8.327	209	2.46	104.5
4.90	1.0854	8.399	200	2.48	111.4
4.94	1.0958	8.53	196	2.5	114
4.98	1.0979	8	193	2.52	114.1
5.02	1.1395	8.105	190	2.54	111.8

Depth (m)	Coef	GS (md)	SUS(cal. to GSDepth)	Depth(SUS)	MS (cal) (High Res.)
5.06	1.1332	8.019	181	2.56	103.8
5.10	1.1551	8.246	200	2.58	112.4
5.14	1.1624	8.297	206	2.6	110.1
5.22	1.1562	7.367	225	2.62	114.3
5.26	1.1395	8.36	229	2.64	114.3
5.30	1.128	7.21	236	2.66	114.3
5.34	1.1322	8.012	265	2.68	116.1
5.38	1.1228	7.705	269	2.7	120.6
5.42	1.1041	7.962	277	2.72	125.7
5.46	1.1124	7.186	275	2.74	117
5.50	1.0812	6.712	265	2.76	122.6
5.54	1.077	8.674	274	2.78	127.2
5.58	1.0593	7.407	277	2.8	127.7
5.62	1.0312	6.936	273	2.82	130.5
5.66	1.0512	7.722	262	2.84	130.9
5.70	1.0375	7.12	260	2.86	131.9
5.74	1.05	8.14	258	2.88	134.1
5.78	1.0448	7.629	251	2.9	135.8
5.82	1.0375	7.408	251	2.92	135.3
5.86	1.0511	7.69	247	2.94	137.9
5.90	1.0188	8.189	238	2.96	132.6
5.94	1.0271	8.366	242	2.98	138.5
5.98	1.025	8.737	232	3	140.7
6.02	1.0334	9.183	224	3.02	139.3
6.06	1.0229	7.268	214	3.04	137
6.10	1.0292	8.6	212	3.06	139.4
6.14	1.0594	9.587	194	3.08	140.4
6.18	1.0302	9.202	218	3.1	141.1
6.22	1.0063	8.476	198	3.12	140.6
6.26	1.0334	9.612	186	3.14	139.5
6.30	1.0271	9.466	180	3.16	147.9
6.34	1.0198	10.972	187	3.18	148.6
6.38	1.0375	9.642	185	3.2	140
6.42	1.0104	9.271	184	3.22	138.3
6.46	1.0334	10.074	177	3.24	139.8
6.50	1.0667	10.348	171	3.26	133
6.54	1.146	10.103	157	3.28	142.5
6.58	1.1658	9.622	155	3.3	150
6.62	1.1772	9.597	157	3.32	141
6.66	1.1209	9.76	161	3.34	145.7
6.70	1.1408	9.563	170	3.36	143.4
6.74	1.1522	9.818	169	3.38	144.5
6.78	1.1147	9.384	191	3.4	147.7
6.82	1.1209	9.584	174	3.42	149.5
6.86	1.1157	9.997	161	3.44	146.4
6.90	1.1418	8.887	162	3.46	145.7
6.94	1.1564	9.372	159	3.48	150.9
6.98	1.1355	9.63	159	3.5	148.4
7.02	1.1376	8.684	156	3.52	148.4
7.06	1.1147	8.42	155	3.54	147
7.10	1.1407	9.223	153	3.56	149
7.14	1.152	8.855	148	3.58	148
7.18	1.1624	7.962	152	3.6	147
7.22	1.1936	9.061	147	3.62	148
7.26	1.1374	8.694	156	3.64	209
7.30	1.1749	8.576	153	3.66	210

Depth (m)	Coef	GS (md)	SUS(cal. to GSDepth)	Depth(SUS)	MS (cal) (High Res.)
7.34	1.153	8.07	152	3.68	214
7.38	1.1666	8.194	154	3.7	213
7.42	1.1426	9.64	154	3.72	218
7.46	1.1686	10.47	154	3.74	212
7.50	1.1676	10.172	153	3.76	208
7.54	1.153	8.724	150	3.78	214
7.58	1.1582	8.782	153	3.8	216
7.62	1.1811	9.47	155	3.82	214
7.66	1.1541	8.932	155	3.84	217
7.70	1.1957	9.47	150	3.86	220
7.74	1.1957	8.389	137	3.88	217
7.78	1.1686	8.427	161	3.9	215
7.82	1.1541	9.592	165	3.92	214
7.86	1.1416	8.524	172	3.94	193
7.90	1.1353	8.65	168	3.96	210
7.94	1.1374	8.622	164	3.98	218
7.98	1.1353	9.401	169	4	215
8.02	1.1374	8.234	171	4.02	212
8.06	1.1759	8.841	173	4.04	215
8.10	1.1478	8.733	162	4.06	215
8.14	1.1437	8.99	168	4.08	217
8.18	1.1291	9.532	164	4.1	214
8.22	1.1145	9.101	157	4.12	213
8.26	1.0802	9.687	151	4.14	214
8.30	1.1187	10.526	148	4.16	211
8.34	1.1353	9.616	145	4.18	211
8.38	1.1253	10.95	144	4.2	211
8.42	1.1253	11.444	145	4.22	212
8.46	1.1691	9.702	150	4.24	213
8.50	1.167	8.739	171	4.26	214
8.54	1.1566	7.642	253	4.28	218
8.58	1.1378	6.21	275	4.3	213
8.62	1.143	8.401	302	4.32	213
8.66	1.1128	6.919	315	4.34	215
8.70	1.1138	7.338	321	4.36	214
8.74	1.096	6.447	322	4.38	215
8.78	1.0898	6.398	315	4.4	216
8.82	1.0741	8.207	307	4.42	216
8.86	1.0714	7.124	307	4.44	212
8.90	1.0668	7.803	299	4.46	211
8.94	1.0585	7.35	310	4.48	215
8.98	1.0376	7.266	318	4.5	211
9.02	1.0501	7.625	345	4.52	212
9.06	1.0386	6.574	359	4.54	213
9.10	1.0104	8.626	370	4.56	209
9.14	1.0282	7.375	366	4.58	210
9.18	1.0188	7.182	373	4.6	208
9.22	1.0271	7.803	376	4.62	206
9.26	1.0188	6.948	374	4.64	198
9.30	1.0167	6.891	357	4.66	204
9.34	1.0177	6.281	381	4.68	205
9.38	1.0021	6.804	371	4.7	207
9.42	1.0063	7.331	368	4.72	205
9.46	1	5.912	360	4.74	211
9.50	1.0021	6.825	347	4.76	210
9.54	1	6.418	331	4.78	208

Depth (m)	Coef	GS (md)	SUS(cal. to GSDepth)	Depth(SUS)	MS (cal) (High Res.)
9.58	1	6.402	331	4.8	201
9.62	1	6.522	344	4.82	192
9.66	1	6.154	341	4.84	208
9.70	1	6.264	334	4.86	209
9.74	1	6.748	332	4.88	201
9.78	1	6.737	336	4.9	200
9.82	1	6.867	332	4.92	199
9.86	1	7.945	333	4.94	196
9.90	1	7.37	341	4.96	193
9.94	1	6.369	340	4.98	193
9.98	1	6.5	345	5	192
10.02	1	6.881	357	5.02	190
10.06	1	5.787	366	5.04	192
10.10	1	6.556	375	5.06	181
10.14	1	6.239	380	5.08	199
10.18	1	6.346	390	5.1	200
10.22	1	5.705	394	5.12	203
10.26	1	5.808	395	5.14	206
10.30	1	5.311	387	5.16	211
10.34	1	6.432	386	5.18	218
10.38	1	5.513	383	5.2	221
10.42	1	5.871	371	5.22	225
10.46	1	7.896	346	5.24	228
10.50	1	5.983	344	5.26	229
10.54	1	5.937	316	5.28	229
10.58	1	6.524	310	5.3	236
10.62	1	5.912	288	5.32	238
10.66	1	7.686	272	5.34	265
10.70	1	6.393	279	5.36	268
10.74	1	6.287	280	5.38	269
10.78	1	6.547	274	5.4	276
10.82	1	6.727	276	5.42	277
10.86	1	5.799	262	5.44	273
10.90	1	5.9	245	5.46	275
10.94	1	6.396	234	5.48	264
10.98	1	6.366	209	5.5	265
11.02	1	7.61	197	5.52	277
11.06	1	7.09	115	5.54	274
11.10	1	8.722	92	5.56	268
11.14	1	7.799	77	5.58	277
11.18	1	7.71	72	5.6	275
11.22	1	7.994	70	5.62	273
11.26	1	9.195	78	5.64	271
11.30	1	7.155	79	5.66	262
11.34	1	6.777	79	5.68	265
11.38	1	9.087	86	5.7	260
11.42	1	8.967	85	5.72	258
11.46	1	9.579	86	5.74	258
11.50	1	8.13	86	5.76	253
11.54	1	9.176	84	5.78	251
11.58	1	10.125	79	5.8	252
11.62	1	10.065	78	5.82	251
11.66	1	11.563	72	5.84	247
11.70	1	10.917	67	5.86	247
11.74	1	12.22	65	5.88	244
11.78	1	12.036	66	5.9	238

Depth (m)	Coef	GS (md)	SUS(cal. to GSDepth)	Depth(SUS)	MS (cal) (High Res.)
11.82	1	12.263	65	5.92	242
11.86	1	13.238	56	5.94	242
11.90	1	15.057	50	5.96	238
11.94	1	13.908	48	5.98	232
11.98	1	13.635	44	6	231
12.02	1	14.902	41	6.02	224
12.06	1	15.897	32	6.04	223
12.10	1	16.481	40	6.06	214
12.14	1	16.441	38	6.08	216
12.18	1	16.035	37	6.1	212
12.22	1	15.21	39	6.12	206
12.26	1	15.987	38	6.14	194
12.30	1	15.936	40	6.16	210
12.34	1	15.482	42	6.18	218
12.38	1	16.39	44	6.2	213
12.42	1	14.796	47	6.22	198
12.46	1	14.376	51	6.24	193
12.50	1	13.977	62	6.26	186